Evaluation of the Mechanistic Empirical Pavement Design Guide (NCHRP 1-37 A)

Ali, O.

Research Report (National Research Council Canada. Institute for Research in Construction); no. RR-216, 2005-09-01

NRC·CNRC Institute for Research in Construction
CNRC·NRC Institut de recherche en construction

http://irc.nrc-cnrc.gc.ca

Evaluation of the Mechanistic Empirical Pavement Design Guide (NCHRP 1-37A)

RR-216

Ali, O.

September 2005

National Research Council Canada
Conseil national de recherches Canada
Canada

Evaluation of the Mechanistic Empirical Pavement Design Guide (NCHRP 1- 37 A)

Author: Osman Ali

Report No: UR 3002.1
Report Date: September 2005
Contract No: Research Report 216
Program: Urban Infrastructure

EXECUTIVE SUMMARY

Current empirical pavement design approaches are in the process of being replaced with mechanistic models. This study reviewed such a model entitled “AASHTO 2002 Design Guide” to examine its sensitivity to variables with known influence on the performance of roads. The study focuses on evaluating the effectiveness of the manner in which material characteristics were incorporated in the analytical model.

- The structure module relies on linear elastic analysis ignoring visco-elastic/plastic responses. Incorporating nonlinear analysis in the future will improve model performance prediction capabilities.
- The proposed guide is sensitive to asphalt concrete related variables such as mix stiffness, layer thickness as influenced by traffic characteristics and elements of the environment.
- The guide is less successful in addressing variables that are related to unbound materials. The study identified a need to introduce nonlinear analytical capabilities to improve the model sensitivity to variation in the materials response.
- Measures, introduced in the proposed guide to circumvent the need for mechanical testing of materials in lower design levels are not effective. The study recommends the use of actual laboratory test results or alternatively use generic properties produced by limited testing of typical local materials.
- The study identified the need to revise AASHTO soil classification to make it more compatible with mechanistic characterization and design.

TABLE OF CONTENTS

LIST OF TABLES

LIST OF FIGURES

CHAPTER 1

INTRODUCTION

1.1 Background

The last 50 years have seen remarkable increases in the demand for moving people and goods. The surface transportation system has been under pressure to sustain the substantial increase in heavy truck traffic volume levels. Considerable annual expenditures worldwide are allocated for developing the transportation infrastructure, including urban roads and highways. In Canada, $ 8 Billion dollars is allocated annually for the rehabilitation of urban roads [1], with overlays being one of the most commonly used techniques. Durability of the pavement structure determines the initial cost of the road and its future maintenance requirements. A reliable analytical model that ensures the structural and functional integrity of the pavement during its design life is needed to optimize the benefits from the significant funds dedicated to construction and maintenance of the roadway network.

Currently, structural design approaches to flexible pavement are empirical in nature. However limitations of the empirical approach are becoming increasingly obvious with developments in the transportation system and increased knowledge in the fields of pavement mechanics and material science. Premature failures of asphalt overlays within few years of construction are not uncommon, and the need for a more comprehensive mechanistic pavement design model has been recognized. Despite efforts by researchers in the last decades to enhance the mechanistic part of the design, no fully satisfactory, comprehensive alternative to the empirical approach has been found [2]. Research conducted by the Directorate for Transportation of the European Commission, in the late 1990s, to evaluate existing advanced analytical pavement design models, showed that the output varied considerably from model to model [3]. Now there is a major effort to develop a new AASHTO Design Guide, [4] with a potential to address the specific effects of the environment and traffic on the materials that relates its structural response to a realistic pavement performance.

1.2 Objective

This study evaluates an emerging mechanistic-empirical analytical model the *AASHTO 2002 Design Guide*, which is intended to replace the current version used by almost all provinces in Canada (AASHTO 93). The beta version of the software is being evaluated by potential users in the United States and Canada to determine its effectiveness and the need for calibration of some of its components. The current version of the software uses US customary units as the measurement system.

1.3 Scope

This study focused on investigating the effectiveness of the material mechanistic characterization techniques adopted in the new AASHTO 2002 to discriminate between various material types and to produce the input parameters required by the proposed mechanistic-empirical model.

- Asphalt concrete (AC) and unbound material samples (crushed stone and clays) were tested in the laboratory to produce mechanistic properties using the complex modulus and the resilient modulus test protocols respectively.

- The output of tests performed on different materials were used as input to the *AASHTO 2002 Design Guide* to conduct sensitivity analysis. The results were then used to evaluate the model's ability to distinguish between materials with a known performance level. The road structure, environmental conditions and traffic volumes were kept constant in these model runs to focus analysis on the influence of the material type on the predicted performance.

- Model runs were performed using different design levels of the *AASHTO 2002 Design Guide* to determine the degree of precision achieved by using the advance design level (Level 1) compared with the routine design level (Level 3). This component of the investigation focused on establishing the benefits gained from using material models formulated based on results of actual mechanical tests performed on the pavement materials (Level 1) with those estimated from physical properties and limited mechanical tests on the binder used in the mix.

The effects of variations in significant independent material variables were quantified by calculating the predicted distress as each significant variable was changed while all other variables were held constant. The results were plotted to display the relative significance of the independent variables.

1.4 Organization of the Report

Chapter 1 introduces the current state of the roadway network and the absence of a sound analytical approach to pavement design. This chapter also includes the study objective and scope of the investigation.

Chapter 2 discusses state-of-the art road design techniques adopted in Canada and highlights the deficiencies in the most commonly used empirically based approach. The chapter discusses the current material characterization techniques and laboratory testing required in support of the pavement design task.

Chapter 3 describes the main features of the *AASHTO 2002 Design Guide,* including the adopted structural response models, performance models, material characterization and other input requirements. This chapter also includes critique of the theoretical construct of the model with emphasis on the empirical nature of the performance models.

Chapter 4 discusses the *AASHTO 2002 Design Guide* evaluation process according to the terms described in the scope of this study. The input parameters related to the material characteristics used in the analysis are listed.

Chapter 5 discusses the results and output of model runs to reflect the impact of material types on the predicted performance. Different asphalt mixes and unbound materials were used in the analysis to examine the model sensitivity to variation in the mechanistic response of these materials.

Chapter 6 provides conclusions and recommendation related to the objectives set for this study.

CHAPTER 2

STATE OF THE ART

2.1 Pavement Design and Analysis

Pavement engineers are continually looking for an effective analytical tool to assist in analyzing pavement structures, taking into consideration the in-service condition of the road. Such a tool will facilitate the establishment of a performance-based design, capable of extending the service life of roads. An ideal design tool consists of a structural model capable of predicting the state of stresses and strains within the pavement structure under the action of traffic and environmental loading. To carry out such analysis effectively, the design tool should be equipped with material models capable of capturing the mechanistic response of the various materials used to construct the road structure. Such a model is considered a mechanistic model. Because of the knowledge gaps in mechanics and material science in the early 1960s, the empirical modeling approach evolved as an alternative. This study examined a typical empirical design model and evaluated a newly proposed model that represents a step toward mechanistic design.

Empirical Design Approach

Current pavement design procedures are based mainly on empirical approaches. In these empirical approaches, equations that estimate the response of the road are developed to guide users to the appropriate design that limits stresses and strains below a critical level. The design inputs include standardized traffic loading, physical properties of pavement materials, and environment conditions to estimate the pavement performance based on results from previous field experiments (AASHTO road test of 1960s) and in some cases, on practical experience. A number of empirical design methods are in use today, such as the Asphalt Institute Thickness Design [5], the National Crushed Stone Association [6], the California Method and the most commonly used pavement design method the AASHTO design guides [7, 8, 9, 10].

Mechanistic-Empirical Design Approach

In the mechanistic approach, the relationship between the structural response (stresses, strains and deflection) and the physical causes (inputs) are described using a mathematical model. The most common models are based on the multilayered elastic theory and some finite element model applications. Since these theoretical approaches are still not capable of fully analyzing pavements, mechanistic-empirical design approaches evolved with empirical elements added to complement the mechanistic models. These empirical elements are usually included, as performance prediction models since it remains difficult to quantify permanent deformation using the linear elastic theory. The performance prediction models use the calculated stresses, strains and deflections to predict pavement distress using the adopted empirical formulas.

2.2 Overview of AASHTO '93

The AASHO road test conducted near Ottawa, Illinois, during the period 1958-62 was the major highway design/traffic field experiment, which became the basis for the design guides used in North America. The original design procedure was modified several times over the last 40 years in an endeavour to improve the procedure and to incorporate new research findings. For example, the reliability concept was introduced with the release of the 1986 Guide to allow for uncertainties associated with design variables. The 1993 Guide, the current design guide used by the majority of Canadian provincial road authorities [11], was an attempt to improve design procedures particularly for the rehabilitation of existing pavements. Some of the new developments introduced in the 1993 Guide included the removal of the pavement support value and replacing it with the resilient modulus M_R (elastic response). Drainage coefficients were added and the regional factor (R) abandoned.

Main features of the ASSHTO 93 structural design procedure are captured in Figure 2.1. The basic equation of the guide for flexible pavement design is shown below as Equation 2.1.

$$\log_{10}(W_{18}) = Z_R \times S_o + 9.36 \times \log_{10}(SN+1) - 0.20 + \frac{\log_{10}\left(\frac{\Delta PSI}{4.2-1.5}\right)}{0.40 + \frac{1094}{(SN+1)^{5.19}}} + 2.32 \times \log_{10}(M_R) - 8.07 \qquad (2.1)$$

where:

- W_{18} = predicted number of 80 kN (18,000 lb.) equivalent standard axle load (ESALs)
- Z_R = standard normal deviate
- S_o = combined standard error of the traffic prediction and performance prediction
- SN = structural number (an index that is indicative of the total pavement thickness required)
  - = $a_1D_1 + a_2D_2m_2 + a_3D_3m_3$+...
    - a_i = i^{th} layer coefficient
    - D_i = i^{th} layer thickness (inches)
    - m_i = i^{th} layer drainage coefficient
- ΔPSI = difference between the initial design serviceability index, p_o, and the design terminal serviceability index, p_t
- M_R = subgrade resilient modulus (in psi)

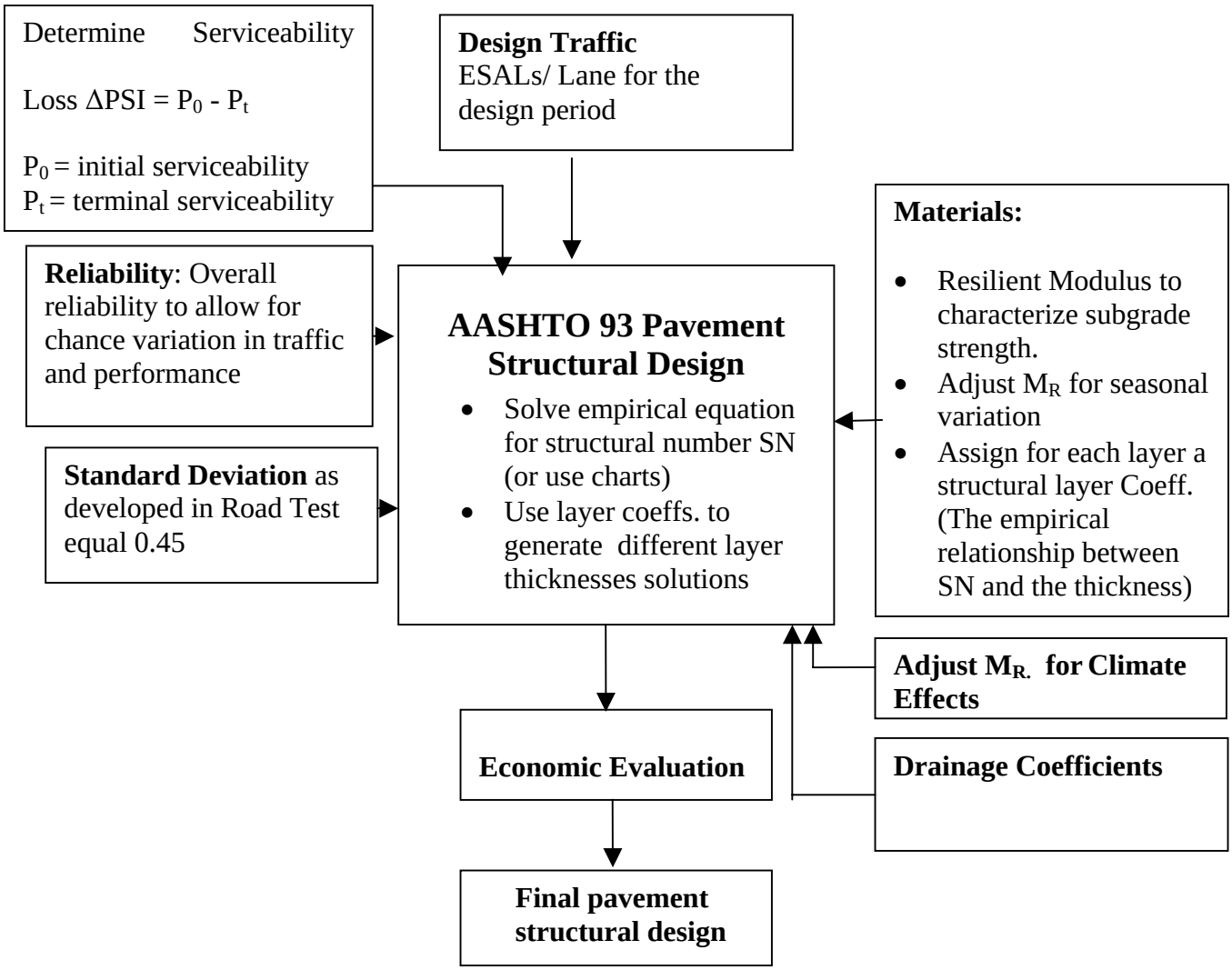

Figure 2.1: AASHTO 93 Structural Design Procedures

Traffic

The current AASHTO 93 is based on the 18-kip single standard axle. Different axle types are converted to ESALs using the load equivalency factors (LEF), defined as the number of repetitions of the 18-kip single standard axle that causes the same damage as a single application of a particular configuration. The concept of the relative damage is not quantifiable and is based on empirical results of the ASSHTO Road Test. One main reason that makes the empirical procedure outmoded is the development that took place in traffic loading conditions. Today, traffic volumes and vehicle characteristics have changed significantly. There are a variety of multiple axle configurations; tire types and pressures have increased substantially. The trucking industry has succeeded in increasing

legal truck loads. Weigh-in-motion (WIM) stations have provided detailed traffic data including traffic counts, actual truck loadings, truck classifications and distribution during the day and the whole year. All the above-mentioned developments have far exceeded the data for which the empirical design was thought to cover. Although it does influence pavement loading, the current AASHTO design practice does not account for vehicle speed. Slower speeds and stop conditions for a longer period of time result in greater rutting damage. Because of an inadequate mix or structural design, the rutting problem becomes evident at bus stops and intersection approaches.

Reliability

Reliability is introduced in the guide as a means of incorporating some degree of certainty into the design process to ensure that the various design alternatives will last for the analysis period. Design performance reliability is controlled through the use of a reliability factor F_R that is multiplied by the design period traffic prediction (w_{18}) to produce design applications (W_{18}) for the design equation. The reliability factor is a function of the overall standard deviation (S_0) that accounts for both chance variation in the traffic prediction and normal variation in pavement performance prediction for a given W_{18}. Suggested levels of reliability in the Guide are associated with the functional classification of the road and whether it is urban or rural.

Materials Characterization

With the exception of the native soil properties, the 93 Guide continued to rely on physical properties to characterize other materials used in the pavement structure.

Roadbed Soil Characterization

Characterization of subgrade soils in the AASHTO 93 is based on the resilient modulus M_R parameter determined using AASHTO Test Method T274. This represents the first attempt at implementing a mechanistic property in pavement design. The original AASHTO M_R test procedure has been modified (SHRP – P-46) to the current procedure entitled “AASHTO T294-92”.

The resilient modulus is a measure of the elastic property of soil recognizing certain nonlinear characteristics. It should be noted that the AASHTO Guide empirical model (Equation 2.1) is sensitive to variations in the M_R parameter. The AASHTO Guide (AASHTO 93) recommends that the resilient modulus test be performed on laboratory samples using relevant stress levels and moisture conditions simulating the primary moisture seasons. When test facilities are unavailable for performing the test, estimation of the resilient modulus can be made from standard CBR, R-value and soil index test results using correlation relationships recommended by the Guide. It provides guidelines for two procedures to be followed for determining the seasonal variation of the modulus based either on the laboratory relationship between the resilient modulus and moisture content, or from backcalculated moduli for different seasons. The Guide includes a procedure for determining the effective roadbed soil resilient modulus based on an estimate of relative damage (u_f) that corresponds to the seasonally adjusted subgrade modulus for each month of the year.

Pavement Layer Material Characterization

In the current empirical design procedure (AASHTO 93), pavement material characteristics are not directly incorporated in the structural design. The layer coefficients representing the various unbound layer materials are related to the resilient modulus determined using AASHTO T274 test methods. Alternatively the bound or asphalt concrete may be characterized using results of the repeated load indirect tensile test (ASTM D 4123). The Guide also provides charts for estimating these coefficients based on physical properties. The layer coefficient, which is a measure of the relative ability of the material to function as a structural component of the pavement, expresses the empirical relationship between the structural number (SN) and thickness [10].

$$SN = a_1D_1 + a_2D_2m_2 + \ldots\ldots + a_iD_im_i \quad 2.2$$

Where:

SN = Structural number of the pavement structure

a_i = Layer coefficient i.

D_i = Thickness of layer i

m = Drainage factor for layer I

It was found that many factors could influence the layer coefficients such as the thickness of the layer and the underlying support and position within the pavement structure. The Guide noted that the laboratory resilient modulus values were significantly different from what may exist for an in situ condition. In practice, experience play a major role in determining the layer coefficients, and long-term pavement response data are considered the most reliable method for determining the structural layer coefficients.

Critique

The empirical equations developed for the specific conditions of the AASHTO Road Test hindered advancement of the earlier developed design approach. Limitations of the approach were recognized, and researchers noted that it is not realistic to use empirically derived relationships to describe phenomenon that occur outside the range of the original data used to develop the empirical relationships. Accordingly, applications of the AASHTO 93 Guide [10] involved significant limitations including the following.

- Since the adopted empirical equations were developed based on only one type of pavement material and roadbed soil at the AASHTO Road Test, extending analysis beyond those materials may result in design errors.
- Limitations associated with the environment at which the AASHTO Road Test was conducted render the results of the design procedure in uniquely different environmental conditions less accurate.
- There are limitations associated with the age at which loading tests were performed. An accelerated two-year testing period was used to develop the test results. The Guide did not consider aging effects, and it is unrealistic to extrapolate the results for a typical 20-year pavement life.
- The maximum load used to develop the equations was approximately one million. The vehicles used in the test had identical axle loads and configurations, as opposed to mixed traffic.

Pavement performance is categorized according to the structural performance and the functional performance. The structural performance relates to the physical conditions of the pavement, such as the occurrence of cracking or any other conditions that might affect the load-carrying capacity of the road. On the other hand,0 the functional performance describes how well the pavement serves the user. It is concerned with the riding comfort and is quantified using the serviceability-performance concept.

In the current AASHTO 93 system, the loss of serviceability, the difference between the initial serviceability and terminal serviceability is the only performance indicator. One major deficiency of the empirical approach is that it proved to be inadequate in evaluating the performance of the pavements. There is no provision to predict other modes of failure, such as fatigue, rutting and thermal cracking. In fact, these types of failures, in many cases dictate the scheduling of maintenance and planning of rehabilitation.

The empirical nature of the design approach does not account for the mechanistic response of asphalt concrete. The mix design procedure relies on physical properties, which cannot be linked to the pavement structural response. Road agencies select a mix type based solely on experience without direct reference to the mix's ability to withstand relevant vehicle load characteristics. The long-term effects of climate on material properties were not considered. In the end, the design process yields a set of layer combinations that satisfy the structural number with the selection of the best solution based mainly on economical analysis.

2.3 Research Work

The limitations of AASHTO road design guides, evolving from the early road test, motivated researchers to pursue improvements in the design process. These improvements benefited from advancements in mechanics and material science leaning toward the development of a mechanistic based design approach.

Materials Characterization

Mechanistic pavement design procedures are complex and involve the interaction of the pavement structure model that estimates the state of stresses and strains with the imposed traffic loads and environmental conditions. The state of stresses and strains changes in response to traffic and seasonal variations in the environment. The state of the different materials forming the road layers and, consequently, the response of the structure, changes with variation in temperature and moisture condition. An effective analytical model should account for all of these factors in analysis leading to a performance-based design. Material characterization models interact with the environmental models. The structural response model should then use material properties to estimate the stresses and strains within the pavement structure. The shift to a mechanistic design approach necessitates the development of procedures to define the material characteristics necessary for the implementation of the proposed analytical model and to establish performance-based specifications for road design and construction.
The following is a review of recent developments in material characterization techniques.

Binder Characterization:

The Strategic Highway Research Program (SHRP), completed in the late 1990's, was one of the largest research projects conducted after the AASHTO Road Tests. One of its major deliverables was the SuperPave system, which included new binder specifications that replaced the penetration grade and a mix design procedure to replace the Marshall approach.

In the past, binders were characterized according to their physical properties, such as penetration, ductility and viscosity. The tests associated with these specifications are empirical and do not provide a comprehensive interpretation of the test results. However the conventional tests do not allow for cold temperature effects. SuperPave uses a binder selection process based on binder performance grading (PG) system and its associated specifications. New binder tests and classification system are designated for expected high and low in-service temperatures. The high pavement temperature is based on the seven-day average high air temperature of the surrounding area while the low pavement temperature is based on the one-day low air temperature of the surrounding area. Using a reliability concept the appropriate PG asphalt binder is determined. SuperPave allows for high pavement temperature adjustment for slow transient loads and stationary loads. Additionally, if the anticipated 20-year loading is in excess of 30 million ESALs, the high temperature grade is increased by one grade.

SuperPave has adopted a new set of tests that can be related to pavement performance.

Rolling Thin-Film Oven (RTFO) Test

The test simulates short-term aging by heating a moving film of asphalt binder in an oven for 85 minutes at 163° C. The quantity of volatiles lost from the binder is an indication of the aging that may occur in the asphalt during mixing and construction time. The AASHTO T240 test, "Effects of Heat and Air on a Moving Film of Asphalt", and the ASTM D 2872 test, "Rolling Thin-Film Oven Test", were adopted to account for the impact of short-term binder aging on the response of asphalt concrete layers.

Pressure Aging Vessel (PAV)

The SuperPave pressure aging vessel test simulates the effects of long-term asphalt binder aging that occur during the in-service time of pavement (AASHTO PP1: Practice for Accelerated Aging of Asphalt Binder Using a Pressurized Aging Vessel).

Dynamic Shear Rheometer (DSR)

This test is used in the SuperPave system for estimating medium to high temperature viscosities of binders. The test is performed between 46°C (115° F) and 82° C (180° F). The test simulates the shearing action of traffic at a certain speed and determines two important parameters used to predict the performance of the hot mix asphalt concrete (HMA). The first is the complex shear modulus (G*) and the second is the phase angle (δ), which represent the time lag between the maximum applied shear stress and the maximum resulting shear strain. By obtaining the values of G* and δ, it is possible to determine the elastic and viscous components of the total complex shear modulus. These binder properties help in predicting the performance of the HMA and specify the minimum value for the elastic component if rutting is of primary concern. On the other hand, it is possible to specify the maximum value of the viscous component when fatigue

is under consideration (see AASHTO TP5 test “Determining the Rheological Properties of Asphalt Binder Using a Dynamic Shear Rheometer”).

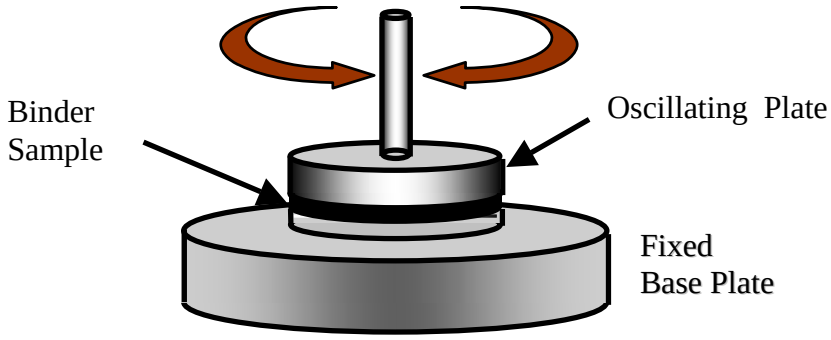

Figure 2.2 Dynamic Shear Rheometer

Bending Beam Rheometer (BBR)

This test measures binder properties at low temperatures (AASHTO TP1: Method for Determining the Flexural Creep Stiffness of Asphalt Binder Using the Bending Beam Rheometer). A simple asphalt beam is subjected to a 980 μN load over 240 seconds to calculate the beam creep stiffness S(t) and the rate of change of that stiffness known as the m-value. The creep stiffness is related to thermal stresses while the m-value indicates how the binder relaxes under load. Cold region specifications may call for a maximum limit on creep stiffness and a minimum limit on the m-value to minimize the potential for thermal cracking.

Direct Tension Tester (DDT)

The DTT test measures the amount of binder strain before failure at low temperatures. The test is implemented for testing asphalt binders with high BBR creep stiffness in excess of 300 MPa (see AASHTO TP 3: Method for Determining the Fracture Properties of Asphalt Binder in Direct Tension). SuperPave specifications call for a minimum failure strain for asphalt binders that have a high BBR creep stiffness to ensure that they will stretch rather than break.
Although the SuperPave goal was to use the above mentioned tests to quantify asphalt performance during mixing, construction and in-service, these tests received little attention by the industry. However, the performance-based binder specifications (PG) was the most popular product of SuperPave and gained wide acceptance and application.

SuperPave Mix Design Method

The superPave mix design method targets the establishment of sustainable aggregate gradation and performance-based binder specifications [12] to produce a durable HMA product. The method was designed to replace the conventional Marshal and Haveem methods. The Marshal method developed in the late 1930s depends on a set of physical characteristics of the mix to arrive at the intended material quality during construction [13]. However, there is a limitation associated with the Marshal tests (Stability and Flow), because of their empirical nature.

SuperPave specifies aggregate by placing restrictions on aggregate gradation using broad control points. In addition, it applies consensus requirements on coarse and fine aggregate angularity, flat and elongated particles, and clay content.
The SuperPave approach relies on using the gyratory compactor for preparing laboratory samples. It was claimed that the gyratory compactor simulates closely actual field compaction.
Density and voids analysis are similar to the conventional mix design methods. The optimum asphalt binder content is selected as the asphalt binder content that results in four percent air voids at the design number of gyrations required to produce a sample with the same density as that expected in the field after the indicated amount of traffic. SuperPave mix design procedure adopted the modified Lottman test, "AASHTO T 283: Resistance of Compacted Bituminous Mixture to Moisture Induced Damage" for moisture susceptibility testing.

Characterization of Asphalt Concrete Mix

Linear viscoelasticity

One principal feature of elastic behaviour is the capacity for materials to store mechanical energy when deformed by loading, and to release this energy totally on removal of loads. Conversely, in viscous flow, mechanical energy is continuously dissipated. A number of engineering materials, such as HMA, simultaneously store and dissipate mechanical energy in varying degrees during a loading and unloading cycle. This behaviour is referred to as viscoelastic [14]. Two main ways to characterize this property in bituminous mixes are the complex modulus and the creep compliance.

The Dynamic Modulus

The bituminous mixture behaviour, similar to its binder, depends on temperature and load frequency. Viscoelastic properties of asphalt materials are generally determined within the linear viscoelastic domain where the material is subjected to sinusoidal loading at different frequencies at small values of strain to keep it within the linear zone. Experimentally, loading can be applied under either a stress or strain controlled mode. The complex modulus (E*) defines the relationship between the stress and strain for a linear viscoelastic material subjected to sinusoidal loading. The complex modulus contains both real and imaginary components as shown in equation 2.3. The absolute value of the complex modulus |E*| is defined as the dynamic modulus.

$$E^* = |E^*|\cos\varphi + |E^*|\sin\varphi \qquad (2.3)$$

The phase angle φ is an indication of the elastic-viscous properties of the mix or binder material. For a perfect elastic material φ is equal to zero and for a perfect viscous material φ is equal to 90º.

The complex modulus test is conducted at different temperatures (usually –10, 0, 10, 20, 30 and 40 °C) over a range of frequencies say (0.1, 0.3, 1, 5, 10, 20 Hz). Isothermal curves can be displayed by plotting the dynamic modulus |E*| as a function of reduced frequency for each temperature tested in a bi-logarithmic scale.

Master curves may be constructed based on the time-temperature superposition properties of asphalt mixes. Different combinations of temperature and frequency can produce the same dynamic modulus. The principle of time-temperature superposition makes it possible to merge the isothermal curves into a single curve at a reference temperature by shifting those curves horizontally relative to that reference temperature.

The resulting master curve of the modulus, as a function of time, describes the time dependency of the material. The amount of shift at each temperature required to form the master curve describes the temperature dependency of the material. In general, the dynamic modulus master curve can be mathematically modeled by a sigmoidal function described by Equation 2.2.

$$\log(E^*) = \delta + \frac{\alpha}{1 + e^{\beta + \gamma (\log(tr)}} \qquad (2.4)$$

Where:

t_r = time of loading at the reference temperature.

δ, α = fitting parameters; for a given set of data, δ represents the minimum value of E* and δ+α represents the maximum value of E* and δ+α represents the maximum value of E*.

β, γ = parameters describing the shape of the sigmoidal function.

The fitting parameters δ and α depend on the physical properties of the asphalt mixes [4]. The model developed by Witczak for predicting the dynamic modulus of HMA has a sigmoidal form similar to the general relation suggested for the master curve in Equation (2.4) [15]. The predictive model is intended to provide an approximation for the dynamic modulus in the absence of conducting the test protocol.

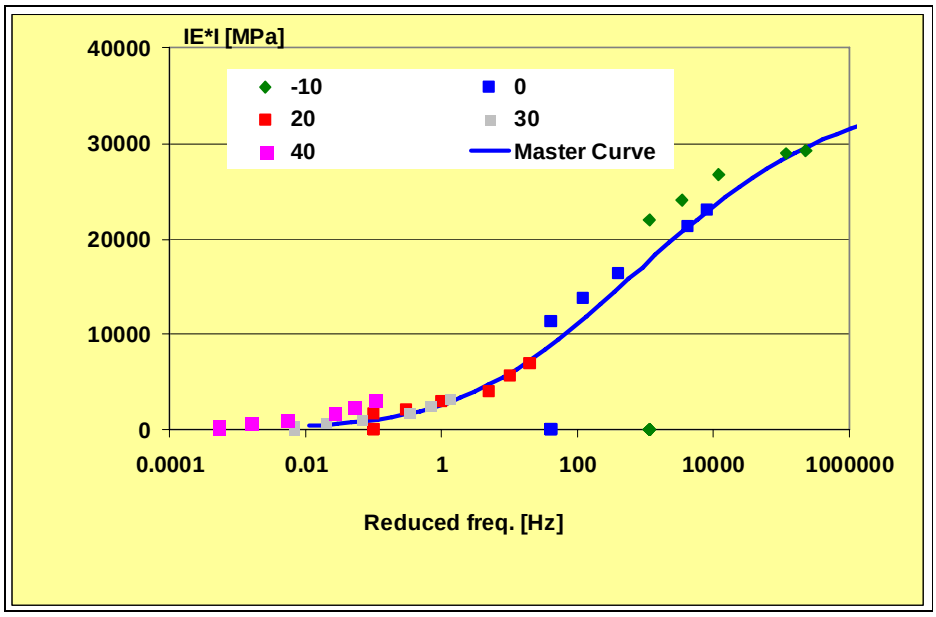

Figure 2.3 Master Curve Developed Using Husaroad Program [16]

Rheological Models

Rheological models are used to capture the material's response to an imposed load. This response is generally used as an input to performance models that predict various types of distress. Many rheological models were developed to describe the mechanistic response of bituminous materials such as the Generalized, Burgers, and Huet-Sayegh (see Figure 2.4). The rheological models are composed of various combinations of springs and dashpots to describe the viscoelastic behaviour of materials.

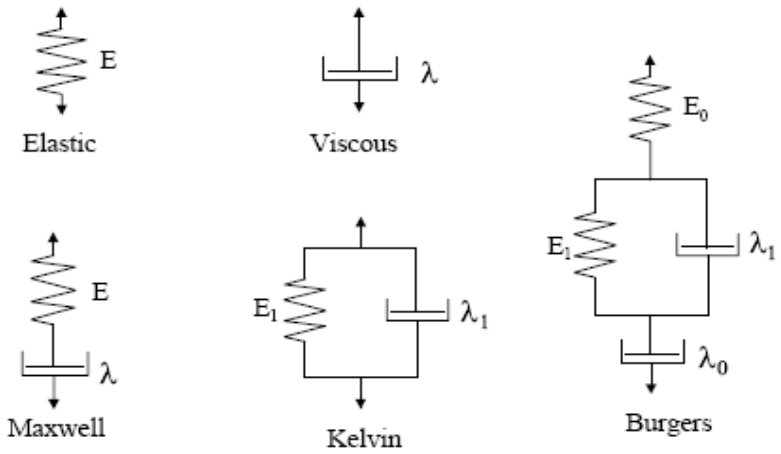

Figure 2.4 Rheological Models Representation

The Huet-Sayegh model [17, 18] has two branches as shown in Figure 2.5. One branch consists of two parabolic dashpots, k and h, associated in series with a spring E_∞ - E_0. The other branch consists of a single spring E_0. The model can be described mathematically using the formula in Equation 2.5.

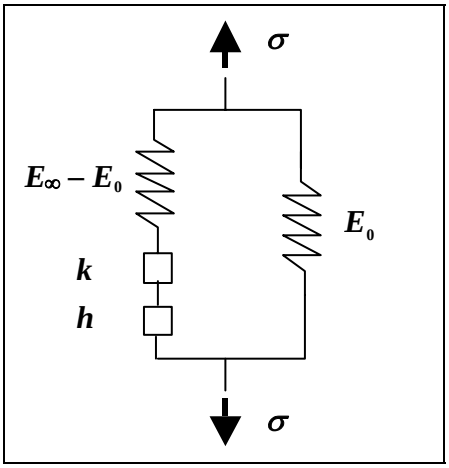

Figure 2.5 Huet-Sayegh Model

$$E^*(i\omega) = E0 + (E_\infty - E_0) / 1 + \delta (i\omega\tau)^{-k} + (i\omega\tau)^{-h} \quad (2.5)$$

E_0 is the high temperature stiffness while E_∞ represents the purely elastic modulus; δ, k and h are parameters of the biparabolic elements of the model. The parameter τ is a temperature dependent variable and is referred to as the characteristics time. The dynamic modulus at any given temperature and frequency can be obtained by fitting the rheological model into the experimental data.

Creep Compliance

The creep compliance is another concept used to characterize the viscoelastic behaviour of bituminous mix. If a constant stress is applied, the strain will increase with time. When this strain is normalized and formulated as a function of time, it is called creep compliance as defined by Equation (2.6)

$$D(t) = \varepsilon(t) / \sigma \quad (2.6)$$

Where

σ = constant applied stress.

$\varepsilon(t)$ = increasing strain with time

The creep compliance must be defined for a number of temperatures. In the laboratory, tensile creep is determined by applying a static load of fixed magnitude along the diametral axis of a specimen. The horizontal and vertical deformations measured near the center of the specimen are used to calculate tensile creep compliance as a function of time (see AASHTO TP9-96 Method for Determining the Creep Compliance and Strength of Hot Mix Asphalt (HMA) Using the Indirect Tensile Test Device). Loads are selected to keep horizontal strains in the linear viscoelastic range. The Poisson ratio can be determined from the test. The tensile strength is determined immediately after determining the tensile creep or separately by applying a constant rate of vertical deformation to failure.
Tensile creep and tensile strength test data are required to determine the master relaxation modulus curve and fracture parameters. This information is used to calculate fatigue performance and thermal cracking of the HMA. The master relaxation modulus curve controls thermal crack development while the fracture parameter defines a mixture's resistance to fracture [19].

Characterization of Unbound Materials

The mechanical response of naturally occurring soils, such as sand, gravel and clays, can be influenced by a variety of factors. These include:

- the shape, size and mechanical properties of the individual soil particles;
- the configuration of the soil structure;
- the intergranular stresses and stress history; and
- the presence of soil moisture, the degree of saturation and the soil permeability.

These factors generally contribute to stress-strain phenomena, which display markedly non-linear, irreversible and time-dependent characteristics, and to soil masses, which exhibit anisotropic and non-homogeneous material properties [20]. The non-linear behaviour of a soil is important for the analytical design and evaluation of pavements. The resilient modulus, M_R, is commonly used in pavement engineering as an appropriate measure of stiffness for the unbound layers.
The selection of an appropriate design M_R value for base, subbase and/or subgrade materials has long been complicated by various test and analysis problems [21]. Since the M_R was introduced in the AASHTO 1986 edition, a set of test protocols was developed and proposed. They include AASHTO T 292-91, AASHTO T 294-92, AASHTO T P46-94, NCHRP 1-28 Draft-96, and the Harmonized Resilient Modulus Test Method for Unbound Pavement Materials NCHRP 1-28A. The main differences between these protocols are in the material type definition, specimen size, compaction method, loading time, stress sequence and the model predictive equation.

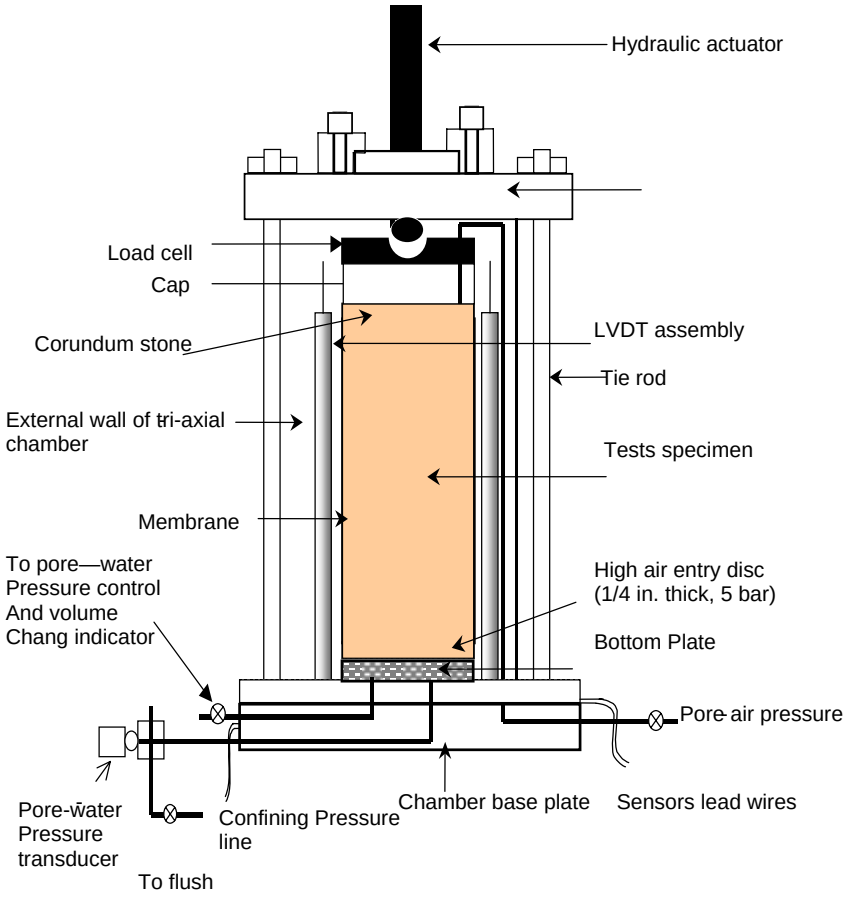

Figure 2.6 Triaxial Pressure Chamber for Determination of M_R

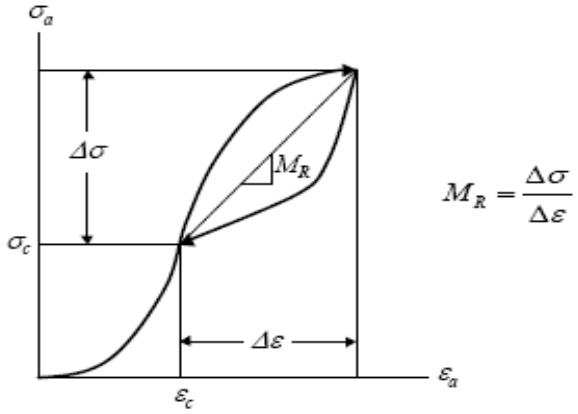

$$M_R = \frac{\Delta\sigma}{\Delta\varepsilon}$$

Figure 2.7 M_R Definition.

Many models were suggested to establish the stress-strain relationship. Course-grained soils exhibit an increase in stiffness with increasing confining stress and are usually represented with a power-law model of the form:

$$M_R = k_1 p_a (\theta/P_a)^{k2} \quad (2.7)$$

Where:

θ = Bulk stress ($\sigma_1 + \sigma_2 + \sigma_3$),

k_1, k_2 = material parameters, with $k_1 > 0$ and $k_2 \geq 0$

P_a = atmospheric pressure.

For fine-grained soils, an alternative equation representing the decrease in stiffness with the increase of deviator stress (σ_d) has the form:

$$M_R = k_1 p_a (\sigma_d/P_a)^{k3} \quad (2.8)$$

Here, the parameters $k_1 > 0$ and $k_3 \leq 0$.

Witzak and Uzan proposed a universal model [22] that combined both the effects into a single equation. The model later modified and adopted in the NCHRP Project 1-37A and has the following form:

$$M_r = k_1 p_a \left(\frac{\theta}{p_a} \right)^{k_2} \left(\frac{\tau_{oct}}{p_a} + 1 \right)^{k_3} \quad (2.9)$$

Where:

τ_{oct} is the octahedral shear stress.

2.4 Summary

Review of current pavement design practices in this study revealed that the AASHTO 93 Guide is relied upon across Canada. Deficiencies of the design process were identified, which were mainly related to limitations in the AASHO Road test performed in the 1960s. The limitations included dependency on information collected for a single native soil and road construction material within unique environmental and traffic conditions. Advancements made in engineering mechanics and analytical modeling encouraged researchers to explore the potential for mechanistic design methods. Material characterization techniques were investigated to produce mechanistic properties suitable for the new trend in modeling. Encouraged by these developments, the road community is now prepared for the mechanistic design approach and the AASHTO 2002 Guide represents the first attempt toward that goal. The next chapter discusses the AASHTO 2002 Guide to reflect improvements achieved with the new approach to pavement design.

CHAPTER 3

OVERVIEW OF THE PROPOSED AASHTO DESIGN GUIDE

3.1 Introduction

The new guide was developed through a National Cooperative Highway Research Program initiative (NCHRP Project 1-37A). The objective of the new Design Guide was to provide the highway community with a state-of-the practice tool for the design of new and rehabilitated pavement structures, based on mechanistic-empirical principles. This chapter includes a brief overview of the theoretical construct of the mechanistic empirical model and its applications. General features of the design procedures and the interaction between materials and of environmental elements are discussed. The chapter also covers the two main features of the analytical model; the structural response model and the distress response models.

3.2 General Features of the Design Model

The design process adopted in the new guide is an iterative process using computational software and a set of documentation. Three design levels were incorporated in the model for users to select according to their needs. Main features of the design process are illustrated in Figure 3.1.

Design Input Levels

The guide provides three levels of input depending on the criticality of the project, the sensitivity of the pavement performance to a given input, the resources available to the designer, and the availability of input information at the time of the design. These three levels are categorized as follows.

Level 1

Site and/or material-specific inputs for the project are to be obtained through direct testing or measurements. This level of input uses the state of the art techniques for characterization of the materials, such as the dynamic modulus of HMA, as well as characterization of traffic through collection of data from (WIM) stations.

Level 2

This level uses correlations to determine the required inputs. For example, the dynamic modulus could be estimated based on results of tests performed on binders, aggregate gradation and mix properties. The level of accuracy for this category is considered as intermediate.

Level 3

This level produces the lowest accuracy. Inputs are typically user selected from national or regional default values, such as characterizing the HMA using its physical properties (gradation) and type of binder used.

Processing of Input Over Design Analysis Period

The design period is divided into incremental analysis periods typically by the month or for two weeks for frost conditions. The design inputs are processed to obtain seasonal values of the traffic, material and climatic inputs needed for each analysis increment. The traffic level and the layer moduli are computed for each increment period. Temperature and moisture profiles in pavement layers are obtained using the Enhanced Integrated Climatic Model (EICM) built in the software. The asphalt global aging model modifies the hot-mix asphalt properties for long-term aging so the dynamic modulus of the asphalt mix is increasing over time.

Pavement Structural Response Models

Two flexible pavement analysis methods have been incorporated in the Design Guide.

1. Multilayer linear elastic analysis method
   The assumptions associated with this method are that each layer is homogeneous, has finite thickness except for the subgrade, is isotropic, full friction is developed between layers at each interface, and there are no surface shearing forces. The elastic modulus and Poisson's ratio of each layer are essential for the stress solution of the problem.
2. Finite element method
   The finite element module is initiated when the unbound material's non-linear behaviour is considered and the coefficient and exponents of the resilient modulus prediction model are entered for level 1 input (of unbound layers).

Critical stress and/or strain values computed by the structural model include:

- tensile horizontal strain at the bottom/top of the HMA layer to predict fatigue cracking;
- compressive vertical stresses/strains within the HMA layer for prediction of HMA rutting;
- compressive vertical stresses/strains within the base/subbase layers for prediction of rutting of unbound layers; and
- compressive vertical stresses/strains at the top of the subgrade for prediction of subgrade rutting.

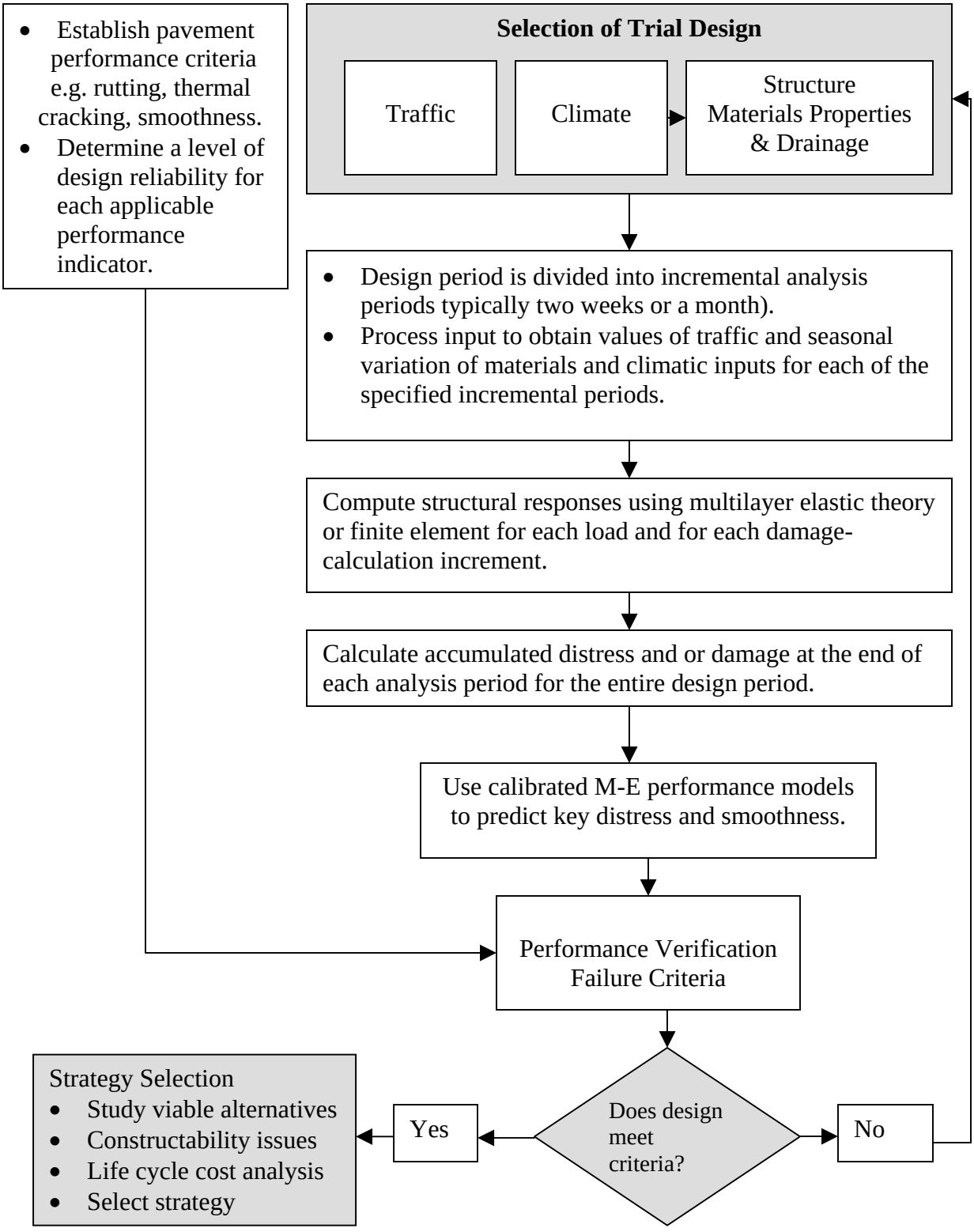

Figure 3.1 M-E Design Process for Flexible Pavement

Distress Prediction

The critical stress and/or strain values obtained from the structural response model are converted to incremental distresses, either in absolute terms, such as in rut depth calculation or in terms of a damage index in fatigue cracking. Distress models, sometimes called transfer functions, relate the calculated damage to field observed distresses. The cumulative damage is converted to physical cracking using calibrated distress prediction models and the output at the end of each analysis period is tabulated by the Design Guide software and plotted for each distress type.
The structural distresses considered in flexible pavement design and analysis include:

- bottom-up fatigue cracking (alligator);
- surface-down fatigue cracking (longitudinal);
- fatigue in chemically stabilized layers (in semi-rigid pavements);
- thermal cracking; and
- permanent deformation (rutting).

Smoothness

All types of structural distresses mentioned above contribute to the loss of pavement smoothness. Users usually rate the road performance by its roughness. The smoothness is defined as the variation of surface elevation that induces vibrations in traversing vehicles. The new guide adopted the international roughness index (IRI) as a measure for smoothness. In addition to the structural distresses, the performance criteria for smoothness is achieved through specifying a terminal IRI at a defined level of design reliability. The smoothness model adds changes to the initial smoothness (IRI) over the design period. These changes are due to the increase in individual distress, site conditions and maintenance activities.

3.3 Reliability

The design of flexible pavements is associated with many factors that introduce a substantial measure of variability. These factors include traffic levels, material properties and construction quality, in addition to model prediction errors and calibration measurement errors. There are two methods of pavement design to cater to these uncertainties: deterministic and probabilistic. In the deterministic method, each design factor has a fixed value based on the factor of safety assigned by the designer. In the probabilistic method, each design factor is assigned a mean and a variance.

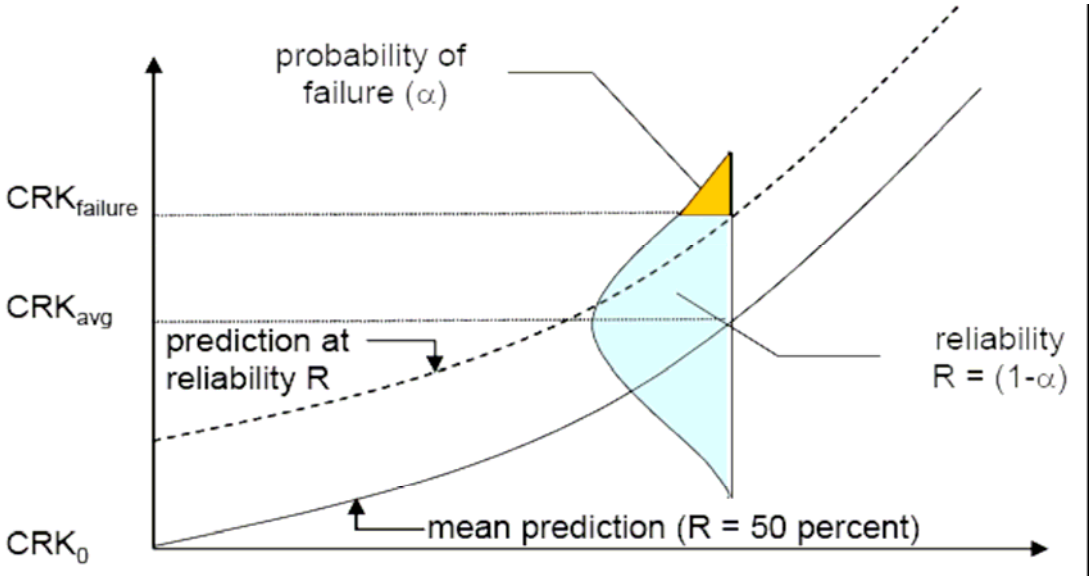

Figure 3.2 Design Reliability Concept for a Given Distress
(Source: Design Guide Documentation- Part1. Introduction)

Reliability is defined as the probability that each of the key distress types and smoothness levels will be less than a selected critical level over the design period. For each trial design, the software provides a prediction based on mean or average values for all inputs that correspond to 50% reliability. The designer usually specifies a higher probability that the design will meet the performance criteria over the design life. The distribution of the error term for a given distress about the mean expected prediction is a function of the many sources of variation and uncertainty mentioned earlier. Distress and IRI are approximately normally distributed. The standard deviation for each distress type was determined from the model prediction error from calibration results. The standard deviation of IRI was determined using a closed form variance model estimation approach while the standard deviation of the distribution of distress was determined as a function of the predicted cracking. The reliability of the design can be calculated using the mean and standard deviation of a normal distribution in two steps

- Predict the cracking level over the design period using mean inputs to the model.
- Estimate cracking at the desired reliability level using the following relationship:

$$Crack\_P = Crack\_mean + STDmeas * Zp \quad (3.1)$$

Where:

Crack_ P = cracking level corresponding to the reliability level p

Crack_ mean = cracking predicted using the deterministic model with mean inputs

STDmeas = standard deviation of cracking corresponding to cracking predicted using the deterministic model with mean inputs

Zp = standard normal deviate corresponding to reliability level p

Recommended levels of reliability for each distress are based on the functional class of the roadway as shown in Table 3.1.

Table 3.1 Illustrative Levels of Reliability for New and Rehabilitation Design

Functional Classification	**Recommended Level of Reliability**	
	Urban	**Rural**
Interstate/Freeway	85 – 97	80 – 95
Principal Arterials	80 – 95	75 – 90
Collectors	75 – 85	70 – 80
Local	50 – 75	50 – 75

Source: Design Guide Documentation- Part1. Introduction.

3.4 Traffic

The traffic characterization method proposed in the new guide is more precise than the conventional ESALs technique adopted in previous guides. The load spectra for single, tandem, tridem and quad axles are introduced. Traffic data, including truck count by class, by direction and lane, are required for traffic characterization. Axle load spectra distributions are developed for each vehicle class from axle weight data. Traffic volumes by vehicle class are forecasted for the design analysis period. The traffic module determines the total number of axle applications for each axle type and load group over the design period. The number of applications for each axle type and load increment is then used in the computation of pavement responses, damage and distress prediction. Additional data related to the axle configuration, such as average axle width, dual tire spacing, tire pressure and axle spacing are used in the pavement response module. Traffic wander influences the number of load applications over a point. This parameter affects prediction of fatigue and permanent deformation. Wander is assumed normally distributed and the standard deviation is used as a measure for it.

An important feature introduced in the guide is the provision for the special axle configuration. This option allows the designer to analyze pavement performance due to special, heavy, non-conventional off-road vehicle systems. Another important input for the flexible pavement design is the vehicle operational speed. It directly influences the stiffness response of the visco-elastic asphalt concrete layers. The magnitude and

duration of stress pulses caused by the moving traffic depend on the vehicle speed, type and geometry of pavement structure, and the location of the element under consideration. The frequencies corresponding to various speeds are used to calculate the dynamic modulus of the asphalt concrete layer. Table 3.2 shows recommendations for selecting vehicle operating speed and the estimated frequency at mid-depth of the asphalt concrete layer.

Table 3.2 Recommendations for Selecting Vehicle-Operating Speed

Type of Road Facility	Operating Speed (mph)	**Estimated Frequency at Layer Mid-Depth (Hz)**		
		Representative HMA layer (4-12 in)	Thin HMA layer wearing surface (1-3in)	Thick HMA layers binder/base (3-12in)
Interstate	60	15-40	45-95	10-25
State primary	45	10-30	35-70	15-20
Urban street	15	5-10	10-25	5-10
Intersection	0.5	0.1-0.5	0.5-1.0	0.1-0.25

3.5 Environmental Effects

Environmental variations can have a significant impact on pavement performance. Moisture and temperature changes can significantly affect the pavement material's properties and, hence, its strength, durability and load carrying capacity. The asphalt bound materials modulus value can rise during the cold winter months by 20 times its value during the hot summer months. Excessive moisture can drastically lead to the stripping of asphalt mixture. Similarly, the resilient modulus of unbound materials at freezing temperatures exhibits high values compared to the thawing months. The moisture content affects the state of stress of unbound materials and it breaks up the cementation between soil particles. Increased moisture contents lower the modulus of unbound materials.

The Design Guide incorporated the Enhanced Integrated Climatic Model (EICM) to simulate changes in the behaviour and characteristics of pavement and subgrade materials that concur with climatic conditions over the design period. The model computes and predicts the modulus adjustment factors, pore water pressure, water content, frost and thaw depths, frost heave and drainage performance. The EICM consists of three components as shown in Figure 3.3. The model role is to record the user-supplied resilient modulus M_R of all unbound layer materials at an initial or reference condition, generally at near optimum moisture content and maximum dry density. The model then

evaluates expected changes in moisture content and the effect on the user-entered resilient modulus.
The model also evaluates the effect of freezing on the layer M_R and the effect of thawing and recovery from the frozen M_R condition. The model provides varying M_R values in the computation of critical pavement response parameters and damage at various points within the pavement system. For the asphalt bound layer, the model evaluates the changes in temperature as a function of time to allow for the calculation of the dynamic modulus and thermal cracking.

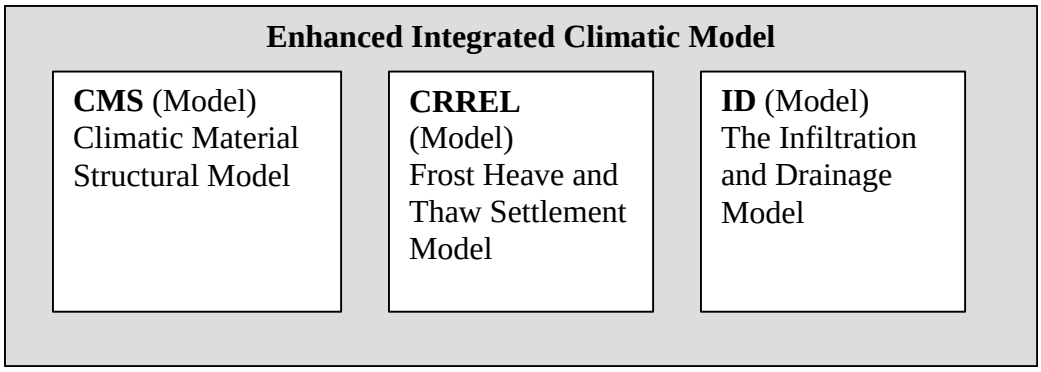

Figure 3.3 Enhanced Integrated Climatic Model Components

The climate module in the Design Guide software requires the user to specify a climate file for the project location stored in the database. The database includes over 800 weather stations around the United States. The user has an opportunity to generate a weather file by interpolating climatic data from selected locations inversely weighted by the distance from the required location.

3.6 Performance Prediction Models

Permanent Deformation

The Design Guide predicts the rutting of each layer in the pavement structure as a function of time and traffic. The Guide models only the initial and secondary permanent deformation stages shown in Figure 3.4. The primary stage is modeled using an extrapolation of the secondary stage trend. The tertiary stage is not considered in the model.

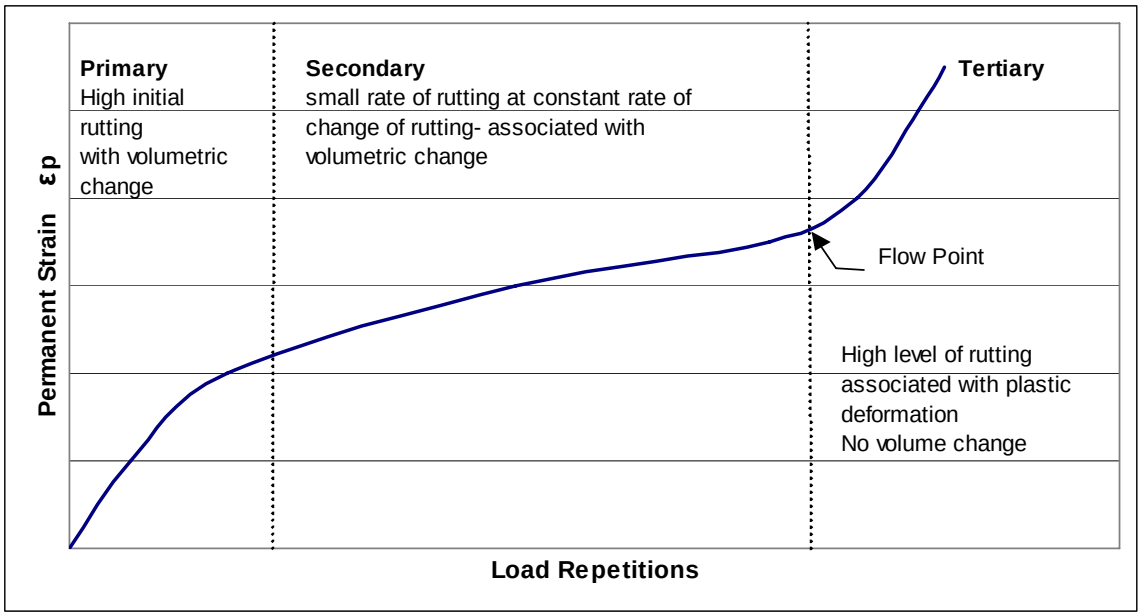

Figure 3.4 Pavement Deformation Behaviour of Pavement Materials

The structural response model calculates the vertical strain in a layered pavement cross-section at any given depth using the elastic properties of the material. Equation 3.2 gives the vertical strain

$$\varepsilon_{rz} = 1/E^* (\sigma_z - \mu\sigma_x - \mu\sigma_y) \quad (3.2)$$

From the knowledge of the resilient strain ε_{rz}, the plastic strain is predicted using an empirical relationship. The selected laboratory model has the following form:

$$\varepsilon_p / \varepsilon_r = a_1 T^{a2} N^{a3} \quad (3.3)$$

Where:

ε_p = accumulated plastic strain at *N* repetitions of load (in/in)

ε_r = resilient strain of the asphalt material as a function of mix properties, temperature and time rate of loading (in/in)

N = number of load repetitions

T = temperature (deg F)

a_i = non-linear regression coefficients

The total permanent deformation needs to be accumulated for different conditions over the design period. To account for the variation in temperature, resilient modulus, and moisture over the incremental periods, the Guide use a special approach called the strain hardening approach to incorporate these variable parameters in a cumulative deformation subsystem. Details of the procedure for calculating the permanent deformation of each layer are given in Part 3-Chapter 3 of the guide documentation.

Fatigue Cracking

Repeated traffic loads cause tensile and shear stresses to develop in the asphalt layer. Fatigue cracking initiates at locations of critical strain and stress. These locations mainly depend on the stiffness of the asphalt layer and the load configuration. Two types of fatigue cracks initiate in the asphalt layer. The first is the commonly known fatigue cracking that initiates due to bending action, which results in flexural stresses at the bottom of the asphalt layer. The second type, which propagates from the surface to the bottom, is believed to be due to critical tensile and or shear stresses developed at the surface due to high contact pressures at the tire edges-pavement interface. Highly aged thin asphalt layers facilitate the initiation of fatigue type two cracks.
Modelling of both types of fatigue cracking is based on one approach. The estimation of the fatigue damage is based on Miner's law [23] given by Equation 3.4.

$$D = \sum_{i=1}^{T} \left(n_i / N_i \right) \qquad (3.4)$$

Where:

D = damage

T = total number of periods

n_i = actual traffic for period *i*

N_i = traffic allowed under conditions prevailing in *i*

The model used for the characterization of the fatigue cracking is as follows:

$$N_f = Ck_1(1/\varepsilon_t)^{k2}(1/E)^{k3} \qquad (3.5)$$

Where:

N_f = number of repetitions to fatigue cracking

ε_t = tensile strain at the critical location

E = stiffness of the material

k_1, k_2, k_3 = laboratory regression coefficients

C = laboratory to field adjustment factor

The transfer function for bottom-up cracking and top-down cracking is calculated from the fatigue damage model and calibrated separately.

Thermal Cracking Model

Thermal fracture analysis in the new Design Guide is based on the visco-elastic properties of the asphalt mixture. The thermal cracking model, TCMODEL, is an improved version of a model developed earlier by (SHRP). The procedure requires the characterization of the HMA mix in an indirect tensile mode to measure the creep compliance at one or three temperatures depending on the level of analysis. The master creep compliance curve is then developed and fit to a power model defined by:

$$D(\xi) = D_0 + D_1\xi^m \quad (3.6)$$

Where

$D(\xi)$ = creep compliance at reduced time ξ

D_0, D_1 = Prony series parameters

m = power slope parameter

The next step is to relate the compliance D(t) to the relaxation modulus E_r of the asphalt mix, using viscoelastic transformation theory. The relaxation modulus is represented by a generalized Maxwell model expressed by a Prony series relationship:

$$E(\xi) = \sum_{i=1}^{N+1} E_i\, e^{-\xi/\lambda i} \quad (3.7)$$

Where:

$E(\xi)$ = relaxation modulus at reduced time ξ

E_i, λi = Prony series parameters for master relaxation modulus curve (spring constants or moduli and relaxation times for the Maxwell elements)

Once the relaxation modulus is known, the thermal stresses in the pavement can be computed using the following constitutive equation:

$$\sigma(\xi) = \int_0^{\xi} E(\xi - \xi') \frac{d\varepsilon}{d\xi'} d\xi' \quad (3.8)$$

Where:

$\sigma(\xi)$ = stress at reduced time ξ.

$E(\xi-\xi')$ = relaxation modulus at reduced time $\xi-\xi'$

ε = strain at reduced time $\xi = (\alpha (T(\xi') - T_0))$

α = linear coefficient of thermal contraction

$T(\xi')$ = pavement temperature at reduced time ξ'

T_0 = pavement temperature when $\sigma = 0$

ξ' = variable of integration

The amount of crack propagation induced by a given thermal cooling cycle is given is predicted using the Paris law of crack propagation

$$\Delta C = A \Delta K^n \quad (3.9)$$

Where:

ΔC = change in the crack depth due to a cooling cycle

ΔK = change in the stress intensity factor due to a cooling cycle

A,n = fracture parameters for the asphalt mixture

The stress intensity K is estimated from the following formula, which was developed based on an analytical finite element method analysis.

$$K = \sigma (0.45 + 1.99 C_o^{0.56}) \quad (3.10)$$

Where:

K = stress intensity factor

σ = far-field stress from pavement response model at depth of crack tip

C_o = current crack length, feet

The value of the parameter (n) in Equation 3.9 is given by Equation 3.11:

$$n = 0.8(1+ 1/m) \quad (3.11)$$

The value of m is obtained from the master creep compliance curve power function (3.6). The fracture parameter (A) is given by Equation 3.12:

$$A = 10^{(\beta^* (4.389-2.52 \log (E\, \sigma m\, n))} \quad (3.12)$$

Where

E = mixture stiffness, psi

σ_m = undamaged mixture tensile strength, psi

β = calibration parameter

Finally, the length of the thermal cracks is predicted from an assumed relationship between the probability distribution of the log of the crack depth to HMA layer thickness ratio and the percent of cracking. The relation between the computed crack depth and the crack frequency is given by the following expression:

$$C_f = \beta * N (\log C/h_{ac}/\sigma) \quad (3.13)$$

Where:

C_f = observed amount of thermal cracking

β_1 = regression coefficient determined through field calibration

N (z) = standard normal distribution evaluated at (z)

σ = standard deviation of the log of the depth of cracks in the pavement

C = crack depth

h_{ac} = thickness of asphalt layer

The thermal cracking model assumes a maximum crack length of 400 ft in every 500ft, which is equivalent to a crack across a lane width of 12 feet spaced at 15 feet along the pavement length. The model can only predict 50% of this maximum amount. The model assumes failure occurs when the average crack depth reaches the thickness of the asphalt layer.

Smoothness Models (IRI)

Distresses predicted by the mechanistic-empirical models, such as fatigue cracking, permanent deformation and thermal cracking are correlated to smoothness. In addition the smoothness model optionally considers other distresses, such as potholes, longitudinal cracking outside the wheel path, and block cracking if there is potential of occurrence. An initial IRI value, typically between 50 to 100 in/mile is required to estimate the terminal distress. There are three models for predicting IRI depending on whether the base type is an unbound aggregate base and subbase, asphalt treated base, or chemically stabilized base.

3.7 Comparison between AASHTO 93 and the Proposed 2002 Guides

Review of the current and proposed AASHTO guides, conducted in this study, revealed significant improvements in the design process achieved in the new Guide.

- The new Guide is capable of addressing a wide range of pavement structures covering new construction and rehabilitation of existing pavements. Analysis of composite structures is now possible, which address the need to overlay AC pavement with PCC or the opposite.

- Significant changes were incorporated in the new guide to improve treatment of traffic related variables. The current guide relies on an equivalent standard axles load (ESAL), which obscures the impact of the various characteristics of vehicles using the roadway network on the type and extent of damage. The new guide expands characterization of road vehicles to account for tire pressure, axle load and distribution.
- The impact of the climate on the material response is adequately captured in the new guide where climate conditions are linked to the material library to facilitate

adjustment of AC dynamic modulus and unbound resilient modulus according to seasonal changes in moisture and temperature condition.

- With the introduction of mechanistic material characterization, the model is now capable of assessing the performance of newly developed materials, such as engineered binders, unconventional gradations and recycled materials. Reliance in the past on field trials proved to be expensive and takes a long time to rate these newly developed materials in comparison with conventional materials.
- Foundation material (native soil) and existing pavement are analyzed adequately in the new guide making it possible for the model to assess a number of design options before implementation.
- The introduction of a performance model (distress prediction) promotes the implementation of performance-based design instead of stress and strain based designs, which proved unreliable in the past. Accumulation of damage with time is an effective tool for designers to plan rehabilitation activities anticipated in the future. Providing designers with the ability to incorporate local preference using acceptance criteria based on a number of distress types and smoothness of the road supports this process.

Capabilities of the proposed guide are expected to encourage users of the current guide to switch to the new application. However, the ability of the new guide to address design requirements should be examined before moving to implementation. Chapter 5 of this study includes the results of a sensitivity analysis performed to test the ability of the new guide in performing a number of design functions. Parameters of the sensitivity analysis and input data used in the model runs are described in Chapter 4.

CHAPTER 4

EVALUATION OF THE PROPOSED AASHTO 2002 GUIDE

4.1 Introduction

The evaluation of an analytical approach to design and analysis usually includes a validation component in the form of field investigations where controlled road sections are built and performance monitored. Comparisons between predicted and actual performance provides a direct indication of the ability of the model to perform the evaluated functions. The Long-Term Pavement Performance (LTPP) program, an element of the Strategic Highway Research Program (SHRP), was one source used to evaluate the AASHTO 2002 Guide. However, since some of the LTPP data has been originally used to generate some of the empirical performance models of the proposed guide, the evaluation process is not adequate for concluding that the model will effectively address combinations of parameters that were not covered in the LTPP experiments such as material characteristics, layer configurations, construction quality and environmental conditions. Accordingly, the AASHTO project committee launched a second series of validation projects (NCHRP 1-30A, NCHRP 1-40A) to further test the model. These new tests will take two to three years and will still fall short of validating the model since they will not address long-term performance.
This study focuses on sensitivity analysis to examine the ability of the model to account for the impact of variables with a known influence on performance, especially material characteristics. This chapter discusses input parameters used in the sensitivity analysis; the results are discussed in Chapter 5.

4.2 Asphalt Concrete Characteristics

Following on the recommendations of the Design Guide, a laboratory investigation was performed at the National Research Council Canada (NRCC) to produce necessary AC input data. Standards of the AASHTO and ASTM were used to perform physical testing on the HMA fractions and to design the different mixes used in the sensitivity analysis. A complete list of the AC and binder tests required by the software for all input levels is shown in Appendix A. For this study the Marshal approach was followed in designing the AC mixes shown in Table 4.1. The two mixes were selected to represent commonly used asphalt mixes in Ontario Canada. The Marshal mixes were designed according to AASHTO standard designated T 245 [24] with different binder types leading to slightly different binder contents.

Aggregate Proportioning

Sieve analysis was performed according to Ontario Ministry of Transportation (MTO) specifications [25]. The MTO specifications were followed to determine the combinations of aggregate fractions that achieve the job mix formulas. The gradation curves for the two mixes are shown in Figures 4.1a and 4.1b. The designed aggregate gradation is shown in Table 4.2.

Table 4.1 Designation of Mixes Used in the Study.

MTO Mix Designation	Function in Road Structure	Nominal Maximum Aggregate Size (mm)
HL3	Surface layer	13.2
HL8	Stabilized base course	19

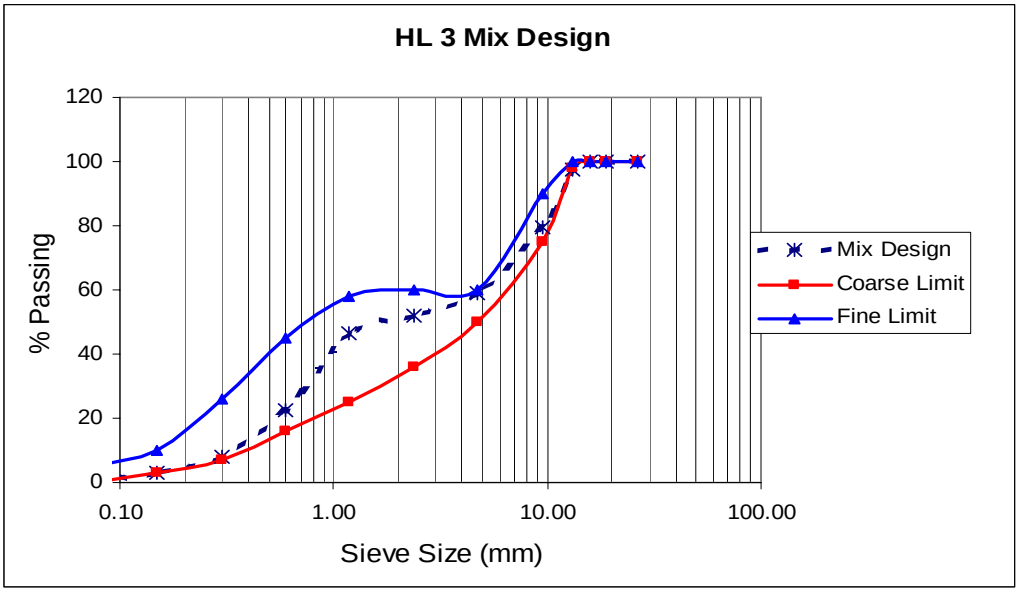

Figure 4.1a Gradation Curve of Mix HL3

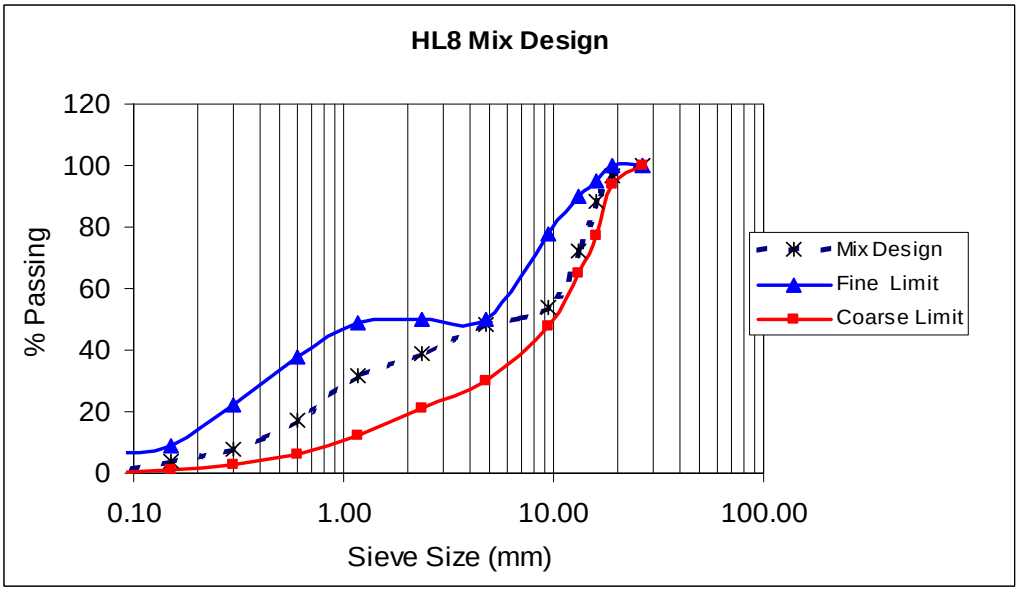

Figure 4.1b Gradation Curve for Mix HL8

Table 4.2 Aggregate Gradations

MTO Sieve Designation (mm)	HL3 Mix Design	HL8 Mix Design
	% Passing	% Passing
26.5	100.0	100.0
19	100.0	96.5
16	100.0	88.5
13.2	97.5	72.2
9.5	79.3	53.8
4.8	59.0	48.6
2.4	52.1	39.1
1.2	46.3	31.9
0.600	22.5	17.3
0.300	7.9	7.8
0.150	3.0	3.6
0.075	0.5	0.5

Binder Characteristics

Asphalt cements were classified according to SuperPave performance grades (PG) specifications. Three binder types were used to prepare the AC specimens. Two binders, PG 58-22 and PG 52-34, were described as neat binders. The third binder (PG 64-34) is an engineered binder and was used in the HL3 mix only, because it is relatively expensive to use in stabilized base courses. Engineered binders are generally used to improve the performance of AC by reducing the potential for rutting or cracking under severe traffic and temperature conditions.

Mix Design Procedure

The Marshal Hammer was used to compact specimens prepared using the Marshal mix design procedure. The optimum binder content was selected following local specifications based originally on the Marshal design approach. The selected binder contents were then used to prepare the specimens for the complex modulus test.
A mechanical mixer was used to prepare the aggregate–binder mixture. It was aged in an oven for two hours at the compaction temperature of the binders in accordance with the short-term aging procedure specified by AASHTO Designation PP2 [26]. The binder manufacturer specifies compaction temperatures. Samples were then compacted using the gyratory compactor. The gyratory compactor was used to produce samples at a specified height and air voids content. The number of gyrations was selected to produce samples with the desired size at the specified air voids percentage. The size of the samples

prepared for the complex modulus tests was determined according to ASTM specification D3497 [27], which is 100 mm for height and diameter.

Standard Physical Tests

Physical properties of the compacted mix specimens were determined to ensure the mix compliance with local criteria. Two different measures of densities were typically taken according to AASHTO specifications T166 [28] and 269-97 [29]: bulk specific gravity (G_{mb}) and theoretical maximum specific gravity (G_{mm}).

These densities were then used to calculate the volumetric parameters of the HMA: air voids (V_a), voids in the mineral aggregate (VMA) and voids filled with asphalt (VFA)

The Marshall stability and flow test was conducted according to AASHTO standard designated T 245 [24]. Physical properties of the selected mix designs that satisfied the mix design criteria are summarized in Tables 4.3 and Table 4.4.

Table 4.3 Physical Properties of Mix HL3

Physical Property	Mix Type		
	HL3- PG 58-22	HL3- PG 64-34	HL3 – PG 52-34
P_b (%)	5	5	4.9
G_{mm}	2.53	2.477	2.50
G_{mb}	2.396	2.337	2.375
G_{sb}	2.72	2.72	2.72
VMA	16.3	18.4	17.0
V_a	5.3	5.7	5.1
V_{beff}	11.0	12.7	11.9

Table 4.4 Physical Properties of Mix HL8

Physical Property	Mix Type	
	HL3- PG 58-22	HL3 – PG 52-34
P_b (%)	4.5	4.5
G_{mm}	2.54	2.56
G_{mb}	2.412	2.429
G_{sb}	2.74	2.74
VMA	15.9	15.3
V_a	5.0	5.3
V_{beff}	10.9	10.0

Mechanical Testing

The primary stiffness property required for the AC analysis is the dynamic modulus (E*). Mechanical testing was performed on HMA samples prepared for the selected mixes and compacted using a gyratory compacter. The NRC test protocol was followed in conducting the complex modulus test. Tests were performed to cover a wide range of pavement temperatures (40^0C to -10^0C) and a frequency sweep from 0.1 Hz to 20 Hz. Typical test output produced from the stress and strain signals generated under a specific temperature and loading frequency is shown in Figure 4.2. Test results for the HL3 mixes made with the three binders for this study are listed in Tables 4.5a, 4.5b and 4.5c in the format required for running the AASHTO 2002 model.

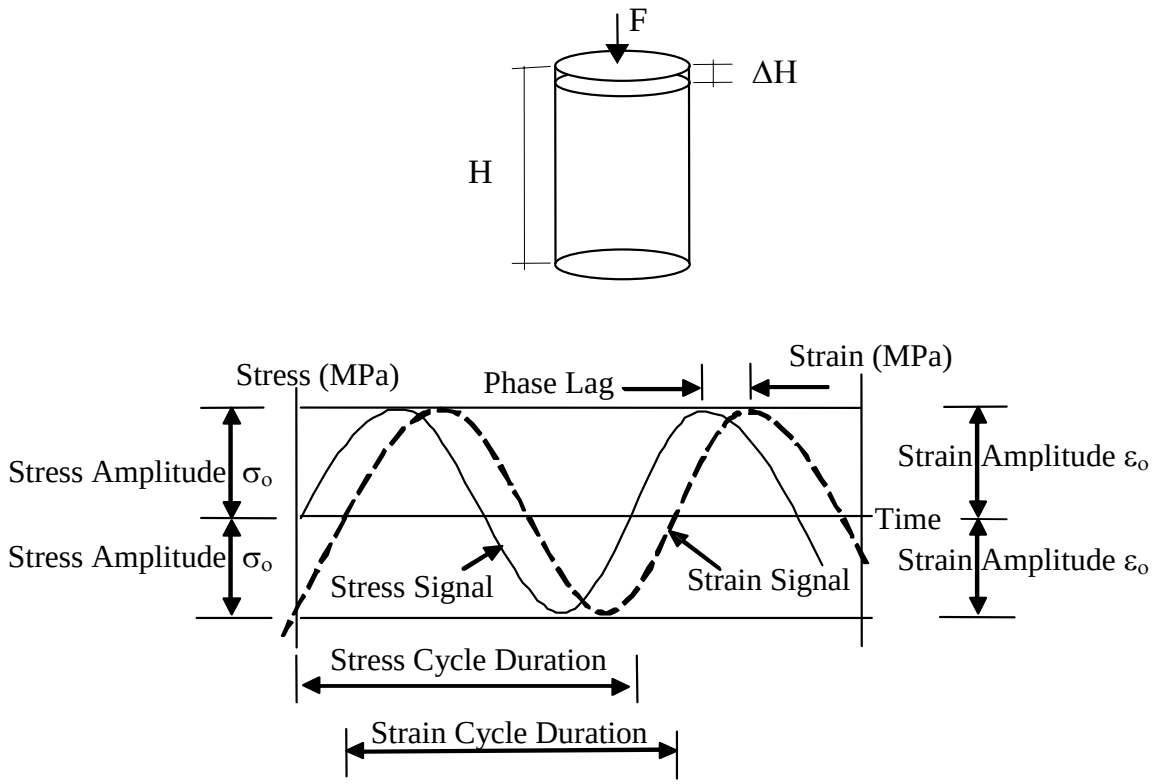

Figure 4.2 Viscous Response of Asphalt Concrete

Tables 4.5 Dynamic Modulus Data Prepared in the Format Required for Running AASHTO 2002 Model

Table 4.5a Dynamic Modulus for Mix HL3- 58-22
Number of temperatures: 5
Number of frequencies: 6

Temperature	Mixture E* (psi)					
^{o}F	0.1	0.3	1	5	10	20
14	2612482	2859216	3120464	3367199	3381713	3497823
32	1582002	1886792	2206096	2656023	2830189	3062409
68	671988	985486	1310595	1785196	1959361	2104499
86	49637	76197	126851	249637	339623	461538
104	20882	26560	42671	87083	119739	172714

Table 4.5b Dynamic Modulus for Mix HL3- 52-34
Number of temperatures: 5
Number of frequencies: 6

Temperature	Mixture E* (psi)					
^{o}F	0.1	0.3	1	5	10	20
14	785195	955007	1169811	1494920	1683599	1901306
32	381712	519593	693759	978229	1120464	1342525
50	99129	142670	211901	349782	431059	551523
86	10885	16981	27866	56313	77503	111901
104	3628	8461	8461	17851	25253	39477

Table 4.5c Dynamic Modulus for Mix HL3- 64-34
Number of temperatures: 5
Number of frequencies: 6

Temperature	Mixture E* (psi)					
^{o}F	0.1	0.3	1	5	10	20
14	917271	1174165	1509433	1770682	1857764	2089985
32	349782	468795	622641	880986	1010159	1178519
68	41074	58055	89550	159651	201741	1178519
86	15674	21770	32801	61683	79390	106966
104	8461	10885	15820	29027	37155	50798

Mix Gradation Used in Predicting the Dynamic Modulus in Level 3

For Levels 2 and 3 analyses, the proposed guide employs a master curve that is developed directly from dynamic modulus values estimated using the predictive equation shown below (Equation 4.1). It predicts the dynamic modulus of asphalt mixtures over a range of temperatures, rates of loading, and aging conditions using data from the volumetric design of the mixture and binder properties. The required mix gradation information for Levels 2 and 3 are shown in Table 4.6.

$$\log\left|E^*\right| = -1.249937 + 0.029232P_{200} - 0.001767(P_{200})^2 + 0.002841P_4 - 0.058097V_a$$
$$-0.802208\frac{V_{beff}}{(V_{beff}+V_a)} + \frac{[3.871977 - 0.0021P_4 + 0.00395P_{38} - 0.000017(P_{38})^2 + 0.00547P_{34}]}{1+e^{(-0.603313-0.313351\log f - 0.393532\log\eta)}} \quad (4.1)$$

Where:

$\left|E^*\right|$ = asphalt mix complex modulus, in 10^5 psi

η = bitumen viscosity, in 10^6 poise

f = loading frequency, in Hz

V_a= percent air voids in the mix, by volume

V_{beff} = percent effective bitumen content, by volume

P_{34} = percent retained on ¾-inch sieve, by total aggregate weight (cumulative)

P_{38} = percent retained on 3/8-inch sieve, by total aggregate weight (cumulative)

P_4 = percent retained on No. 4 sieve, by total aggregate weight (cumulative)

P_{200} = percent passing No. 200 sieve, by total aggregate weight.

Witczack's model (Equation 4.1) is one of numerous methods used for predicting the modulus of AC mixtures. However, the equation needs the binder viscosity as an input. The model uses default viscosity data and empirical approximations to obtain viscosity values at intermediate and lower temperatures. The actual binder characteristics in all cases would not match the empirically approximated values. In Chapter 5, the difference in performance predictions between Levels 1 and 3 is discussed while looking into the difference between the dynamic modulus measured in the laboratory and that estimated by the prediction equation used in Level 3.

Table 4.6 Aggregate Gradation Data Required For Level 2 and 3 Input:

	Mix Type	
	HL3	HL8
Cumulative % Retained on 3/4 in. sieve:	0.0	3.5
Cumulative % Retained on 3/8 in. sieve:	20.7	46.2
Cumulative % Retained on #4 sieve	41.0	59.0
% Passing #200 sieve:	0.5	0.5

Binder Characterization

The binder complex modulus and phase angle data are needed over a range of temperatures for a loading rate of 1.59 Hz (10 rad/sec) as input for Level 1 design. Typical values of dynamic shear rheometer measurements for PG 58-22 are shown in Table 4.7.

Table 4.7 SuperPave Binder Test Data

Temperature (^{o}F)	Angular Frequencies = 10 rad/sec	
	G* (psi)	Delta (^{o})
59	2605000	50
77	572800	56
95	120800	63
113	23440	69
140	3267	78

The design guide software converts the binder stiffness data at each temperature to viscosity using Equation 4.2.

$$\eta = \frac{G^*}{10}[1/\sin\delta]^{4.8628} \qquad (4.2)$$

Where:

G* = binder complex shear modulus, Pa
δ = binder phase angle.

The parameters of the A and VTS of the ASTM Equation below [30] are then found by the linear regression of Equation 4.3.

$$\text{Log log } \eta = A + VTS \text{ Log } T_R. \quad (4.3)$$

Where:

η = viscosity, cP

T_R = temperature, Rankine

A = regression intercept

VTS = regression slope of viscosity temperature susceptibility.

Master Curve for Level 1

After establishing the viscosity–temperature relationship, the laboratory dynamic modulus test data are shifted to construct the master curve represented by Equation 4.4.

$$\log(E^*) = \delta + \frac{\alpha}{1 + e^{\beta + \gamma [\log(t) - c(\log(\eta) - \log(\eta Tr))]}} \quad (4.4)$$

Where:

E* = dynamic modulus, psi

t = time of loading, sec

η = viscosity at temperature of interest, CPoise

η_{Tr} = viscosity at reference temperature, CPoise

$\alpha,\beta,\delta,\gamma,c$ = mixture specific fitting parameters.

The shift factors are calculated using Equation 4.5. The viscosity at the age and temperature of interest are obtained from the global aging model incorporated in the software. The Global Aging System comprises a number of models for adjusting the viscosity of the original binder for short-term aging that occurs during mixing and lay-down operations and for in-service long-term aging.

$$\log(t_r) = \log(t) - c(\log(\eta) - \log(\eta_{Tr})) \quad (4.5)$$

Where:

t_r = reduced time, sec

t = loading time, sec

η = viscosity at the age and temperature of interest, CPoise

η_{Tr} = viscosity at reference temperature and RTFO aging, CPoise

Master Curve for Level 3

The input at Level 3 includes the mix data, as mentioned before, in addition to the performance grade of the asphalt binder. As no testing is required for the binder, the viscosity is estimated from default temperature-viscosity A and VTS values. Typical values built in the software are shown in Table 4.8.

Table 4.8 Recommended RTFO A and VTS Parameters Based on Asphalt PG Grade

Binder Grade	A	VTS
PG 58-22	11.787	-3.981
PG 52-34	10.707	-3.602
PG 64-34	9.461	-3.134

Poisson's Ratio for Bituminous Materials

Poisson's ratio for asphalt concrete usually ranges between 0.15 and 0.5 and is a function of the asphalt mix and temperature. This study used a typical value of 0.35.

Other HMA Material Properties

Tensile Strength

Tensile strength values required as input for Level 3, calculated internally by the software, were used in this study. These values were based on a regression equation developed under NCHRP 1-37A. The indirect tensile strength at 14 ºF is calculated as a function of as-constructed air voids, as constructed voids filled with asphalt, the binder penetration at 77 ºF and the viscosity-temperature susceptibility intercept A.

Creep Compliance

Values for creep compliance used in this study as input for Level 3 design were estimated using a regression equation developed under NCHRP 1-37A, and were calculated by the software using the as built air voids (V_a), as built voids filled with asphalt (VFA) in addition to the binder penetration at 77 ºF.

Table 4.9 Thermal Properties of Asphalt Concrete

Thermal conductivity BTU/hr-ft-^{o}F	0.67
Specific heat (BTU/lb-^{o}F)	0.23
Reference temperature	70 ^{o}F

4.3 Unbound Materials

Attempts were made to adopt non-linear resilient modulus models in the design and analysis of unbound pavement layers including the granular base course and subgrade, which is usually a native soil consisting of a cohesive material. However, the finite element model incorporated in the AASHTO model for non-linear analysis is not calibrated and is being reviewed. Instead, linear elastic analysis is available which is performed with Level 3 input data covering a number of parameters that include the AASHTO soil classification designated M 145[31] and other physical properties. The data for two soils used in this study were produced in NRC laboratories based on testing of different soil categories as shown in Table 4.8. Both Granular materials A and B were classified as A-1-a according to AASHTO specifications. The properties of these granular materials are used in Chapter 5 of this study to assess the implications of using Level 3 in estimating the resilient modulus based on AASHTO classifications.

The sensitivity analysis conducted in this study covered other parameters that directly or indirectly influence the material response. These parameters included traffic and seasonal changes in moisture and temperature conditions as discussed below.

Table 4.10 Properties of Different Granular Materials (A-1-a)

Property	**Measured Property**		**Guide Proposal**	
	Granular A	**Granular B**	**Lower Limit**	**Upper Limit**
Plasticity index	0	0	0	6
Passing #200 (%)	6	7	0	15
Passing #4 (%)	19	21	15	30
D60 (mm)	11	7	2	25
MDD (pcf)	147.7	150	120	150
Specific gravity	2.72	2.73	2	4
OMC (%)	5.0	5.4	2	40
Resilient modulus (psi)	26124	51700	38500	42000

4.4 Traffic Data

Data input for the sensitivity analysis were formulated to account for the wide range of traffic variables and requirements of the different levels of design included in the proposed AASHTO Design Guide. The variables cover the wide axle load spectra, speed, gear/axle configuration/tire spacing, tire pressure, traffic wander and the factors that capture monthly and daily traffic distribution. Traffic data for the sensitivity analysis were selected to establish categories that represent low, medium, medium to heavy and heavy volumes as shown in Table 4.11. The model uses these data to calculate pavement responses and the number of axle load applications over a point for predicting distress and performance. (See the results in Chapter 5) The AADTT in Table 4.11 is the average daily number of trucks traffic (FHWA vehicle classes 4-13) expected over the base year. The traffic growth factor was considered as 3% compound growth. The default traffic volume adjustment factors were selected since there were no WIM station data and were found reasonable; for example the monthly adjustment factor was set to one to indicate

that the volume of trucks is evenly distributed over the months of the year. The default truck traffic classification is shown in table 4.12. The truck traffic classification represents the percentage of each type of vehicles in the traffic stream. The axle load distribution was taken as the default. General traffic input values are shown in Tables 4.13 to 4.15.

Table 4.11 Traffic Data

Initial Two-Way AADTT	200 1000 2000 4000	Low, Medium, Medium to High High
Number of lanes in design direction	2	
Percent of trucks in design direction	50	
Percent of trucks in design lane	95	
Operational speed (mph)	5 25 45 60	Low, Medium, Medium to High High

Table 4.12 Truck Traffic Classification (Default)

Truck Traffic Classification	%
Class 4	1.3
Class 5	8.5
Class 6	2.8
Class 7	0.3
Class 8	7.6
Class 9	74.0
Class 10	1.2
Class 11	3.4
Class 12	0.6
Class 13	0.3
Total percentage	100

Table 4.13 Traffic General Input

Mean wheel location (inch from the lane marking)	18
Traffic wander standard deviation (in.)	10
Design lane width (ft.)	12

The average number of axles for each truck class (classes 4-13) for each axle type (single, tandem, tridem and quad) is calculated from WIM data measured over time by dividing the total number of a specific axle type measured for a truck class by the total number of trucks in that class. The traffic module assumes that the number of axles for each axle type is constant with time. The proposed Design Guide software contains a default set of values estimated using LTPP data.

Table 4.14 Number of Axle/Truck

Vehicle Class	Single Axle	Tandem Axle	Tridem Axle	Quad Axle
4	1.62	0.39	0.00	0.00
5	2.00	0.00	0.00	0.00
6	1.02	0.99	0.00	0.00
7	1.00	0.26	0.83	0.00
8	2.38	0.67	0.00	0.00
9	1.13	1.93	0.00	0.00
10	1.19	1.09	0.89	0.00
11	4.29	0.26	0.06	0.00
12	3.52	1.14	0.06	0.00
13	2.15	2.13	0.35	0.00

Table 4.15 Axle Configuration

Average axle width edge to edge outside dim. (ft.)	8.5
Dual tire spacing (in.)	12
Tire pressure – Single tire (psi)	120
Tire pressure – Dual tire (psi)	120
Average axle spacing – Tandem axle (in.)	51.6
Average axle spacing – Tridem axle (in.)	49.2
Average axle spacing – Quad axle (in.)	49.2

4.5 Climatic Data

The database incorporated in the current version of the proposed guide does not include climatic information for Canadian regions. However, the Transportation Association of Canada (TAC) is considering such a project to compile a climatic database using Environment Canada data. The input parameters include air temperature, precipitation, water table depth, wind speed and sun radiation. The model uses EICM input to adjust unbound material properties, mainly the resilient modulus. An hourly temperature profile was also used to adjust the dynamic modulus and all other parameters built in the distress module to estimate accurately the potential for rutting. In this study, USA geographical sites with climatic conditions available in the database were selected to represent warm and cold regions to test the model's ability in accounting for the impact of seasonal variation in moisture and temperature conditions on predicted performance.

Table 4.16 Climatic Input

Weather Station	Description	Mean Annual Air Temperature
Minnesota	Relatively cold region	461°F
Chicago	Intermediate	52 °F
Dallas	Relatively warm region	67 °F

Table 4.17 Drainage Input

Drainage and surface properties	Cross slope	2%
	Drainage path from the center line to the edge drain adjacent to the lane shoulder (ft.)	12
	Surface shortwave absorptivity	0.85

4.6 Sensitivity Analysis

The collected input data discussed above was designed to serve the sensitivity analysis performed in this study covering four major items while focusing on material characteristics to evaluate the impact on performance associated with the type of pavement structure, seasonal variations in climatic conditions and traffic volumes. Results produced by running the proposed AASHTO design software associated with variations in those design parameters are discussed in Chapter 5.

Structural considerations

The performance of roads constructed over subgrades with different levels of support was examined. Native soils with a different resilient behaviour were used to perform the analytical runs. The predicted performance was used to evaluate the adequacy of the structure based on comparisons with a preset tolerance level for specific performance criteria (rutting, fatigue cracking). Additional runs were then performed after introducing of some design solutions, such as increasing the thickness of the AC layer or the granular base.

Material Considerations

The model application covered a number of material variables to examine the sensitivity of the design guide to material characteristics. Mix designs involving different aggregate gradations and binder types were used in the analysis**.** The AC layers involving mixes that include binders with different performance grades (based on SHRP specification) were simulated to determine the effectiveness of typical design solutions based on manipulation of binder characteristics (engineered binders).

Design Levels

The above model applications were performed using Level 1 AC input and Level 3 for unbound materials. However, separate runs were performed to assess performance predictions based on applications of Level 3 and the output was compared with that produced earlier using Level 1 AC input.

4.7 Model Limitations in Predicting Fatigue Cracking

Sensitivity analysis outlined in Section 4.6 produced results that facilitated assessment of the model ability to evaluate the resistance of AC mixes to permanent deformation and fatigue cracking. Fatigue-related damage is well defined in the literature, and most models use an approach similar to that adopted in the proposed Design Guide. Most of the adopted transfer functions relate the AC tensile strains to the allowable number of load repetitions. The asphalt institute and shell models relate the allowable number of load repetitions that cause fatigue cracking to the tensile strain at the bottom of the AC layer and the AC modulus (E). However, it is essential to carefully calibrate the transfer function by applying appropriate calibration parameters so that the predicted distress can match field observations. Such a process will be needed in the calibration of the proposed guide before it can be used with confidence.

Longitudinal Fatigue Cracking (Surface/Down) Model

The longitudinal fatigue cracking model in the 2002 Design Guide was based on the same concept on which the conventional fatigue model was constructed [32]. This type of fatigue is not as well defined in the proposed Design Guide from a mechanistic viewpoint as the more classical bottom/up fatigue. The Design Guide suggested that the cause of

this type of fatigue is due to critical tensile and/or shear stresses developed at the surface and caused by extremely large contact pressures at the tire edges pavement interface, coupled with a highly aged stiff thin surface layer that has become oxidized.
The results of model runs conducted in this study produced fluctuating and unstable trends when Level 1 AC input was used. On the other hand, input Level 3 functioned better producing stable results that were similar to the conventional fatigue model. However, it is not yet shown which of the two approaches quantifies better the damage associated with fatigue.
Currently NCHRP Project 1-42 is investigating the top-down fatigue cracking of hot asphalt layers. The conducted literature search suggests that top-down cracking in flexible pavements is primarily caused by traffic-associated fatigue and/or thermal stresses. Top-down cracking is significantly affected by the interaction between many factors, including poor compaction and segregation during construction, pavement structure, modulus gradients within the pavement, age hardening of the pavement surface, moisture damage and mixture fracture toughness [33].

Thermal Cracking Model

Thermal stresses are predicted by the TCMODEL based on viscoelastic characteristics of the AC mix at low temperatures. The model was last calibrated in 2003 to be consistent with current SuperPave IDT protocols. The original 1000-second creep data files were changed to 100-second creep data. The calibration report [34] included in the design documentation has highlighted future research areas to improve the model prediction capabilities. After the study, the effect of mix aging in the field on thermal cracking development will be incorporated in the model. Another topic relates to fracture and the utilization of tensile strength data. The current model uses mixture tensile strength at a single test temperature of -10 ºC, and then develops fracture parameters by taking this value as an estimate of the undamaged tensile strength of the mixture. In the future, the model can be improved once a better understanding of mixture fracture behaviour is obtained. A third study area relates to the recent finding that traffic loads applied during critical cooling events can increase tensile stresses by more than 50% [35].
The most recent calibration process is considered insufficient, because of the shortage of field data and site-specific information. The 14 CSHRP sites could not be used, because the Design Guide does not include climatic data for Canadian weather stations. Additionally, not all GPS (SHRP general pavement sections) sites could be interpolated from suitable weather stations at currently available sites.
Two main points affect the accuracy of the thermal cracking prediction process: the reliability of the climatic model that will be used to determine the pavement temperature and eventually the stresses as discussed in the following subsection and the definition and identification of the thermal cracking patterns in the field. There is a misconception that all transverse cracks are due to thermal cracking. Poor compaction methods using conventional rollers would result in hairline cracks [36, 37, 38, 39, 40], which widen and propagate with time in the presence of specific environmental factors. These cracks, left behind by conventional compactors on a freshly compacted asphalt layer, are oriented in a transverse direction. Another point is associated with the fact that temperature is not unidirectional. The thermal crack may follow any direction similar to the thermal cracks that occur on plain concrete ground slabs, a pattern similar to block cracking.

The Climatic Model

The climatic model has an essential and direct influence on the pavement performance prediction process. It is essential to develop unique environmental regions and construct the climatic database files. The validation of the EICM using regional data is important. A recent study [41] to validate the Model, pointed out that the variation in climatic patterns from region to region coupled with the variation in site-specific conditions across North America make it difficult to develop standard models to account for seasonal variation in material properties for all regions. The results of the validation study did not indicate a high correlation between EICM-predicted temperature and moisture profiles for the various pavement layers as compared to measured values. The findings of this study should receive high consideration, because of the direct impact of the climatic model on the whole analysis process

CHAPTER 5

RESULTS AND ANALYSIS

5.1 Introduction:

Results of the sensitivity analysis exercises discussed in Chapter 4, designed to evaluate capabilities of the Design Guide are discussed in this chapter. Analysis addresses the impact of changes in each individual design feature on performance as reflected on the extent of damage accumulating under the action of traffic loading. It should be noted that the stress/strain profiles are not presented as an output of the model application (see typical software run in Appendix B). Accordingly, it is not possible to evaluate stresses and strains predicted by the proposed AASHTO model using another analytical model or field data. Instead, this study reviews model output to examine its conformance with basic mechanics rules and make sure performance predictions agree with trends known for the investigated materials. Analysis also covers the performance of the modules incorporated in the guide to identify areas of future research that may be pursued and the outcome used to improve the accuracy of the Design Guide.
This study covers the primary distress types: permanent deformation and fatigue cracking. It also discusses fatigue longitudinal cracking and thermal cracking models, and evaluated the impact of using hierarchical input levels on the performance prediction process.

5.2 Performance Based Design and Analysis

The guide predicts permanent deformation in each individual layer and finally sums up these values to arrive at the total permanent deformation in the entire pavement structure. The plastic strain is estimated empirically under specific pavement conditions for a total number of traffic repetitions, and the strain hardening approach is then used to accumulate the deformations from sub-seasons to obtain the total plastic deformation. The output of several runs conducted to investigate the impact of changes in the magnitude of various input variables on the predicted permanent deformation is discussed in the following section. The runs were conducted for a design life of 20 years and a reliability level of 90%.

Road Built over a Weak Subgrade

A number of runs were performed to examine the ability of the Design Guide in evaluating the impact of a problem, such as a weak subgrade, and the information it provides to assist the designer in arriving at a sound design alternative. A trial design was modified several times to improve the performance of the road structure. The trial design assumed an urban road with medium traffic (AADTT = 1000) with an operating speed of 25 mph, located in a relatively warm region and having a mean annual air temperature of 67° F. The adopted road structure is shown in Figure 5.1

AC: 4 in. HL3 – PG 58-22

Base: 10 in. GB type A-3 (M_R = 24000 psi)

Subgrade: A-7-6 (M_R = 5000 psi)

Figure 5.1 Reference Pavement Structure

A one-inch tolerance level (design limit) for total rutting and 0.33 in. for AC rutting were selected based on 90% reliability. Analysis performed on the output of the initial design trial revealed there would be excessive rutting in the road exceeding the one-inch design limit as shown in Figure 5.2. The AC layer and subgrade showed the greatest permanent deformation levels. Rutting in the AC layer exceeded the design limit of 0.33 in. Although exposed to low stresses, rutting in the subgrade exceeded that predicted in the granular base. Accordingly, the initial design should be adjusted to improve the road performance as discussed in the following subsection.

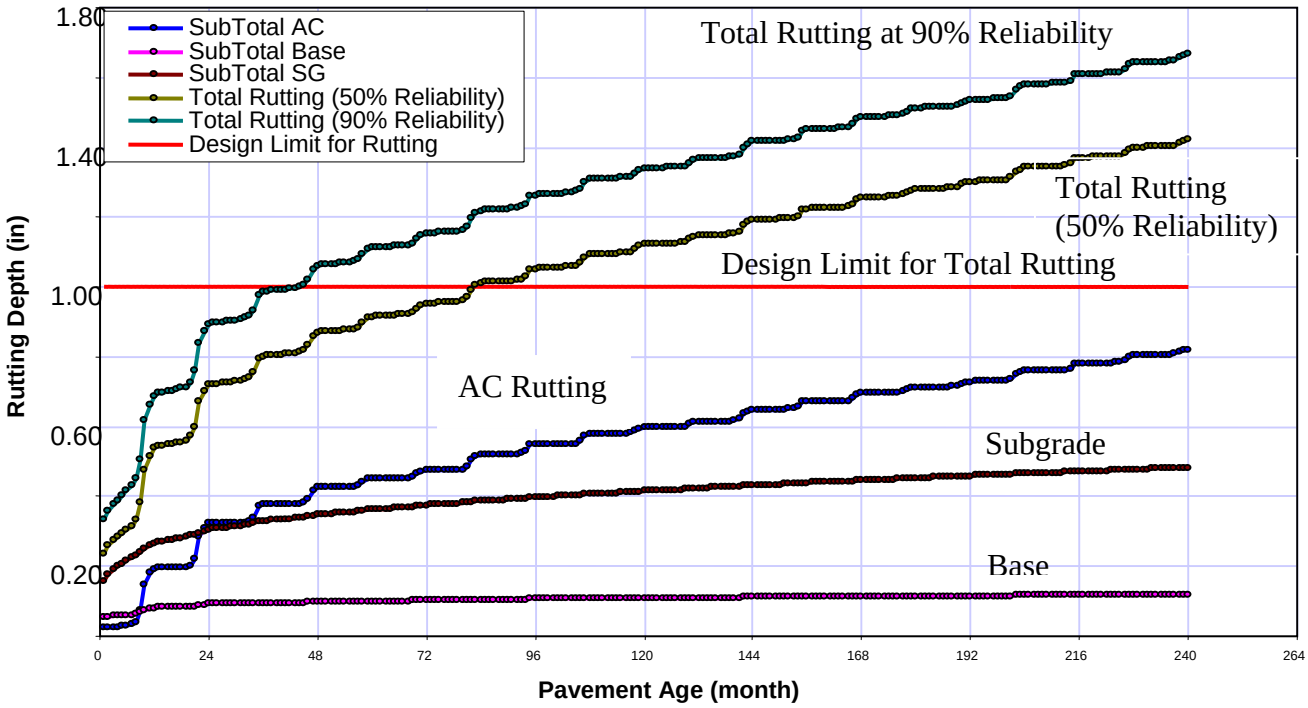

Figure 5.2 Permanent Deformation Predictions

Effect of HMA Thickness on Permanent Deformation

The solution to the weak subgrade problem lies in stiffening the pavement layers above the subgrade. Because of the absence of good quality base course material (a scenario selected here because of the lack of the current model sensitivity to variation in unbound material parameters), adjustment of the AC layer thickness was investigated. Five AC layer thicknesses were used as input to investigate the model's ability to capture the reduction in traffic-induced stresses and strains transmitted to the weak subgrade and as a consequence, limiting build up of rutting in the pavement.

The AC thickness was increased from 4 to 6, 8 and 10 inches, while keeping the base course thickness constant at 10 inches. The effects of AC thickness increase on the total rutting as well as the contribution of individual pavement layers were examined. The results are shown in Table 5.1 and plotted in Figure 5.3.

Increasing the AC layer thickness reduces the total permanent deformation in the pavement structure as shown in Figure 5.3. The result agrees well with what have been established theoretically and in field performance records, where increasing the HMA layer thickness increases the stiffness of the asphalt layer and the overall structure and hence decreases stresses and strains in layers below. Rutting, in the subgrade, diminished by 34% when the AC thickness was increased from 4 to 10 inches. Similarly, AC rutting dropped by 26% resulting in an overall drop in rutting of 43%. No visible change was observed in base course rutting as a result of AC thickness changes. None of the evaluated design options, based on changing the AC layer thickness, satisfied the design limit involving a maximum tolerance of 1.0 in rutting.

Table 5.1 Predicted Permanent Deformation for Different AC Layer Thicknesses

(Base course thickness 10 in., M_R = 24000 psi - weak subgrade, M_R = 5000 psi)

AC Thickness (in)	Total Rutting (in.)	AC Rutting (in.)	Base Rutting (in.)	SG Rutting (in.)	Decrease in Total Rutting %
4	1.4	0.83	0.13	0.44	Reference
6	1.27	0.79	0.1	0.38	9
8	1.12	0.71	0.08	0.32	20
10	0.97	0.61	0.067	0.29	43

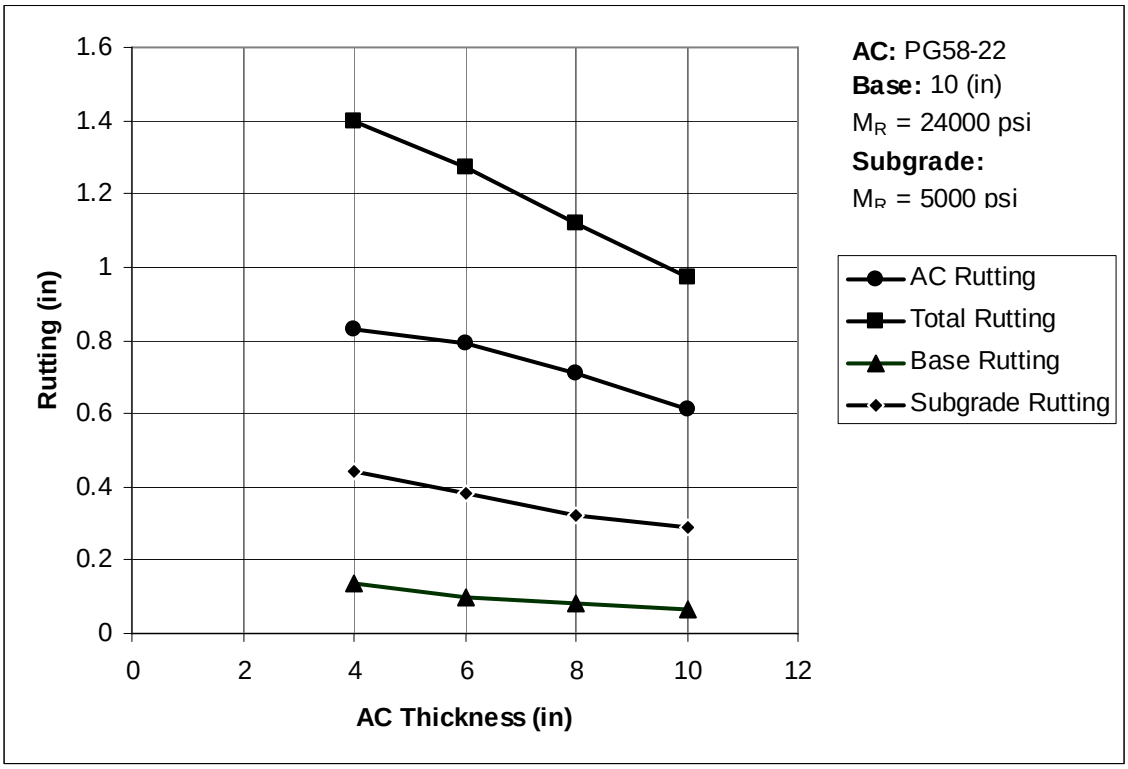

Figure 5.3 Effect of HMA Layer Thickness Changes on Predicted Rutting.

Effect of Base Thickness on Permanent Deformation

The effect of increasing the base course thickness on predicted total permanent deformation of the pavement structure as well as on individual layers of the pavement was also investigated. The base course thickness was increased from 10 to 12, 14,16, and 18 inches while keeping the AC layer thickness constant at 6 inches. Results are shown in Table 5.2 and were plotted in Figure 5.4. Increasing the base thickness has no effect on the rutting of the AC layer. However, the increase in the base resulted in a slight decrease in permanent deformation in the subgrade, probably as a result of a drop in the vertical compressive strain. None of the evaluated design options, based on changing the granular base layer thickness, satisfied the design limit involving a maximum tolerance of 1.0 in. rutting.

Table 5.2 Predicted Permanent Deformations for Different Base Layer Thicknesses (AC thickness 6 in., binder PG 58-22 , weak Subgrade M_R =5000 psi)

Base Thickness (in.)	Total Rutting (in.)	AC Rutting (in.)	Base Rutting (in.)	Subgrade Rutting (in.)	Change in Total Rutting %
8	1.28	0.78	0.0887	0.4115	+ 0.3
10	1.275	0.79	0.101	0.3802	Reference
12	1.294	0.805	0.1228	0.3656	-1.5
14	1.286	0.814	0.1311	0.3412	-0.86
16	1.295	0.818	0.1474	0.3296	-1.56
18	1.28	0.83	0.147	0.303	-0.4

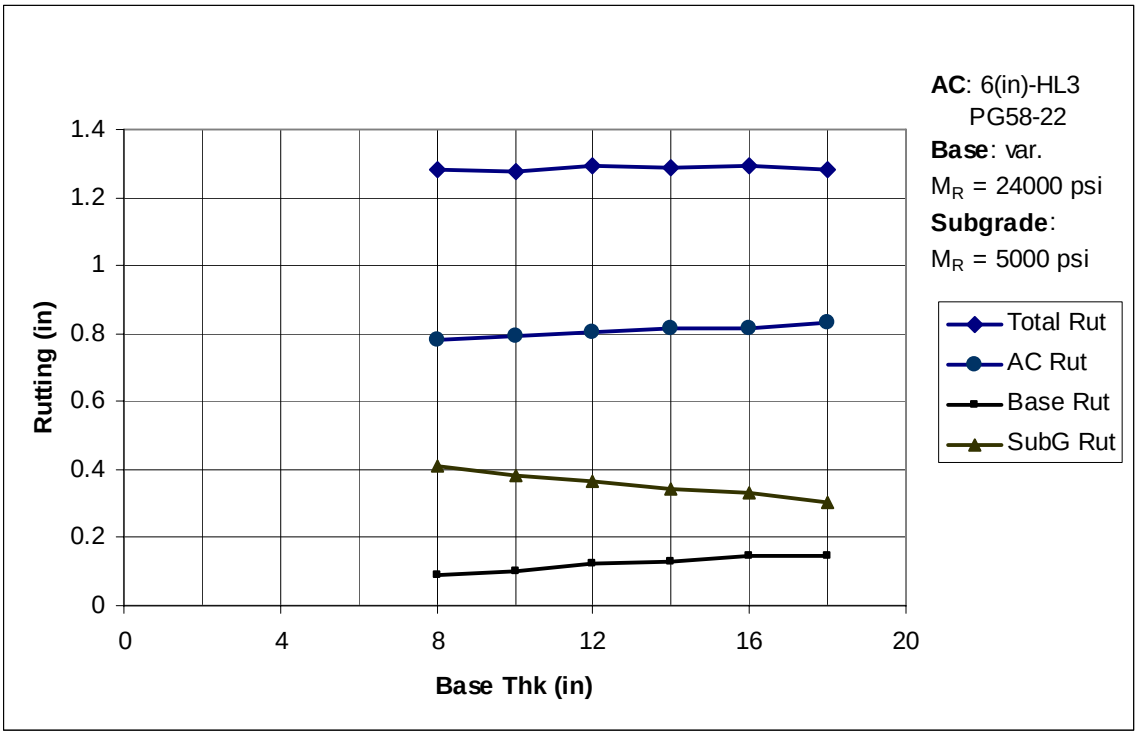

Figure 5.4 Effect of Base Thicknesses on Rutting.

In summary, model predictions indicate that none of the attempted design alternatives (increasing the thickness of the AC or base course layers) will satisfy the set design criteria (maximum of 1.0 in. total rutting depth). Accordingly, a number of other options involving a combination of design solutions were attempted to overcome the problem; the results are shown in Table 5.3.
Combination 1**:** Increase AC layer thickness to10 in. base course to 18 in.(see Figure 5.5)

AC: 10" HL3 – PG 58-22

Base: 18" GB type A-3 (M_R = 24000 psi)

SG: A-7-6 (M_R = 5000 psi)

Figure 5.5 Combination 1

Analysis of the results produced by the model application considering the configuration of the road structure and materials included in Combination 1 reflected a drop in total permanent deformation (at 50% reliability) to 0.98 in, which is below the tolerance level of 1.0 in.. However, predicted damage at 90% reliability level is still above the design limit (predicted rutting at 90% reliability = 1.18 in.) rendering this solution unsuitable for the investigated subgrade condition.

Combination 2: This design trial involves a combined change in layer thicknesses (compared with the reference structure shown in Figure 5.1). Application of a stiffer HMA was achieved by using a binder grade with more stability at relatively high temperatures (see Figure 5.6). A binder designated PG 70-22 was incorporated in the mix to replace the PG 58-22 binder. Total permanent deformation of 0.66 in. was predicted by the model, which satisfies the design limit specified under a reliability level 90%.

AC: 10 in. HL3 – PG 70-22

Base: 18 in. GB type A-3 (M_R = 24 000 psi)
(Note: the only base material available

SG: A-7-6 (M_R = 5000 psi)

Figure 5.6 Combination 2

Combination 3: This combination was selected in conformance with practice in many geographical zones, where an HMA mix with lower binder content (4%) and larger maximum nominal aggregate size is used beneath the surface course and is referred to as either the binder course or a stabilized base. A typical mix in MTO specifications, designated as HL8, was investigated in this study. The depth of the surface course was limited to 6 in. with a 6 in. HL8 layer, prepared using a PG 58-22 binder, introduced

beneath the HL3 layer. The aggregate base course was 14 in thick resting directly on the native subgrade as shown in Figure 5.7. Results of the model run performed using details of Combination 3 as inputs are shown in Table 5.3 and plotted in Figure 5.8. The results indicated that this combination is superior to all others evaluated in this exercise where predicted permanent deformations in all layers are lower.

AC: 6 in. HL3 – PG 70-22

AC: 6 in. HL8– PG 58-22

Base: 14 in. GB type A-3 (M_R = 24 000 psi)

SG: A-7-6 (M_R = 5000 psi)

Figure 5.7 Combination 3

According to analysis of model outputs, combinations 2 and 3 seem to meet the design limits, and the user may make a final choice between the two options based on the cost effectiveness of the design solution.
The exercise performed to investigate the three combinations demonstrates the opportunity offered by the application of the proposed AASHTO Design Guide where an evaluation of design alternatives is possible. No such capabilities are offered by any of the current design approaches.

Table 5.3 Performance Predicted for the Three Design Alternatives

Combination	AC Thickness (in.)	Base Course Thickness (in.)	Total Rutting at 50% Reliability	Total Rutting at 90% Reliability
1	10	18	0.98	1.18
2	10	18	0.66	0.83
3	12	18	0.57	0.73

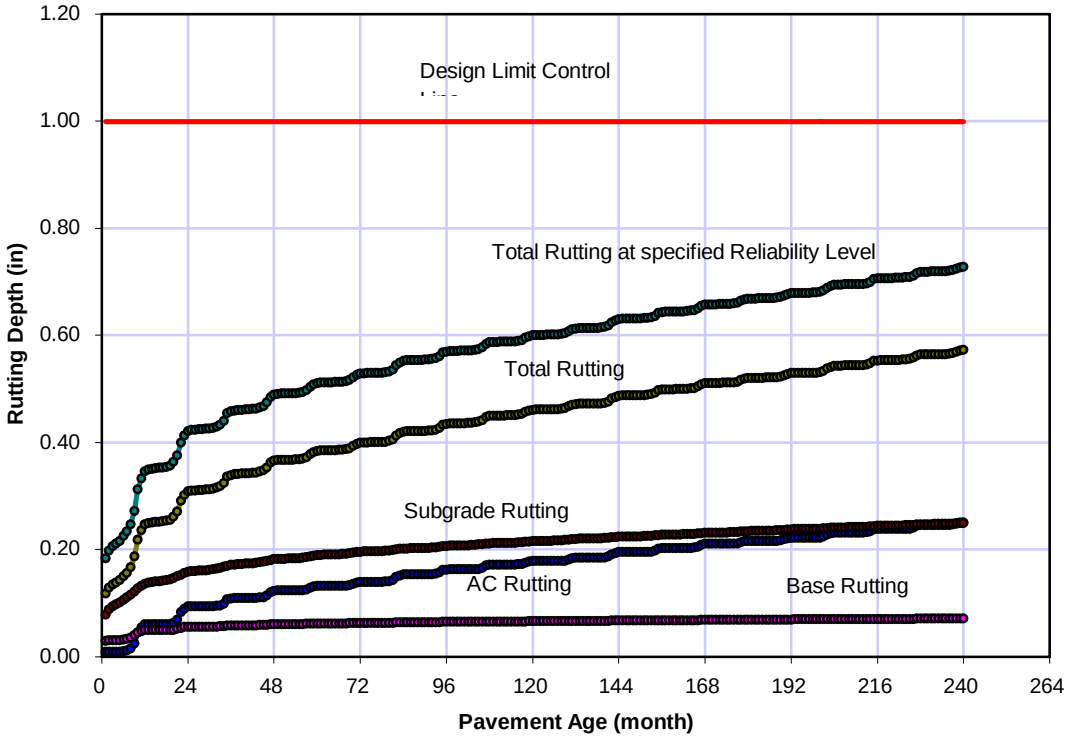

Figure 5.8 Combination 3 that Satisfies the Design Limit

5.3 Unbound Material Characterization

Unbound material characterization based on the resilient modulus approach, implemented in the proposed guide was examined in this study. In the absence of a working module that captures the nonlinear behaviour of the material (currently being redeveloped), only input Levels 2 and 3 were used in this study.
A conventional application of the model was used to gauge the sensitivity of the model to changes in unbound material types with a different resilient modulus. The results are discussed below.

Granular Aggregate Used as a Base Course

Properties of the granular material types, classified by AASHTO M145 (*The Classification of Soils and Soil-Aggregate Mixtures for Highway Construction Purposes*) as A-2-7, A-2-4, A-1-b, A1-a, were used as input to the model considering the road cross section and materials shown in Figure 5.9. Other input parameters covering load characteristics were also specified (medium traffic with an AADTT of 1000, operating speed of 25 mph, and an MAAT = 67°F. Permanent deformations that accumulated in the

road as predicted by the model for the different material types attempted as a base course are shown Table 5.4. Permanent deformation results that reflect the impact of changing the resilient modulus of the granular base material are shown in Figure 5.10.

AC: 10 in. HL3 – PG 58-22

Base: 18 in. GB-M_R Varies 21 500, 28 000, 36 000, 44 000 (psi)

SG: A-6 (M_R = 15000 psi)

Figure 5.9 Pavement Structure with Different Granular Base Moduli

Table 5.4 Predicted Permanent Deformations Considering Different Base Modulus (AC 10 in. thick, binder PG 58-22, Medium subgrade strength, M_R 15 000 psi)

Base Modulus (psi)	Total Rutting (in.)	AC Rutting (in.)	Base Rutting (in.)	Subgrade Rutting (in.)
21 500	0.82	0.60	0.09	0.13
28 000	0.82	0.61	0.08	0.13
36 000	0.81	0.62	0.07	0.12
42 000	0.81	0.63	0.06	0.12

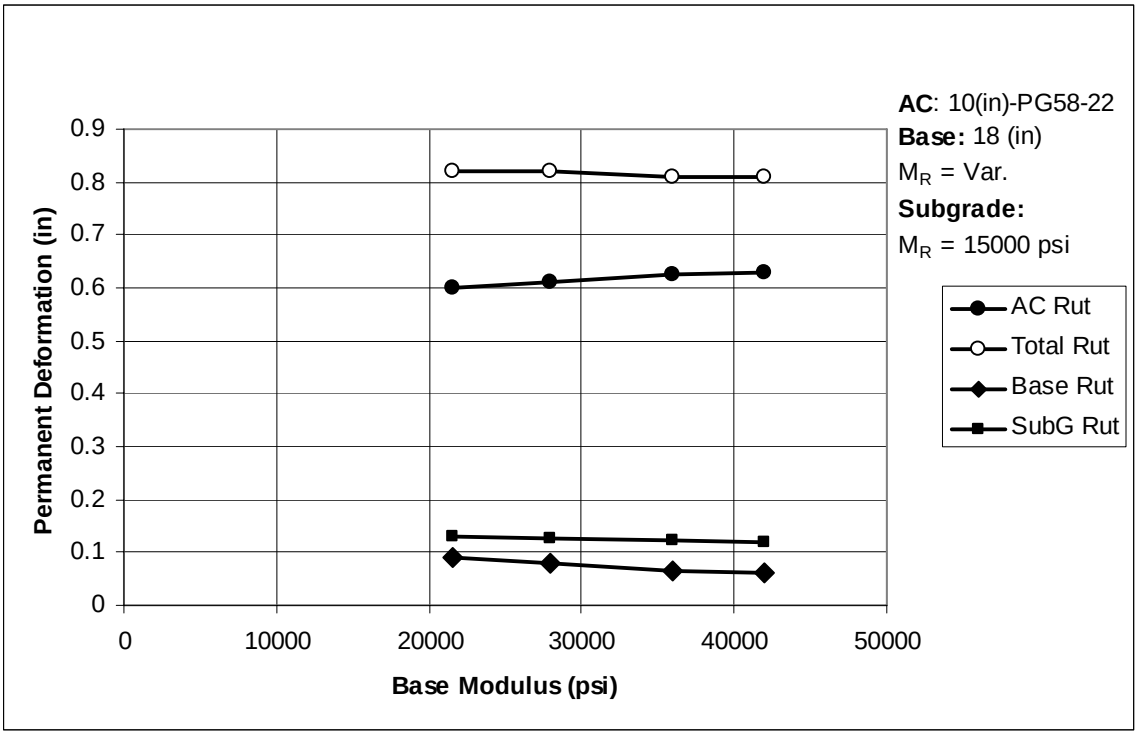

Figure 5.10 Effect of Base Modulus on Permanent Deformation

The effect of changing the quality of the granular base material on the magnitude of predicted permanent deformation is insignificant. A slight decrease in permanent deformation is predicted in the base course with the increase in the base modulus. However there seems to be no effect on the subgrade layer as the base layer modulus changed. The result does not agree with basic rules of pavement mechanics where changes in the base course modulus from 21 500 to 42 000 psi are expected to have a considerable effect on the stresses transmitted to the subgrade.

Cohesive Native Soils Representing Road Subgrade Layers

Similar to the base course investigation discussed above, inputs pertaining to a number of native soils that may exist in the road as a subgrade, were used to perform model runs analyzing the structure depicted in Figure 5.11. The resilient modulus of these soils ranged from 10 000 to 35 000 psi. The AASHTO classification for these materials includes an A-7-5 (MR = 10 000 psi), an A-2-7 (MR = 21 500 psi), A-2-4 (MR = 28 000 psi) and A-2-4 (MR = 35 000 psi). These different materials and the permanent

deformations predicted for the structure shown in Figure 5.11 are listed in Table 5.5. The results are plotted in Figure 5.12.

AC: 4 in. HL3 – PG 58-22

Base: 10 in. GB-M_R = 38 500 psi

SG: var M_R = 10 000, 21 500, 28 000, 35 000 (psi)

Figure 5.11 Pavement Structure with the Different Subgrade Moduli Investigated

Table 5.5 Predicted Permanent Deformations Considering Different Subgrade Modulus (AC 4 (in.) thick –PG 58-22, base 10 (in.) M_R = 38 500 (psi))

Subgrade Modulus (psi)	Total Rutting (in.)	AC Rutting (in.)	Base Rutting (in.)	Subgrade Rutting (in.)
10 000	1.19	0.84	0.10	0.25
21 500	1.15	0.85	0.10	0.21
28 000	1.11	0.84	0.09	0.17
35 000	1.08	0.84	0.09	0.14

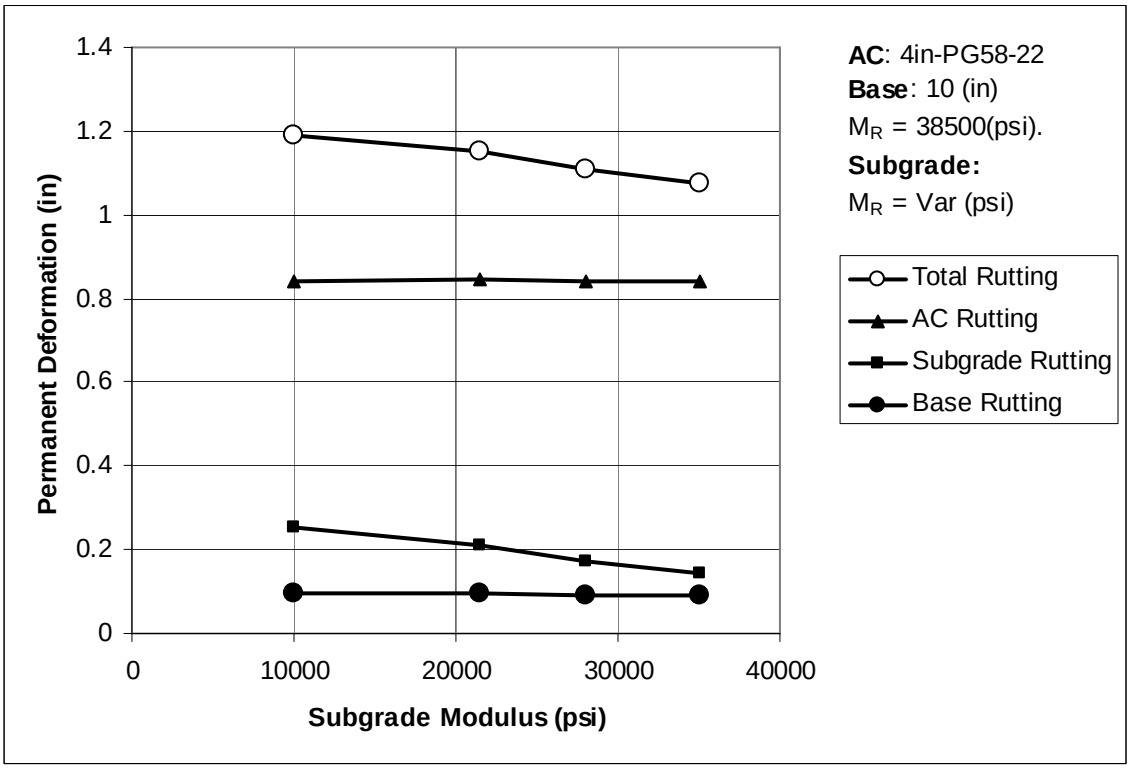

Figure 5.12 Effect of Subgrade Modulus on Permanent Deformation

Results of model runs related to various soils evaluated as subgrades suggest the increase in the modulus has a slight effect on the total permanent deformation predicted for the pavement structure (10%). This effect is directly related to the permanent deformation acquired in the subgrade. On the other hand, Figure 5.12 shows that the influence of the subgrade modulus on the AC and granular base layers is insignificant. This result has been expected, since the structural model employs linear elastic analysis, with permanent deformation prediction depending on the empirical model, which may require further calibration.

In summary, the model reflected insufficient sensitivity to unbound materials. Changes in one unbound material do not reflect on the other unbound material in the structure (from a granular base to a subgrade and vice versa). Accordingly, further investigation of unbound material characterization application in the Design Guide was performed; the results are offered in Subsection 5.12 comparing output of the different input levels (comparison between input Levels 1 and 3).

5.4 Asphalt Concrete Characterization

This section investigates the AC characterization focusing on the HMA dynamic modulus as implemented in the Design Guide. Permanent deformation in the pavement structure associated with two mix types prepared using different binders was predicted to evaluate the model sensitivity to variables associated with the AC mix. Initially, an HL3 mix prepared with a PG 58-22 binder and an HL3 mix prepared with a PG 52-34 binder were evaluated considering the road structure shown in Figure 5.13. The magnitude of permanent deformations shown in Figure 5.14 reflects sensitivity of the model to variations in the dynamic modulus of the mix.

AC: thickness 8 in., Mix 1: HL3-binder PG 58-22 / Mix 2: HL3-52-34

Base: Thickness 10 in. GB-A-1-a, M_R = 38 500 psi

SG: M_R = A-2-7, M_R = 21 500 (psi)

Figure 5.13 Pavement Structure – Two AC Mixes

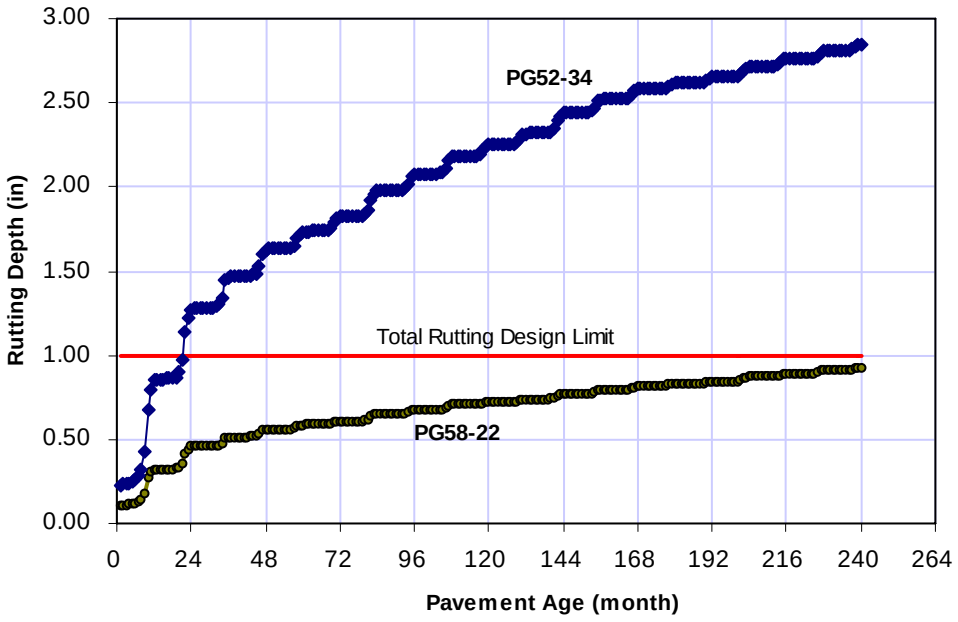

Figure 5.14 Permanent Deformation of Two HMA Mixes

According to the results shown in Figure 5.14, permanent deformation of the HL3 mix prepared with the PG 58-22 binder was substantially lower than that predicted for the HL3 mix prepared with the PG 58-22 binder. Permanent deformation in the mix prepared with the PG 58-22 binder evaluated at an average annual air temperature of 67° F, exceeded the design limit set for this study (1.0 in.). Permanent deformation at the end of the second month in the less stiff mix (prepared with PG 52-34 binder) is more than twice that in the relatively stiffer mix prepared with the PG 58-22 binder. The results agree with the design objectives intended by the producer of the binder where high stability at relatively high temperatures offers adequate resistance to permanent deformations. The mix with the PG 58-22 binder decreased substantially the accumulation of permanent deformation in the course of the 20-year design life (70% less rutting compared with the HL3 mix prepared with the PG 52-34 binder).

The Design Guide showed sufficient sensitivity to mix stiffness while predicting permanent deformation potential. Sensitivity of the model for other HMA characteristics is discussed below based on the results of evaluations performed using the appropriate performance criteria and under relevant environmental and traffic loading conditions.

5.5 Influence of the Environment on Permanent Deformation

This section discusses sensitivity of the model to the effect temperature has on permanent deformation. The climatic files for three cities with uniquely different mean annual air temperatures (MAAT) were implemented in the model runs. The temperature and load repetitions are the only implicit principal parameters in the empirical model used to predict permanent deformation.

Results of permanent deformations predicted by the model for the three MAAT are listed in Table 5.6 and plotted in Figure 5.15. Rutting that accumulated throughout the design life of 20 years for the warm city (Dallas) was 80% more compared with that in the relatively cold region (Minnesota). Clearly, the designer in the warm region will opt to use a different mix design in order to reduce rutting below the design limit of 1.0 in. The model proved capable of capturing the effect of the temperature on stiffness of the AC layer.

Table 5.6 Predicted Permanent Deformations for Different MAATs
(AC 4 (in.) thick, PG 58-22, base 10 (in.) M_R = 38 500 (psi))

Mean Annual Air Temp.	Total Rutting (in.)	AC Rutting (in.)	Base Rutting (in.)	Subgrade Rutting (in.)
46 ºF	0.64	0.34	0.08	0.21
53 ºF	0.68	0.38	0.09	0.21
67 ºF	1.15	0.85	0.09	0.21

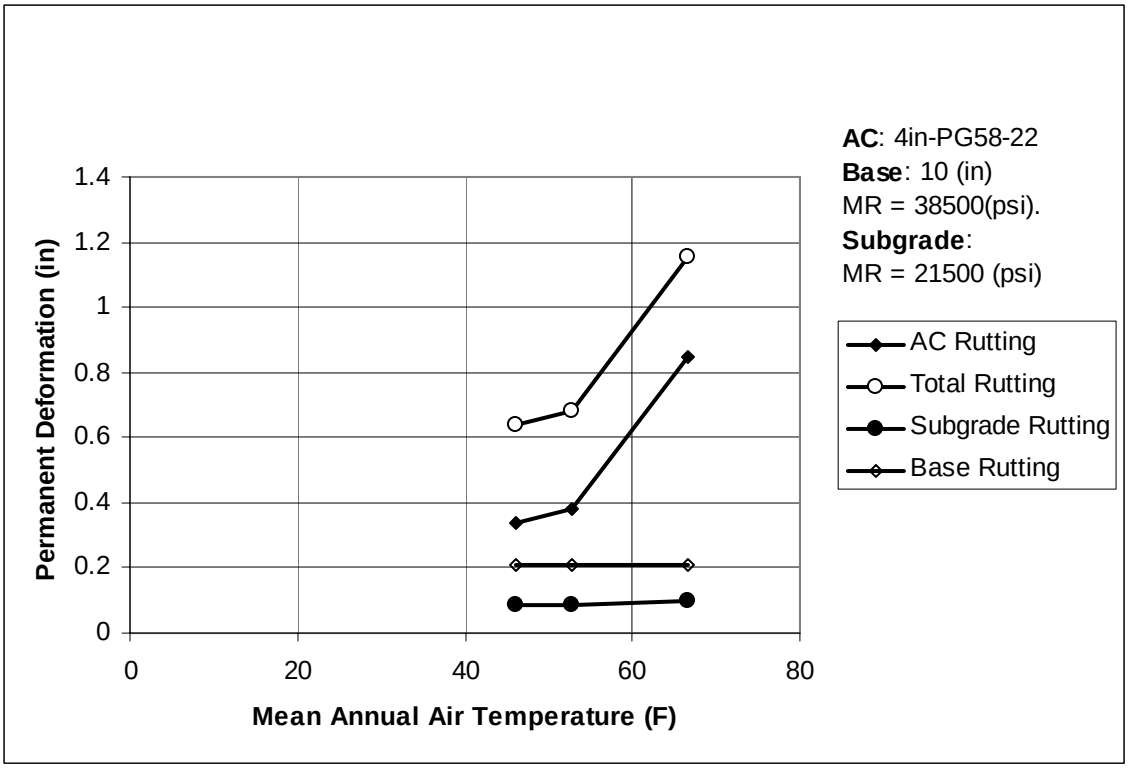

Figure 5.15 Permanent Deformation Evaluated for Different Mean Annual Air Temperatures

5.6 Traffic Characteristics

Traffic speed

Sensitivity of the AC response to the loading rate makes traffic speed an important parameter to incorporate in road structure analysis and design tools. The magnitude and duration of stress pulses resulting from moving vehicles depend on the vehicle speed. This effect diminishes toward deeper sub-layers. Lower frequencies from slower traffic are associated with a lower AC modulus and, accordingly, higher permanent deformations. To evaluate the sensitivity of the proposed guide to this phenomenon, permanent deformation predictions were made using the input data shown in Table 5.7. Model predictions are also shown in Table 5.7 and plotted in Figure 5.16 reflecting a drop of 42% in total rutting associated with the increase in speed from 10 to 60 mph. The results also indicate that the difference is mainly due to rutting in the AC layer with no change in rutting magnitude in other layers associated with a change in speed. The model is clearly sensitive to the dependency of the HMA response to the loading rate as reflected in the increase in permanent deformation associated with the drop in vehicle speed.

Table 5.7 Permanent Deformations Predicted at Different Traffic Speeds
(AC 4 in. thick, PG 58-22, granular base 10 in., M_R =38 500 psi, subgrade M_R =21 500) (psi))

Traffic Speed (mph)	Total Rutting (in.)	AC Rutting (in.)	Base Rutting (in.)	Subgrade Rutting (in.)
10	1.55	1.24	0.10	0.21
25	1.15	0.85	0.09	0.21
45	0.97	0.67	0.09	0.21
60	0.90	0.60	0.09	0.21

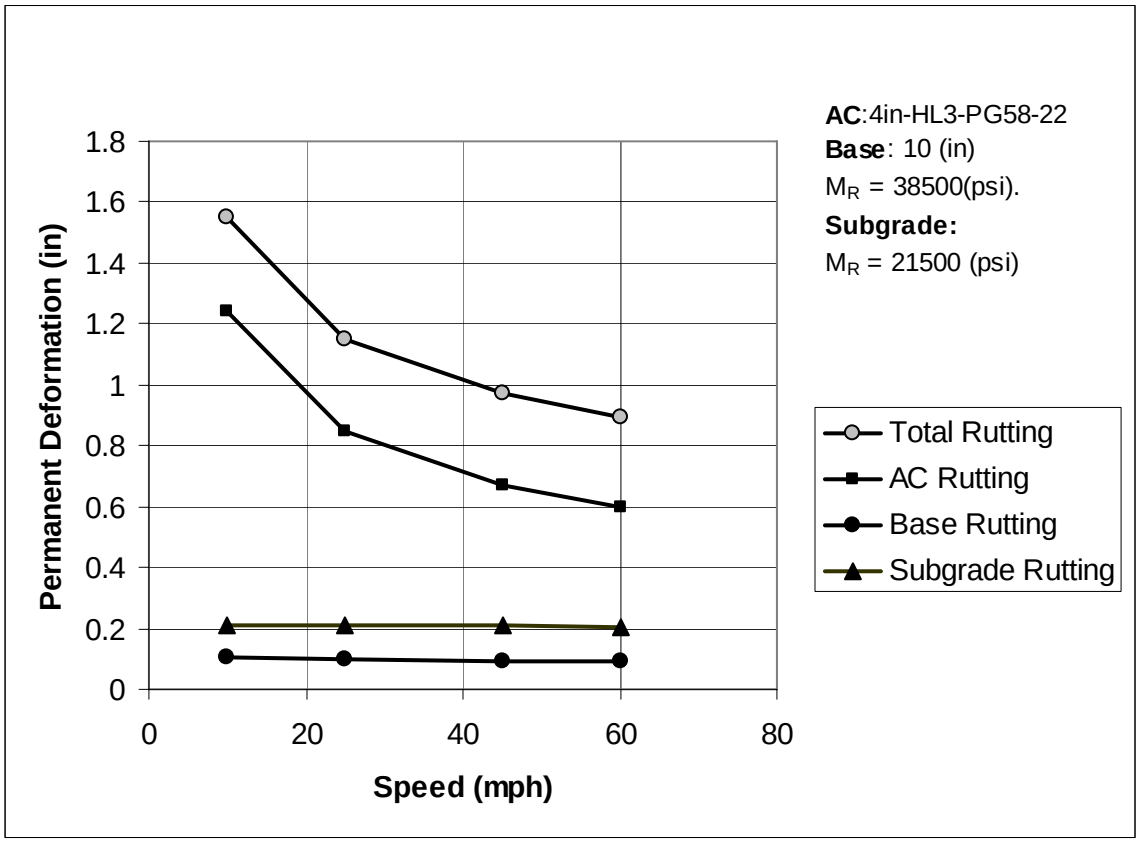

Figure 5.16 Effect of Traffic Speed on Permanent Deformation

Traffic Volume

Traffic volume, quantified as the number of load repetitions, is known to influence the magnitude of permanent deformations in AC roads. Different average annual daily truck traffic (AADTT) values and other inputs shown in Table 5.8 were used to investigate the model sensitivity to the number of load repetitions that reflect traffic volume differences. Predicted permanent deformations are shown in Table 5.8 and plotted in Figure 5.17. Permanent deformation increased with higher traffic volume. The AC layer absorbed the majority of the impact of the increase in traffic volumes. The proposed Design Guide is noticeably sensitive to the number of load repetitions, which is incorporated in the model as a principal input parameter.

Table 5.8 Permanent Deformations Predicted for different Traffic Volumes
(AC 6 in. thick –PG 58-22, base 10 in., M_R =38 000 psi - subgrade M_R =15 000 psi)

Traffic Volume AADTT	Total Rutting (in.)	AC Rutting (in.)	Base Rutting (in.)	Subgrade Rutting (in.)
200	0.56	0.37	0.06	0.13
1000	1.05	0.80	0.069	0.18
2000	1.39	1.11	0.07	0.20
4000	1.86	1.55	0.08	0.23

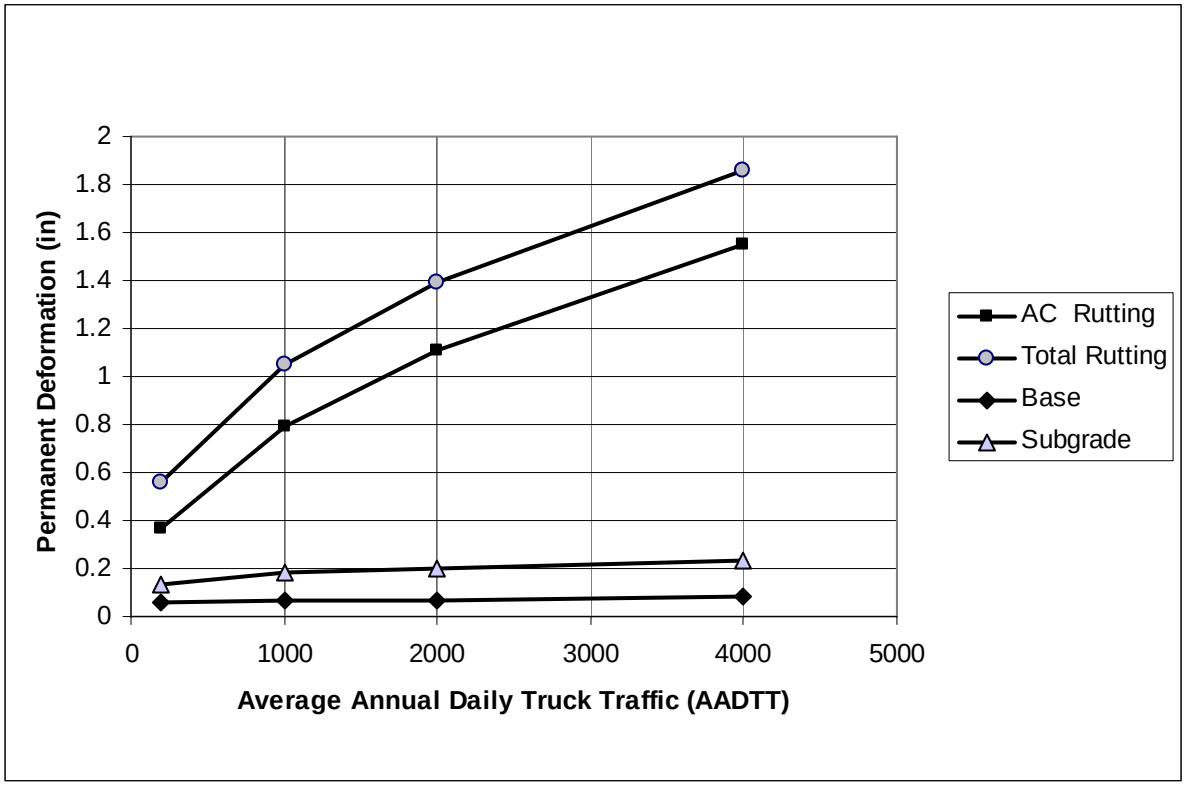

Figure 5.17 Impact of Traffic Volume on Predicted Permanent Deformations

5.7 Construction Related Variables

The proposed Design Guide requires input for three as built volumetric properties related to AC; the effective binder content percentage, air voids percentage and total unit weight. The effects of these parameters are discussed below.

5.7.1 Influence of HMA Air Voids on Predicted Permanent Deformations

The impact of air voids content has been incorporated in the empirical predictive equation. They are mainly used to construct the master curve for levels 2 and 3 inputs. The global aging system model included in the Design Guide also uses the air voids to adjust the viscosity of the original binder for in-service short and long-term aging.

The use of Level 1 AC input for a complex modulus yielded no changes in the output and the investigation switched to the use of level 3. As constructed air voids of 4%, 6%, 8% and 10% were used as input to examine the model sensitivity to variations in this important construction variable (see Figure 5.18 for structural details and air voids investigated). Results of the runs are shown below.

The model captures the effect of increasing the air voids by showing an increase in the permanent deformation. The increase in air voids will result in lower mix stiffness. The voids filled with binder have a direct impact on the mix tendency for permanent deformation.

AC: 6 in. HL3 – PG 58-22, air voids as built 4%, 6%, 8%, 10%

Base: 10 in. GB-A-1-a, M_R = 38 000 psi

SG: M_R = A-7-5, M_R = 15 000(psi)

Figure 5.18 Pavement Structure for the Air Voids Study

Table 5.9 Permanent Deformations Predicted for Different Air Void Contents
(AC 6 in. thick, PG 58-22, base 10 in., M_R =38 000 psi, subgrade M_R =15 000 psi)

AC Mix Air Voids (As Built)%	Total Rutting (in.)	AC Rutting (in.)	Base Rutting (in.)	Subgade Rutting (in.)
4	0.88	0.63	0.07	0.18
5.9	0.95	0.7	0.07	0.19
8	1.08	0.82	0.07	0.19
10	1.25	0.98	0.08	0.19

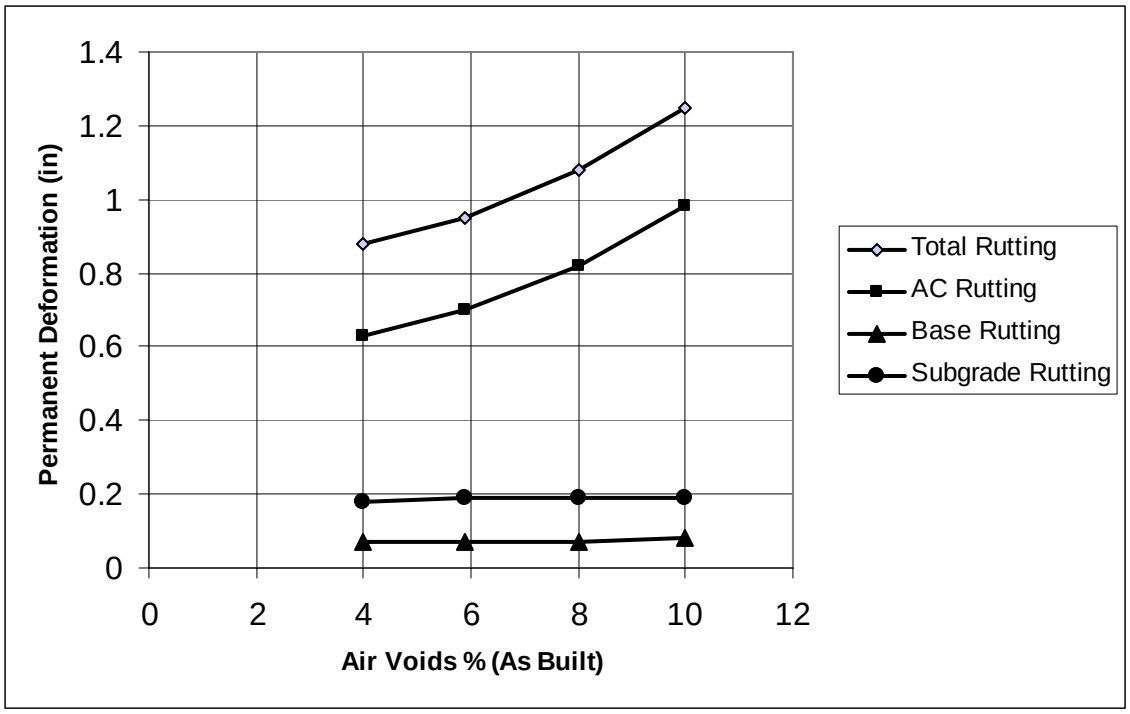

Figure 5.19 Impact of Air Voids Content on Permanent Deformation

Influence of Effective Binder Content on Predicted Permanent Deformations

The predictive equation, used in levels 2 and 3 includes effective binder content as an input parameter. The sensitivity of these two design levels to variations in effective binder content was evaluated using three uniquely different mixes as shown in Table 5.10. Permanent deformation predictions associated with these different effective binder contents are shown in Figure 5.20. Permanent deformations increased with the increase in effective binder content. The entire change is related to the AC layer as indicated by the results plotted in Figure 5.20.

Table 5.10 Permanent Deformations Predicted for Different Binder Contents
(AC 4 in. thick, PG 58-22, base 10 in., M_R =38 000 psi, subgrade M_R =15 000 psi)

Total Rutting (in.)	AC Mix Binder Contents (As Built)%	AC Rutting (in.)	Base Rutting (in.)	Subgade Rutting (in.)
0.86	8	0.61	0.07	0.18
0.95	10.5	0.7	0.07	0.19
1.05	14	0.79	0.07	0.19

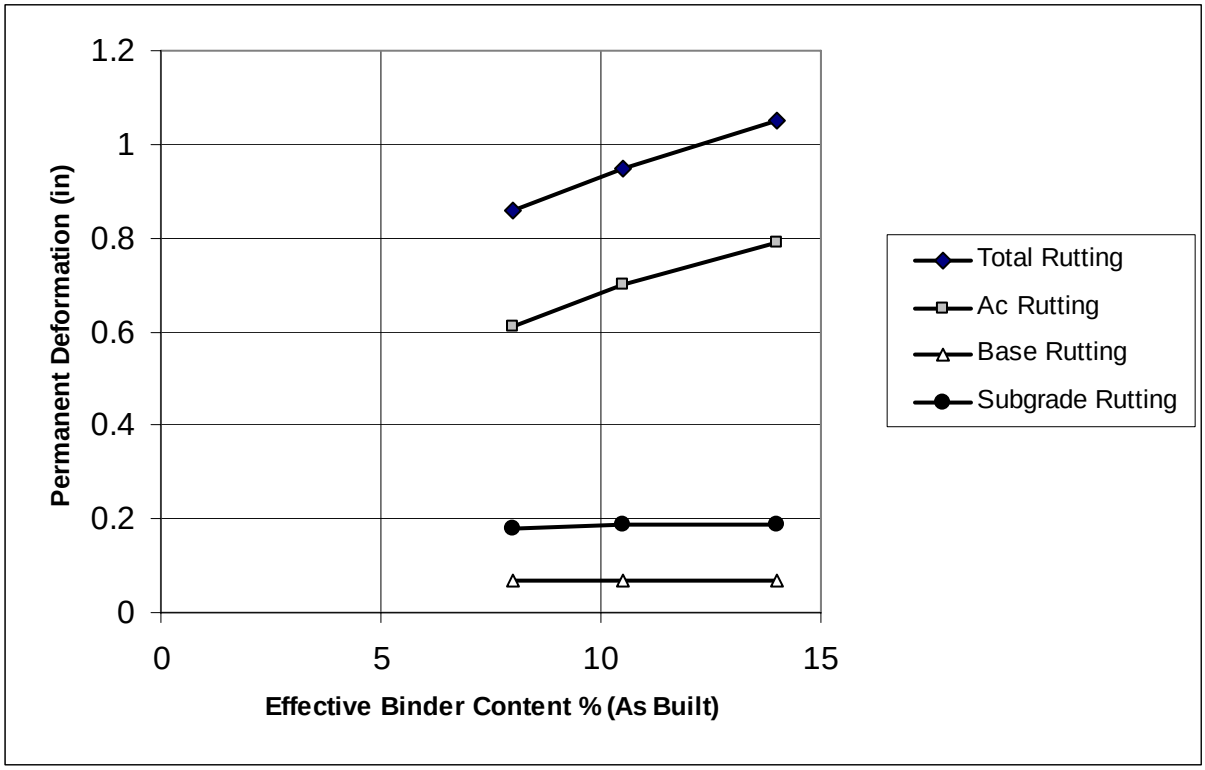

Figure 5.20 Effective Binder Content Impact on Permanent Deformation

5.8 General Comments Related to Model Predictions of Permanent Deformations

Model applications for predicting permanent deformation as the performance criteria to be used in selecting a design proved effective for AC layers. The model showed sensitivity to the thickness of the AC layer and to the mix stiffness associated with the binder used in the manufacturing process. It has also responded clearly to changes in traffic volume and operating speed. Construction related parameters such as mix air voids and effective binder contents have shown to be effective in input level 3 rather than level 1. The predictive equation used in levels 2 and 3 includes these two parameters as a direct input that estimates the dynamic modulus. Accordingly, Level 1 applications should be complemented by laboratory tests performed on samples prepared at the as built air voids content and effective binder content.

Apparently, the model is less successful in addressing analysis requirements related to unbound materials. The model lacks sensitivity toward variations made in this study to parameters known to influence performance, such as the base course depth and the resilient modulus, where model predictions of permanent deformation show little or no effect. These findings are discussed further using different model application runs in the following sections. However, model calibration reports suggest the performed calibration exercise for unbound materials did not progress as anticipated. The calibration of the permanent deformation characteristics within each major pavement layer could not be achieved due to the fact that LTPP data only provides the total (surface) rutting present in the test section. The unbound base, subbase and subgrade rut depth predictions were calibrated to a special study involving the use of numerous test sections designed by the 1993 AASHTO Design Guide [42]. Recommendations were issued suggesting that problems and limitations of the performed calibrations may be avoided benefiting from the results of a local calibration stage to achieve a more reasonable degree of confidence.

The performance of the model is expected to improve when the nonlinear behaviour of unbound materials is included in the analysis.

The NRC is performing an R&D program involving a modification to the current resilient modulus test geared toward developing a process for modeling permanent deformation of unbound materials [43]. Future research is expected to incorporate AC viscoelastic behaviour and permanent deformation in the structural model and reduce dependency on the empirical models included in the proposed guide.

5.9 Fatigue Cracking

Fatigue cracking is a main pavement distress affecting the performance of roads. Repeated traffic loads induce tensile and shear stresses at critical locations causing cracks to initiate and then propagate through the asphalt layer. Environmental conditions aggravate this damage type and cause the pavement structure to lose its structural integrity. Results of a sensitivity analysis are discussed in the following section to address the impact of the factors that affect fatigue cracking in flexible pavements, such as layer thickness, AC dynamic modulus, binder grade, air voids in the asphalt layer, effective binder content, base thickness, the subgrade modulus, traffic and environmental conditions.

The pavement structure details shown in Table 5.1.1, subjected to a medium traffic load of 2000 AADTT and a medium traffic speed of 25 mph in a relatively warm climate (MAAT = 67°F) was analyzed using the proposed Design Guide. The results of the model runs are discussed below

Effect of AC Thickness on Bottom/Up Cracking

The magnitude of fatigue cracking associated with different AC layer thicknesses was investigated. The results of varying the AC thickness from 2 inches to 12 inches are shown in Table 5.11 and plotted in Figure 5.21. Fatigue cracking increased between 2 inches and 4 inches, and then decreased with the increase in the AC layer thickness. The decrease in fatigue cracking with the increase in layer thickness, above 4 inches, is a direct result of the decrease in tensile strain at the bottom of the AC layer and, consequently, the amount of fatigue cracking. It is interesting to note that fatigue cracking peaks at an AC layer thickness of 4 inches, which is supported with observations documented in the literature [44]. The decrease in fatigue cracking for thicknesses below 4 inches may be justified by the fact that at HMA thickness below the maximum level between 3 and 5 inches, tensile strains actually decrease and may become compressive in nature. Similar findings were reported [45] using the Kenlayer computer program. They concluded that for thin asphalt surfaces, say less than 2 inches thick, the use of a single tire results in a smaller tensile strain and is unsafe for the prediction of fatigue cracking.

Table 5.11 Predicted Fatigue Cracking (Bottom/Up) for Different AC Thicknesses
(AC var. thick –HL3-PG 58-22, base 10 in., M_R =38 000 psi, subgrade M_R =15 000 psi)

AC thickness in.	2	4	6	8	10	
Fatigue cracking %	6.8	13.2	3.4	1	0.3	0.1
% Decrease in fatigue cracking	48	Reference	74	92	98	99

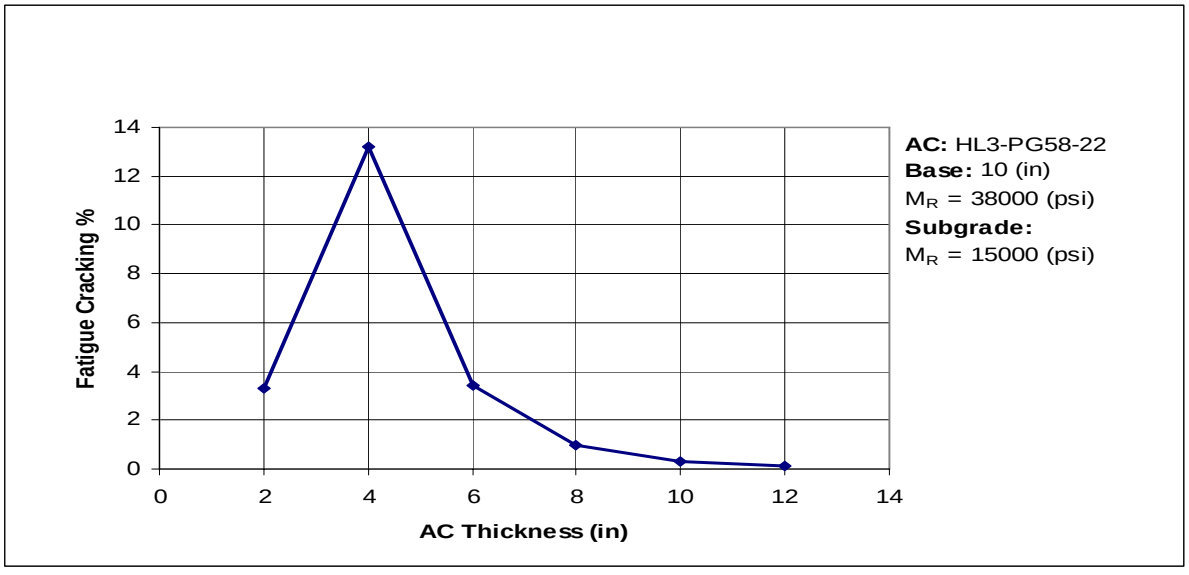

Figure 5.21 Effect of AC Thickness Changes on Fatigue Cracking

Effect of Binder Properties on Fatigue Cracking (Bottom/Up)

Three HL3 mixes prepared with different performance grade binders (PG 58-22, PG 64-34, and PG 52-34) were used to investigate the effect of the binder properties on the amount of fatigue cracking. The dynamic modulus of the three mixes is shown in Figure 5.22. Predicted fatigue cracking is shown in Figure 5.23. As expected, fatigue cracking decreased for mixes with high binder stiffness. Using the softer binder PG 52-34 resulted in an increase of 40% in fatigue cracking compared with PG 58-22. However, the use of the mix with the PG 64-34 binder resulted in 45% higher fatigue cracking compared with the mix prepared with the PG 58-22 binder. Although the PG 64-34 was supposed to be stiffer, predicted performance is in agreement with the laboratory determined dynamic modulus, which indicated that the PG 58-22 produced a stiffer mix than that produced using the PG 64-34 binder.

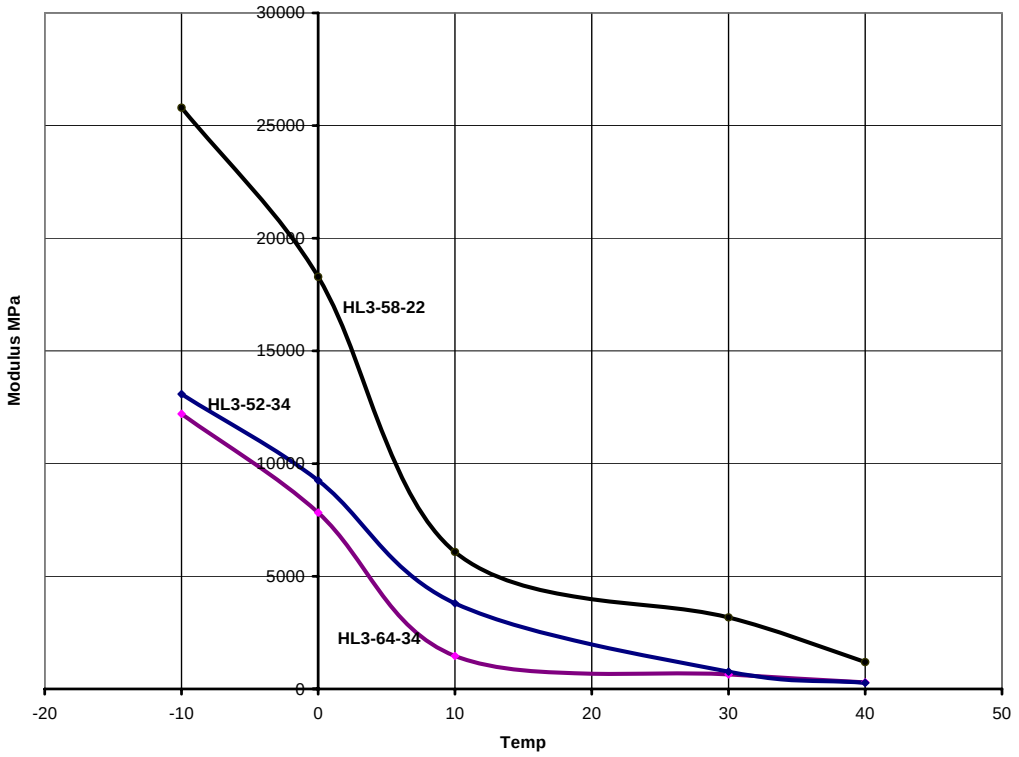

Figure 5.22 Dynamic Modulus of HL3 Prepared with Different Binders

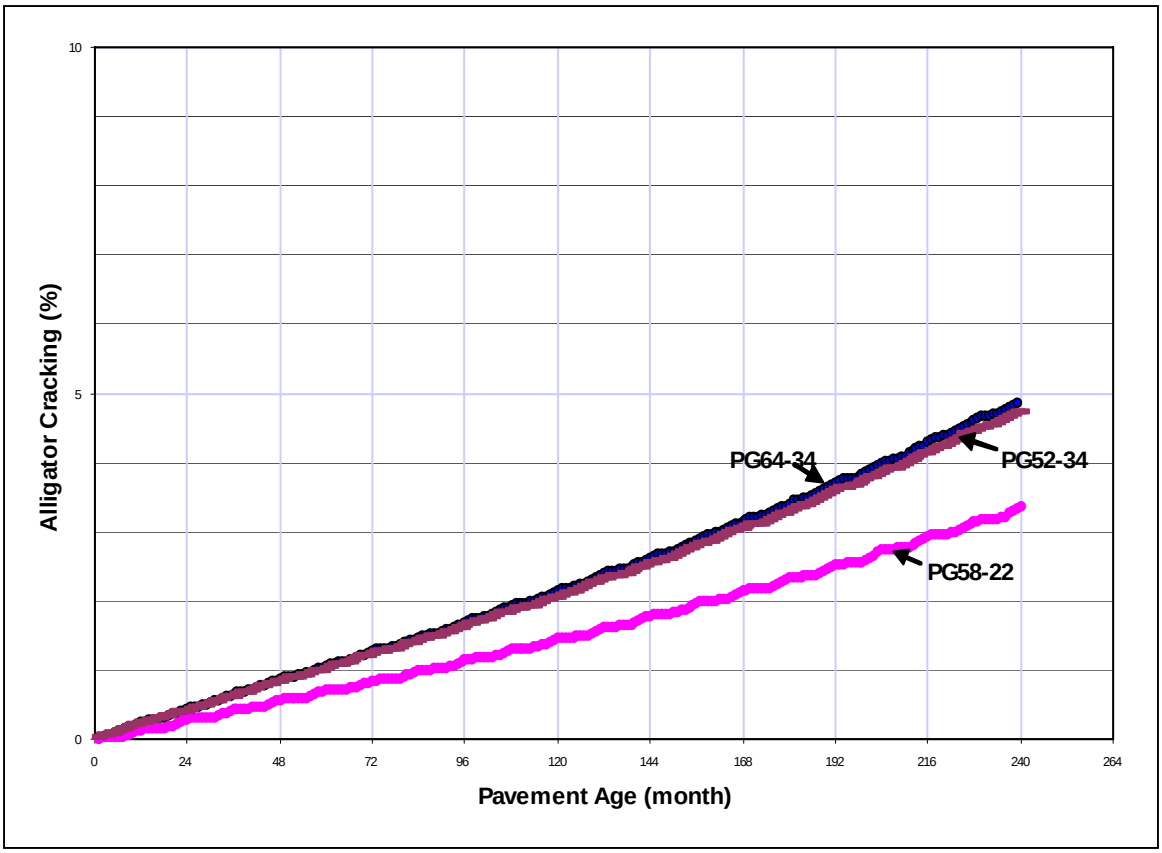

Figure 5.23 Fatigue Cracking Predicted for Three Mixes Prepared with Different Binders

Effect of Unbound Materials Characteristics Used as a BaseCourse

Properties of the different pavement layers influence its response (stresses and strains). Thus, the quality of the granular base course and that of the subgrade acting as a supporting foundation are important factors in evaluating road performance. This subsection evaluates the sensitivity of the model to changes in the resilient modulus of the base course.

The AASHTO soil classification system classifies soils based on particle-size distribution and Atterberg limits. Properties of a number of granular material types, classified by AASHTO (M145) as A-2-7, A-2-4, A-1-b and A-1-a were used as input to the model considering the road cross section and material properties shown in Figure 5.24. Other input parameters covering load characteristic were also specified (medium traffic with an AADTT of 1000, operating speed of 25 mph, and an MAAT = 67 °F). The percentage of fatigue cracking predicted by the model for the different material types simulating the road base course are shown in Table 5.12. These

percentages reflect the impact of changing the resilient modulus of the granular base material as shown in Figure 5.25.
The results indicate that fatigue cracking predicted by the model is very low, but still seem sensitive to changes in the resilient modulus of unbound material below the AC layer. Percentage reduction in the magnitude does not improve the overall performance of the road related to fatigue cracking.

AC: 10 in HL3–PG 58-22

Base:18 in.GB-M_R varies 21 500, 28 000, 36 000 and 42 000 psi

SG: A-6 -M_R = 15 000 psi

Figure 5.24 Pavement Structure with Different Granular Base Modulus

Table 5.12 Predicted Fatigue Cracking (Bottom/Up) for Different Base Modulus Values (AC 10 in. thick –HL3-PG 58-22 - Base 18 in. M_R = Var. - Subgrade M_R =15000 psi)

Base modulus psi	21 500	28 000	36 000	42 000
Fatigue cracking %	0.9	0.5	0.3	0.2
% Decrease in fatigue cracking	Reference	44	67	78

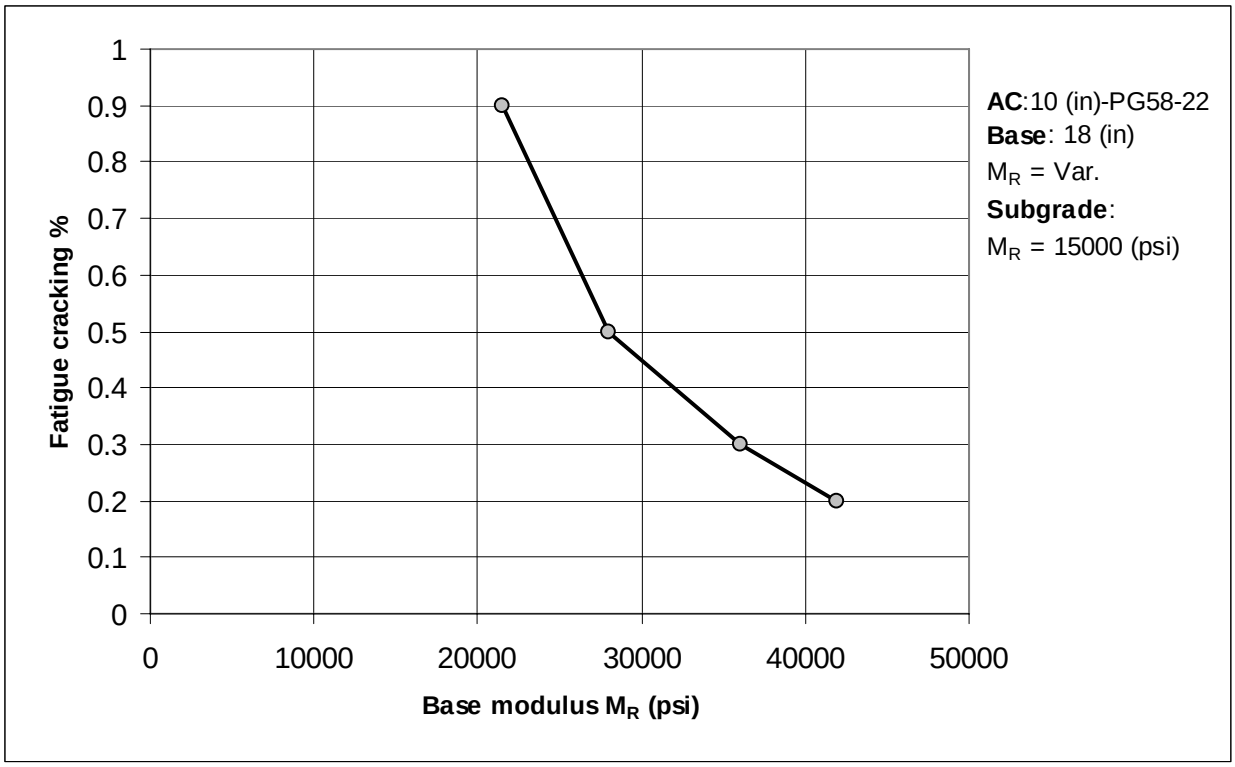

Figure 5.25 Effect of Base Quality on Fatigue Cracking (Bottom/Up)

Effect of Effect of Unbound Materials Characteristics Used as a Subgrade

Similar to the above base course investigation, inputs pertaining to a number of native soils that may exist in the road as a subgrade were used to perform model runs to analyze the structure depicted in Figure 5.26. The resilient modulus of these soils ranged from 5000 to 30 000 psi. AASHTO classification for these materials includes an A-7-6 (MR = 5000 psi), A-7-5 (MR = 10000 psi), A-6 (MR = 15000 psi) and A-2-4 (MR = 30000 psi). These different materials and the percentage of fatigue cracking predicted for the structure shown in Figure 5.26 are listed in Table 5.13. The results are plotted in Figure 5.27.

AC: 6 in. HL3 – PG 58-22

Base: 10 in. GB-M_R = 38 500 psi

SG: var M_R = 5000, 10 000, 15 000, 30 000 psi

Figure 5.26 Pavement Structure with Different Subgrade Modulus

Table 5.13 Predicted Fatigue Cracking (Bottom/Up) for Different Subgrade Modulus (AC 6 in. thick –HL3-PG 58-22, base 10 in., M_R = 38000 psi)

Subgrade modulus psi	5000	10 000	15 000	30 000
Fatigue cracking %	4.5	3.8	3.4	1.5
% Decrease in fatigue cracking	Reference	15	24	67

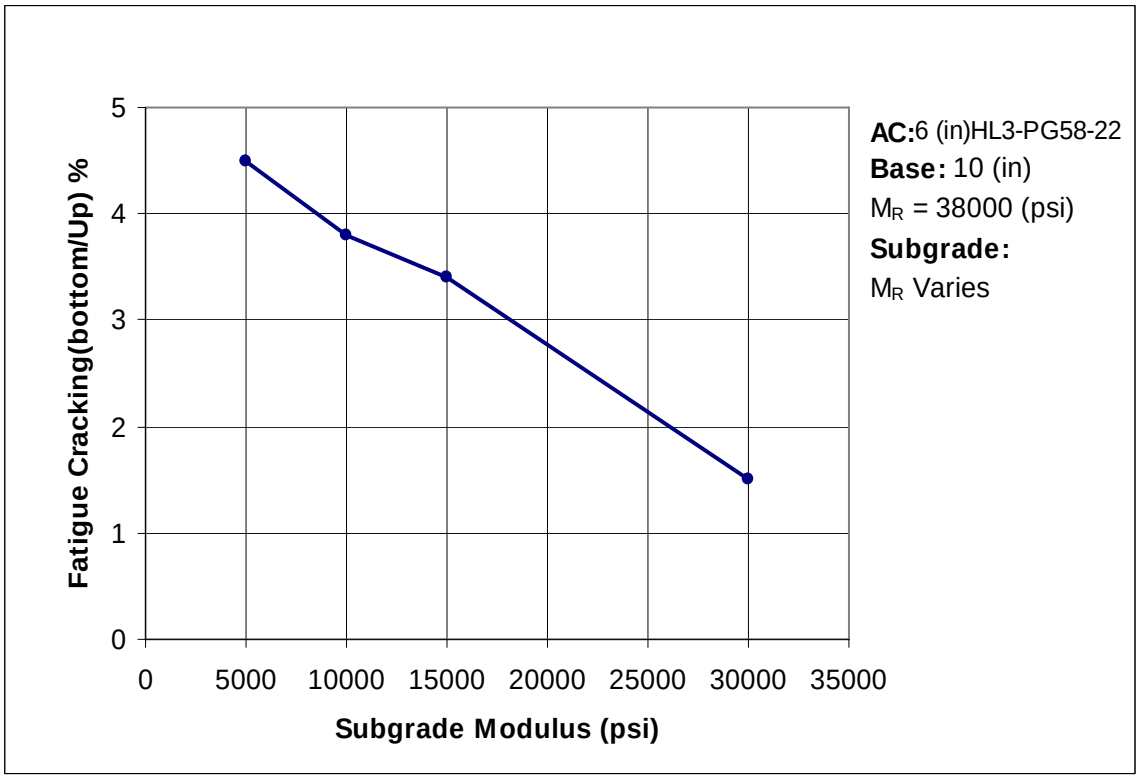

Figure 5.27 Effect of Subgrade Modulus on Fatigue Cracking (Bottom/Up)

Similar to the base course situation, the subgrade modulus has little effect on fatigue cracking. Results of model runs related to various soils evaluated as subgrades suggest the increase in the modulus has affected fatigue cracking as predicted by the model. An increase in the modulus from 5000 psi to 30 000 psi resulted in a decrease of 67% in the predicted fatigue cracking.

Influence of the Environment on Bottom/Up Fatigue Cracking

The influence of the environment on fatigue cracking, focusing on temperature effect, was investigated in this study using the database of the model that houses climatic files of different cities. Climatic files of three cities with uniquely different mean annual air temperatures

(MAAT) were used to run the model. Results of fatigue cracking predicted by the model for the three MAAT are listed in Table 5.14 and plotted in Figure 5.28.
Fatigue cracking in the relatively warm city is 40% more than that predicted for the relatively cold city. The results are in agreement with the impact of temperature on the AC layer stiffness where an increase in the air temperature makes the pavement more vulnerable to fatigue cracking. However, the percentage of fatigue cracking estimated for the warmest city after the design life is lower than what is considered a critical level (25%).

Table 5.14 Predicted Fatigue Cracking (Bottom/Up) – Different MAAT.
(AC 4 in. thick –HL3-PG 58-22, base 10 in., M_R = 38 500 psi,
subgrade M_R = 21 500 psi)

MAAT (^{o}F)	46	53	67
Fatigue cracking %	10.1	12.6	14.2
% Increase in fatigue cracking	Reference	25	40

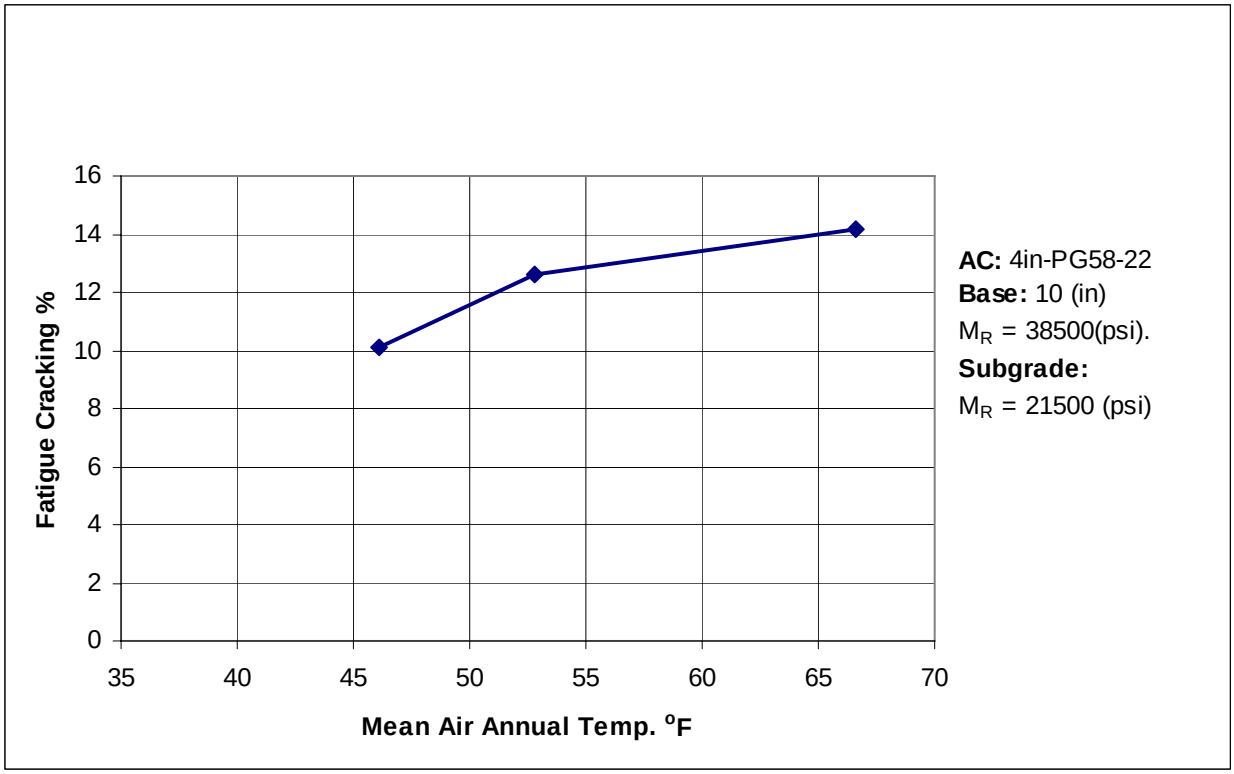

Figure 5.28 Fatigue Cracking (Bottom/Up) Predicted for Three Cities with Different MAAT

Effect of Traffic Characteristics on Fatigue Cracking

The influence of traffic speed and volume on fatigue cracking was investigated in this study. Traffic speed was used as input to perform runs at a medium traffic volume (2000 AADTT). Traffic speeds of 10, 25, 45 and 60 mph were used interchangeably in the model. The structure details are shown in Table 5.15. The climate selected is relatively warm (MAAT = 67 °F). Results of the runs are shown in Table 5.15 and plotted in Figure 5.29. The results show a decrease in the fatigue cracking associated with the increase in traffic speed. The decrease in the magnitude of fatigue cracking reflects the concept that higher speeds result in higher loading frequencies and, consequently, the dynamic modulus of the asphalt layer increases and the induced tensile strains decrease.

Table 5.15 Predicted Fatigue Cracking (Bottom/Up) at Different Traffic Speeds
(AC 4 in. thick –PG 58-22, base 10 in., M_R =38 500 psi, subgrade M_R =21 500 psi)

Traffic Speed Mph	10	25	45	60
Fatigue cracking (bottom/up)%	15.1	14.2	13.5	13.2
% Decrease in fatigue cracking	Reference	6	12	13

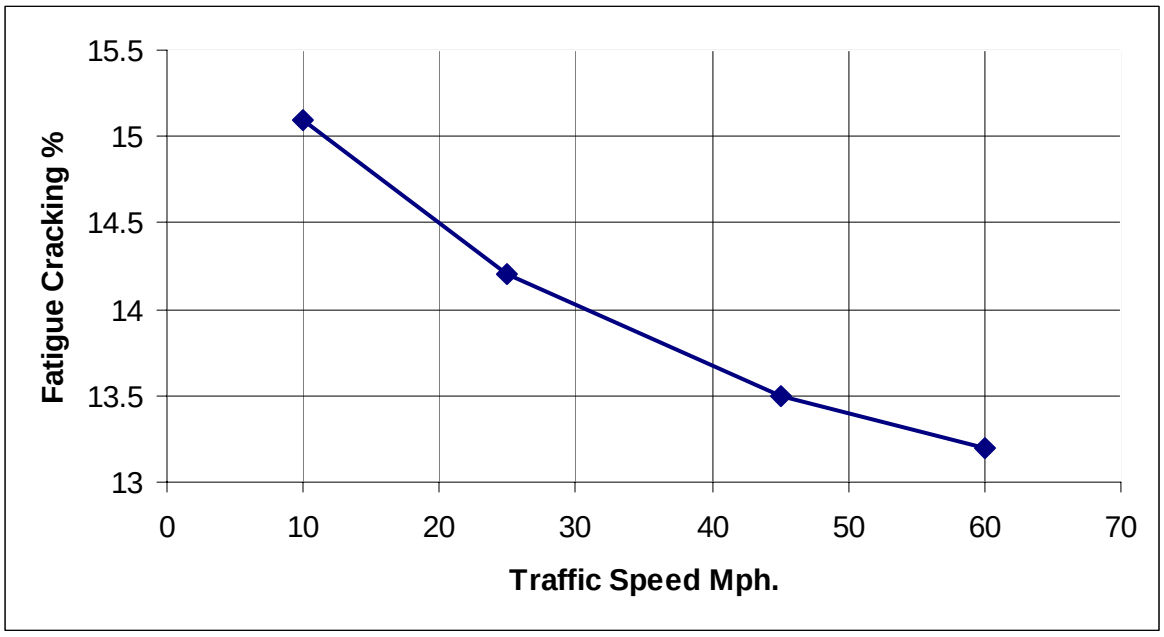

Figure 5.29 Fatigue Cracking (Bottom/Up) Associated with Different Traffic Speeds

Traffic volume is another critical traffic characteristic that influences pavement damage. Different truck volumes were used to investigate the model sensitivity to the number of load repetitions that simulate different traffic volumes (see input in Table 5.16). The predicted percentages of fatigue cracking are shown in Table 5.16 and plotted in Figure 5.30. The model

predictions are in agreement with the fundamentally established relationship between the number of load repetitions and fatigue cracking.

Table 5.16 Predicted Fatigue Cracking (Bottom/Up) – Varying Traffic Volumes
(AC 6 in. thick, PG 58-22, base 10 in., M_R =38 000 (psi), subgrade M_R =15 000 psi)

ADDT	200	1000	2000	4000
Fatigue cracking (bottom/up)%	0.6	5.5	7	14
% Change in fatigue cracking	-89	Reference	+23	+155

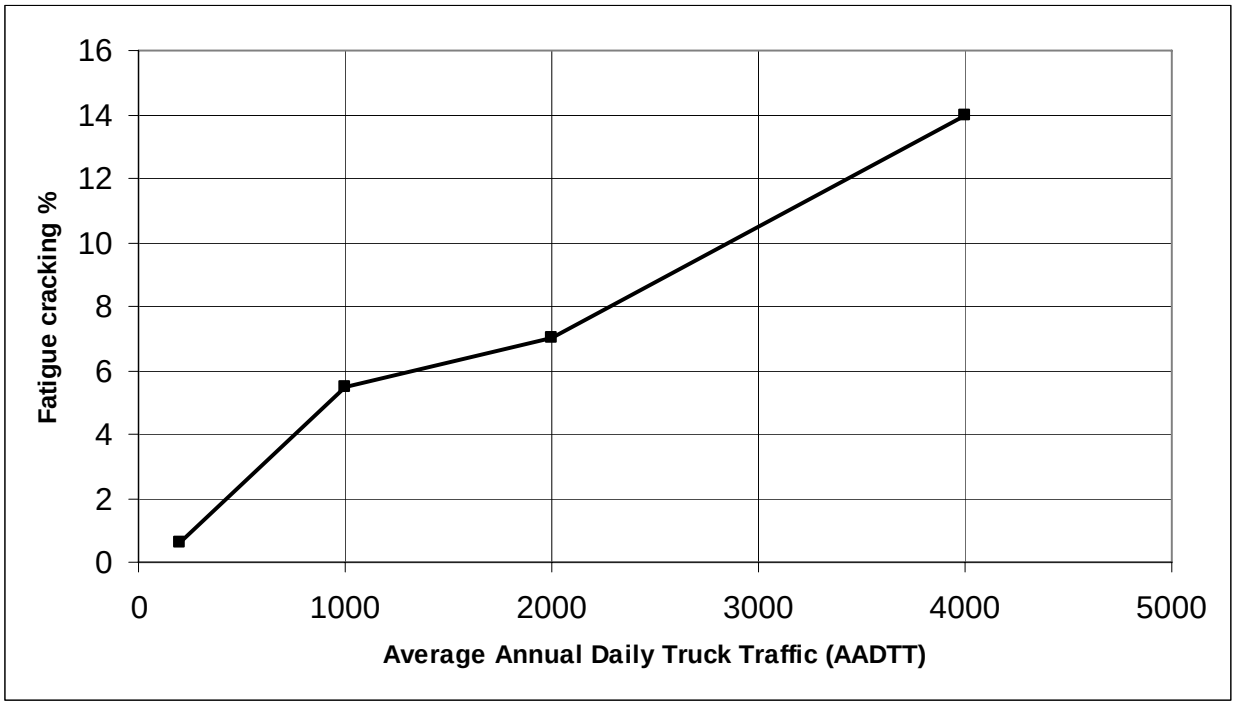

Figure 5.30 Fatigue Cracking (Bottom/Up) Predicted for Different Traffic Volumes

Impact of Construction Related Variables on Fatigue Cracking

This subsection investigates the impact of air voids on fatigue cracking. The Percentage of air voids, together with the percentage of effective binder content, are used in the Asphalt Institute model [46] as an input for obtaining "the laboratory to field adjustment factor (C)" shown earlier in Equation 3.5. As-constructed air voids of 4%, 6%, 8% and 10% were used in this study as input to examine the model sensitivity to variations in this construction related variable. Results of the performed runs are shown in Table 5.17 and Figure 5.31. As expected, high air voids resulted in high fatigue cracking.

Table 5.17 Effect of AC Mix Air Voids (As Built) on Fatigue Cracking (Bottom/up)
(AC 6 in thick, PG 58-22, base 10 in., M_R =38 000 psi, subgrade M_R =15 000 psi)

Air Voids %	4	6	8	10
Fatigue Cracking (Bottom/Up)%	1.6	4.8	11.8	22.2
% Increase in Fatigue Cracking	Reference	67	637	1288

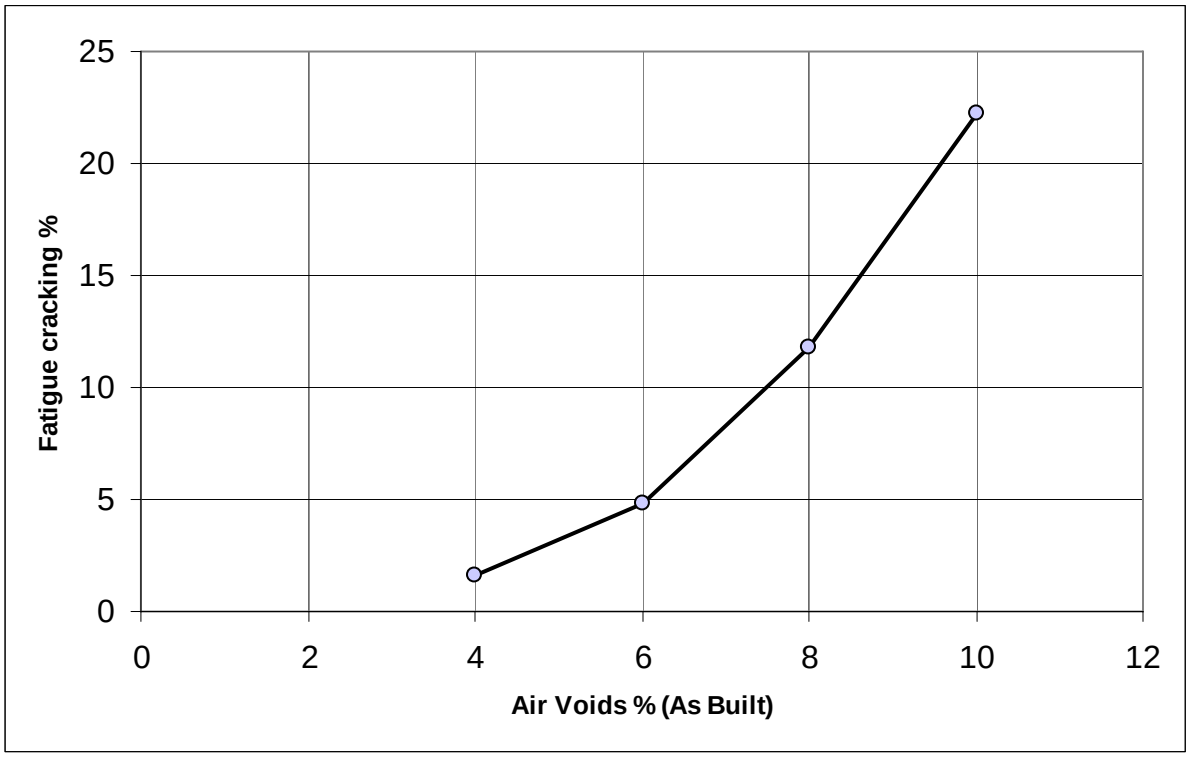

Figure 5.31 Effect of Air Voids (As Built) on Fatigue Cracking

To examine sensitivity of the model to changes in the effective binder content, as constructed effective binder contents of 8%, 10.5% and 14% were used as input to the model. Results of the runs are listed in Table 5.18 and plotted in Figure 5.32. The results suggest the effective binder content has a slight impact on fatigue cracking. Increasing the binder content within a commonly adopted range decreased the percentage of fatigue cracking in the road surface as shown in Figure 5.32

Table 5.18 Effect of AC Mix Effective Binder Content (As Built) on Fatigue Cracking (AC 6 in thick, PG 58-22, base 10 in., M_R =38 000 psi, subgrade M_R =15 000 psi)

Effective binder content %	8	10.5	14
Fatigue cracking (bottom/up)%	9.4	4.8	2.4
% Decrease in fatigue cracking	Reference	49	74

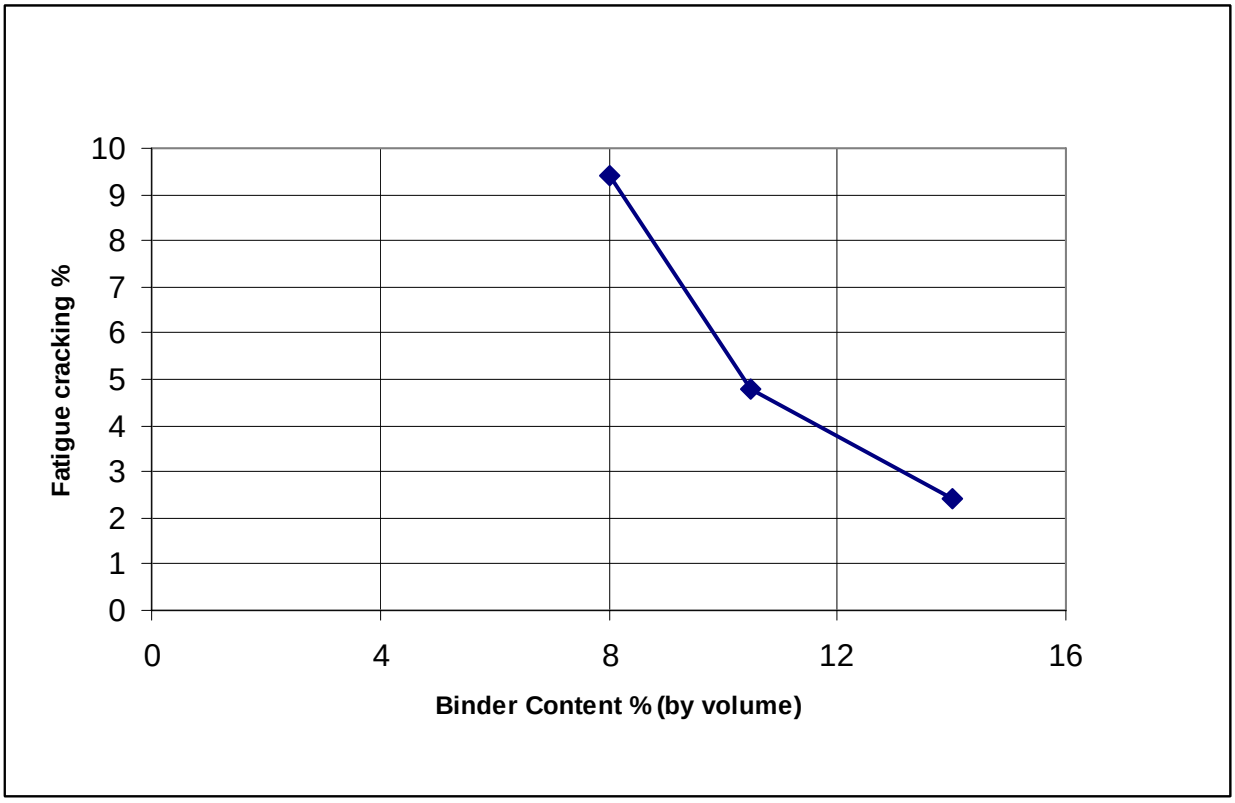

Figure 5.32 Fatigue Cracking for Different Binder Contents

5.10 Comparison between Design Input Levels

The main objective of the hierarchical approach of the design input levels is to provide users with a flexible design system that allows them to use the software of the proposed Guide depending on availability of data and local resources, taking into consideration the complexity of the project. Concerns may arise as to whether pavement engineers can start applying Level 3 and later progress to analysis with the ideal approach (Level 1) when testing resources in Canada match model requirements. The impact of using Level 3 on the accuracy of the analysis is not well known. This section discusses results of analysis using data produced with different design input levels.

Impact of Using AC Design Inputs Level 1 and Level 3 on Performance Prediction

To investigate the impact of using level 1 and level 3 on pavement performance prediction, six model runs were conducted. The first three runs were performed with Level 1 input data using the complex modulus of HL3 mix determined in the laboratory. The three performance graded binders, shown earlier in Table 4.5 were used to prepare the mix design. The other three runs were performed using Level 3 for the same mixes. The pavement structure used to perform the analysis is shown in Figure 5.33 together with other input parameters shown in Chapter 4. Analysis was performed for a design life of 20 years in a relatively warm climate. The predicted total deformations using the two levels of input are shown in Figure 5.34. Permanent deformation varied considerably depending on the binder type used. In general, Level 3 analysis tends to under predict permanent deformation as shown in Figure 5.34.

AC: 6 in. HL3 – PG 58-22, PG 52-34, PG 64-34

Base: 10 in. GB type A-1-b (M_R = 38 000 psi)

SG: A-7-5 (M_R = 15 000 psi)

Figure 5.33 Pavement Structure – Comparison of Design Levels

The calculated difference based on level 1 ranged from 10% for the mix made with the PG 58-22 binder to 60 % for the mix made with the PG 52-34 binder. Level 1 seems to be able to discriminate between the evaluated binder types more than Level 3.
On the other hand, using Level 3 resulted in 40% overestimation of fatigue cracking for mix made with the PG 58-22 binder and by 10% for the mix made with PG 52-34 binder as shown in Figure 5.35.

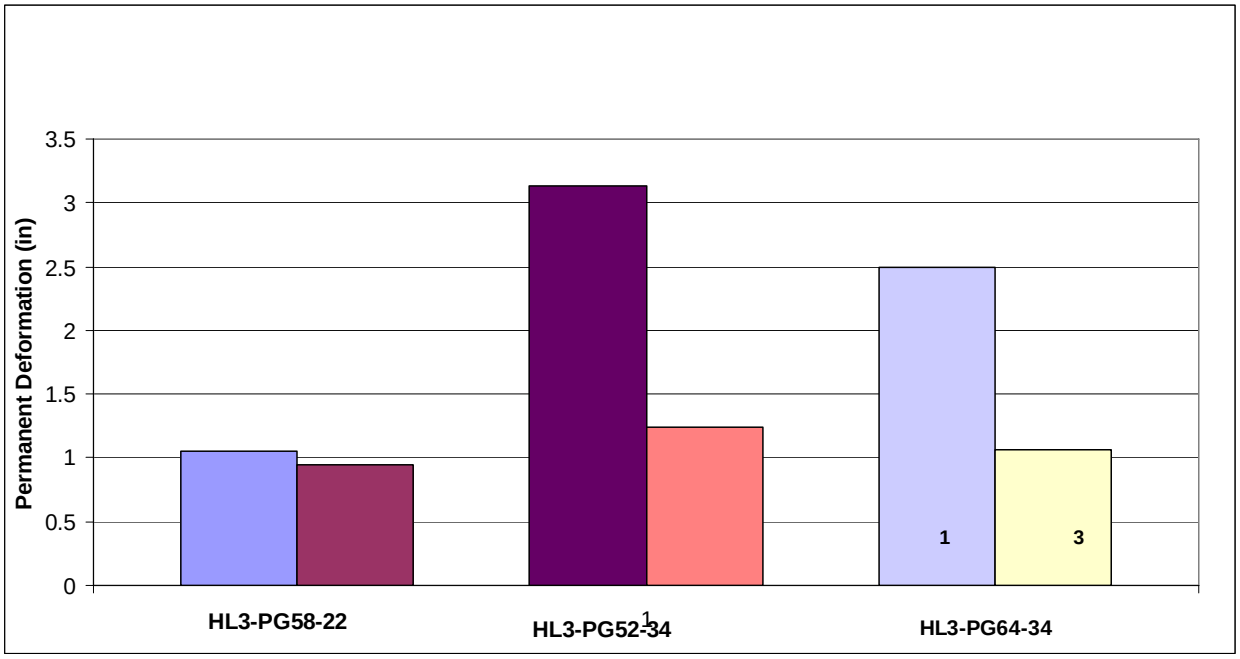

Figure 5.34 Permanent Deformation Prediction Using Levels 1 and Level 3

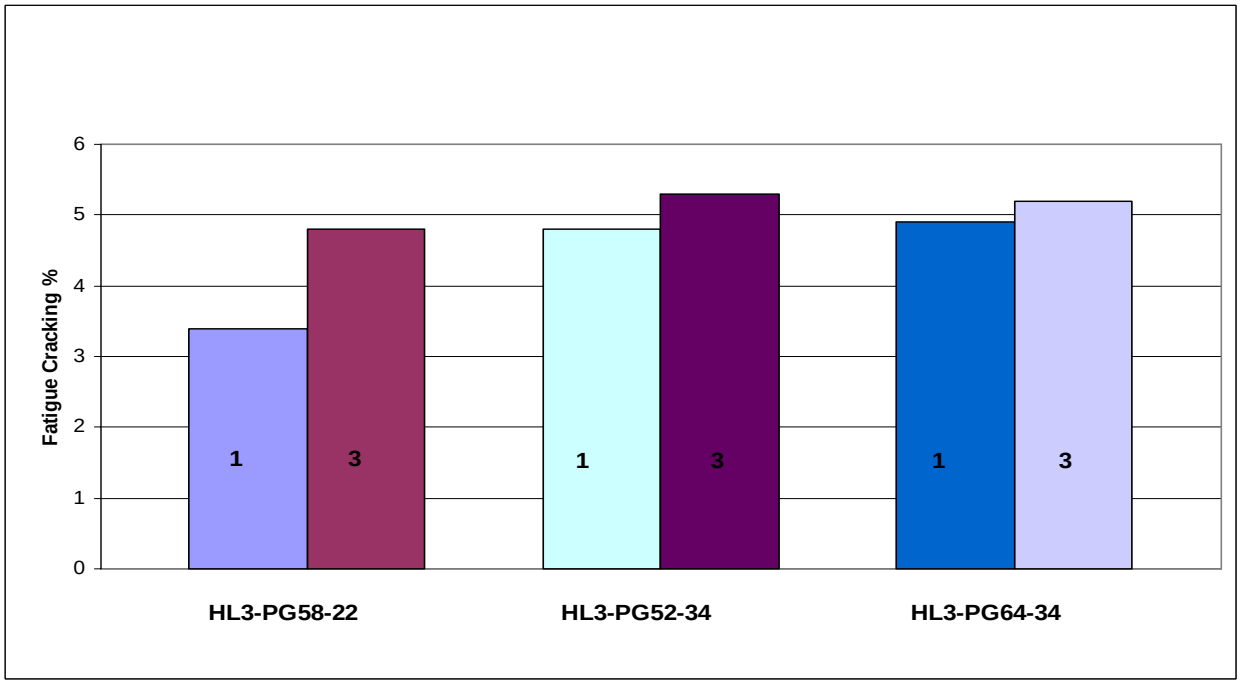

Figure 5.35 Fatigue Cracking Prediction Using Level 1 and Level 3

The difference in pavement performance predictions is apparently due to the accuracy of material properties used in each modeling approaches associated with the two design levels. With level 1 design, the model uses complex modulus values established in the laboratory, determined at relevant temperatures and loading frequencies for the specific mix. Level 3 uses the empirical model incorporated in the Design Guide to calculate the dynamic modulus of AC mix using physical properties as outlined in Equation 4.1[47].

5.11 Measured vs. Predicted Dynamic Modulus

The substantial difference in performance predictions between Level 1 and 3 was discussed in the previous subsection looking into the difference between dynamic modulus measured in the laboratory and that estimated by the prediction equation used in Level 3. The dynamic modulus values were determined in the laboratory simulating cold, moderate and warm operating temperatures. The selected loading frequencies (0.1, 1 and 20 Hz) represent slow, medium and high speeds. The ability of the dynamic modulus to discriminate between two mixes prepared with uniquely different binder types (PG 64-34 and PG 58-22) is demonstrated in Figure 5.36. The response of the engineered binder (PG 64-34), compared with the neat binder, suggests the objectives set for the binder design, aimed at reducing its brittleness at low temperatures to minimize the potential for cracking, are fulfilled. The measured dynamic modulus of the HL3 mix prepared with a PG 64-34 binder is half that prepared with a PG 58-22 binder (see Figure 5.36). However, both binders produced similar dynamic modulus values at relatively high temperatures, reinforcing the widely accepted role played by the aggregate skeleton at such a temperature condition.

The level 3 inputs (mix gradation and binder type) pertaining to the same mixes were entered in the model to estimate the dynamic modulus using the empirical predictive equation incorporated in the model. Dynamic modulus values predicted for the different temperatures for the two binders are shown in Figure 5.36. The predictive equation managed to correctly rate the mix response at low temperatures as influenced by the properties of the two binders. However, the predictive equation was less successful in quantifying the difference between the two binders as measured in the laboratory using the complex modulus test. The predicted responses of the two binders suggest a difference of less than 10% whereas the measured response reflected a difference of 100%.

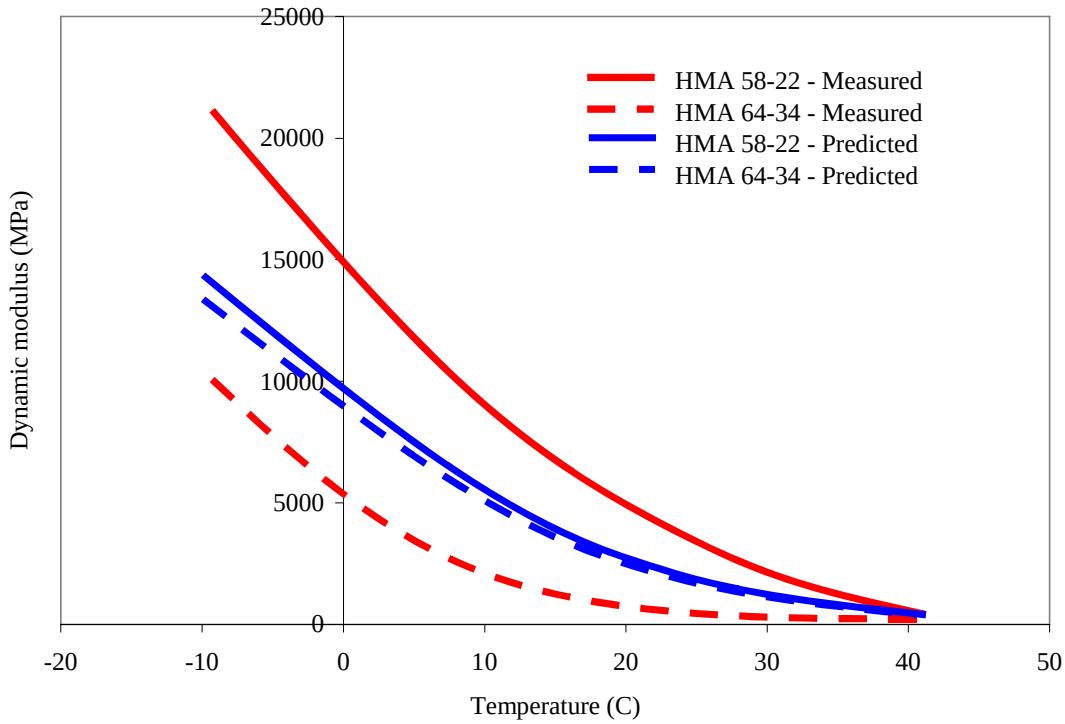

Figure 5.36 Measured and Predicted Modulus for Two HL3 Mixes with Different Binders

Data points representing all mixes examined in this study produced using the predictive equation and laboratory measurements were plotted in Figure 5.37. A comparison between the two approaches represents an excellent opportunity to evaluate the ability of the predictive equation to estimate the dynamic modulus, at least for the specific mixes used in the study. Comparison between estimated and measured values was conducted by examining the distribution of data points along the equality line drawn at 45^{o}. Points located above this line indicate the equation over-predicted the dynamic modulus value and those below suggest under-prediction. Actual co-ordinates of data points (measured and predicted) were used in this study to quantify the deviation of predicted values from those measured in the laboratory at specific conditions associated with speed and temperature. Lines that represent different percentages of deviations from the equality line were used to highlight deviation observed under the different conditions. The results plotted in Figure 5.37 show that the predictive equation over-estimated the value of the dynamic modulus under conditions of relatively high temperature and low loading frequency (low speed). These conditions are marked in Figure 5.37 at measured dynamic modulus values lower than 5000 MPa. The deviation reached as high as 300% under these conditions. Data for measurements made above the 5000 MPa modulus value are scattered above and below the equality line with prevalence of over-estimation, which reached as high as 100%. The average percent error calculated considering all data points produced by the predictive equation was 77%.

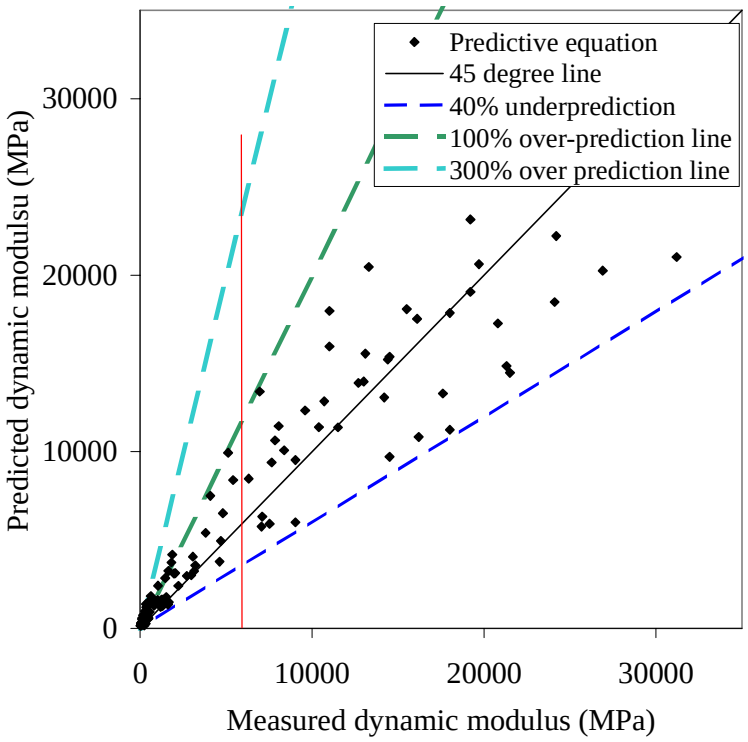

Figure 5.37 Predicted vs. Measured Dynamic Modulus

5.12 Unbound Materials Inputs for Level 1 and 3

The need for considering non-linear material behaviour in unbound materials is as important as the case in AC materials. The results of pavement analysis using linear elastic approximations of unbound material behaviour are no longer acceptable in pavement analysis. Errors from such approximations have been noted and documented [48]. Dependency of the response on the state of stress in soil-based materials must be considered for effective analysis of road pavements. Repeated load resilient modulus test has been recommended as the primary characterization method for unbound materials in the proposed AASHTO Design Guide.

Different levels of input are incorporated in the proposed Guide as a mean for obtaining the resilient modulus of unbound layers. Level 1 resilient modulus is determined from laboratory testing of representative material samples. Two standard test methods are recommended in the Guide (NCHRP 1-28A and AASHTO 307). Results of the laboratory test are used to determine the non-linear elastic coefficients and exponents of the modified universal model [21] described by Equation 2.9.

Currently, no access has been offered in the model to Level 1 input and, hence, no evaluation has been performed in this study to examine the proposed characterization of unbound materials at this level. At Level 2 inputs, the resilient modulus may be estimated using certain correlations established in the model between the resilient modulus and physical material properties, such as the CBR, R-value. At Level 3 inputs, typical resilient modulus values and ranges are recommended based on AASHTO and unified soil classifications.

In the absence of laboratory resources for conducting the resilient modulus, Canadian users of the proposed Guide are expected to rely on Levels 2 and 3. The effectiveness of the approach base on using physical properties as indicators of the expected mechanical response of unbound materials was evaluated in this study. The study examined two granular materials (A and B), which were tested in the laboratory using standard AASHTO techniques for evaluation of physical and mechanical properties. Relevant properties for the two materials, considered suitable for the construction of a base course, are shown in Table 4.10. Based on the determined physical properties, these materials are classified as A-1-a according to AASHTO specifications. Using input level 3 and entering the material class, one resilient modulus range will be proposed. Commonly, users are expected to select the average of the two limits. However, laboratory experiments conducted in this study revealed that the measured resilient modulus of the two materials differed substantially from the recommended average (see Table 4.10). Actually, the measured modulus of the two materials was found to be outside the proposed range, one above and one below the two limits.

To highlight the impact of the difference between the measured and recommended modulus, the software of the proposed AASHTO Design Guide was used to predict performance levels associated with the four different moduli. Base rutting and bottom-up fatigue cracking were selected as the performance criteria for the software applications. Base rutting predictions are shown in figures 5.38 and 5.39. Base rutting predictions were

different for the different modulus values used as input. The application of the two resilient moduli limits proposed in the guide resulted in the prediction of relatively low rutting, which is similar for both materials. However, the application of the modulus measured in the laboratory for Granular A resulted in a base rutting magnitude that is 25% higher than that produced based on applying modulus values estimated by the guide (see Figure 5.38).

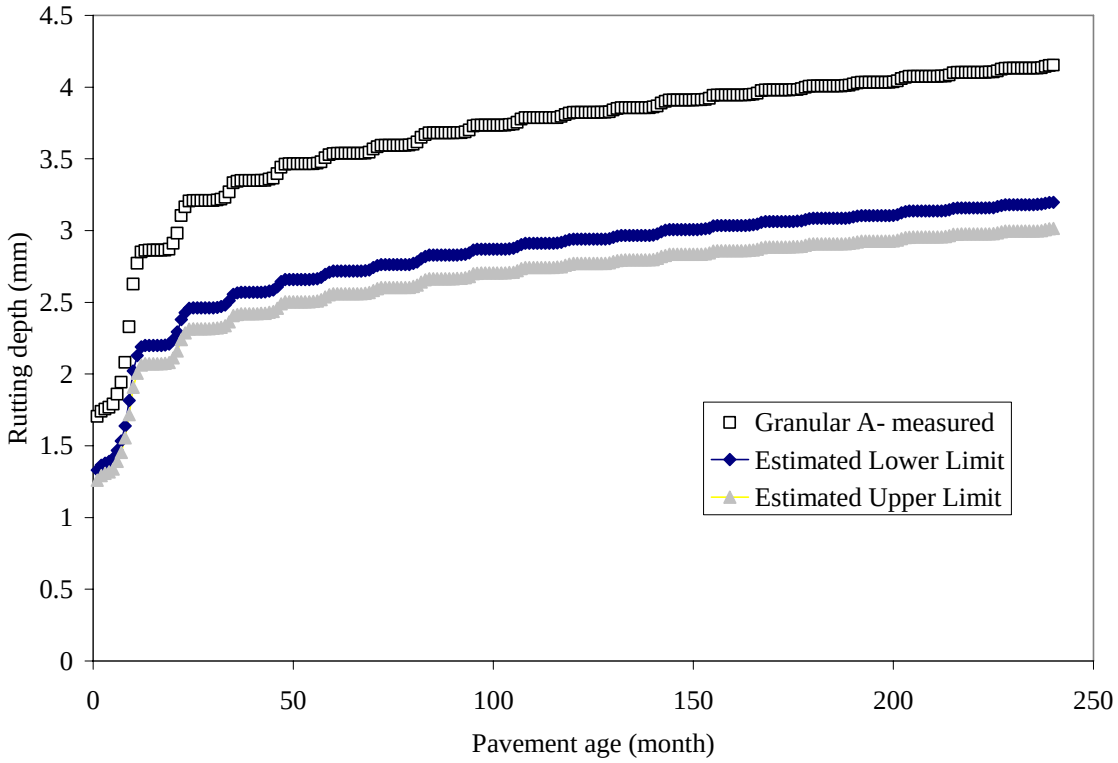

Figure 5.38 Base Rutting for Granular A

Similarly, the application of the modulus measured in the laboratory for Granular B resulted in a granular base course rutting that is 20% lower than that produced based on applying modulus values estimated by the guide (see Figure 5.39). Accordingly, it possible to conclude that reliance on the AASHTO classification to estimate the resilient modulus, as suggested in the proposed Guide, may under- or over-estimate permanent deformations.

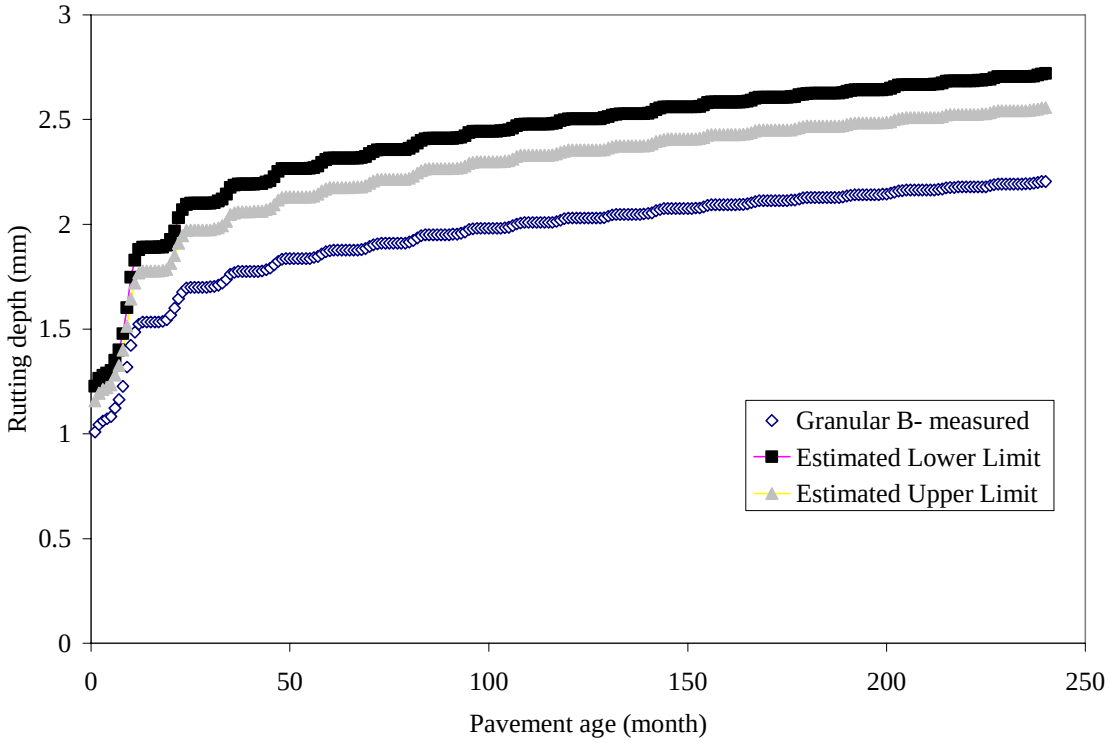

Figure 5.39 Base Rutting for Granular B

Similarly, analysis based on another performance criteria, namely fatigue cracking, produced high error rates when resilient modulus values estimated by the proposed Design Guide were used instead of actual values measured in the laboratory (see figures 5.40 and 5.41). For granular A, an under-estimation of 45% was predicted (see Figure 5.40) and for granular B and over-estimation of 77% was noted (see Figure 5.41).

In summary, the application of Level 3 to predict performance may produce erroneous results and lead to under or over design of unbound pavement layers. A research project, currently underway at the NRC, is pursuing an alternative approach based on using generic material properties and applying level 1 instead of Level 3 which relies on the predictive equation. These generic values may be produced using a limited number of tests performed on typical materials used locally.

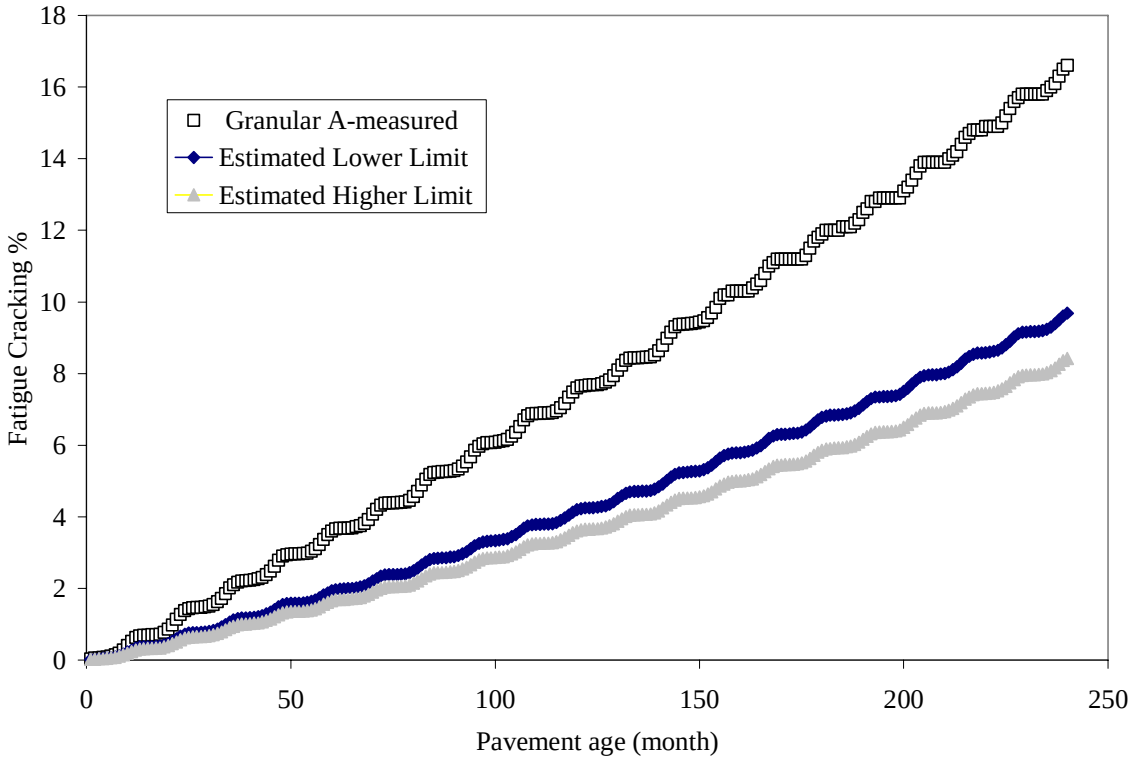

Figure 5.40 Fatigue Cracking for Granular A

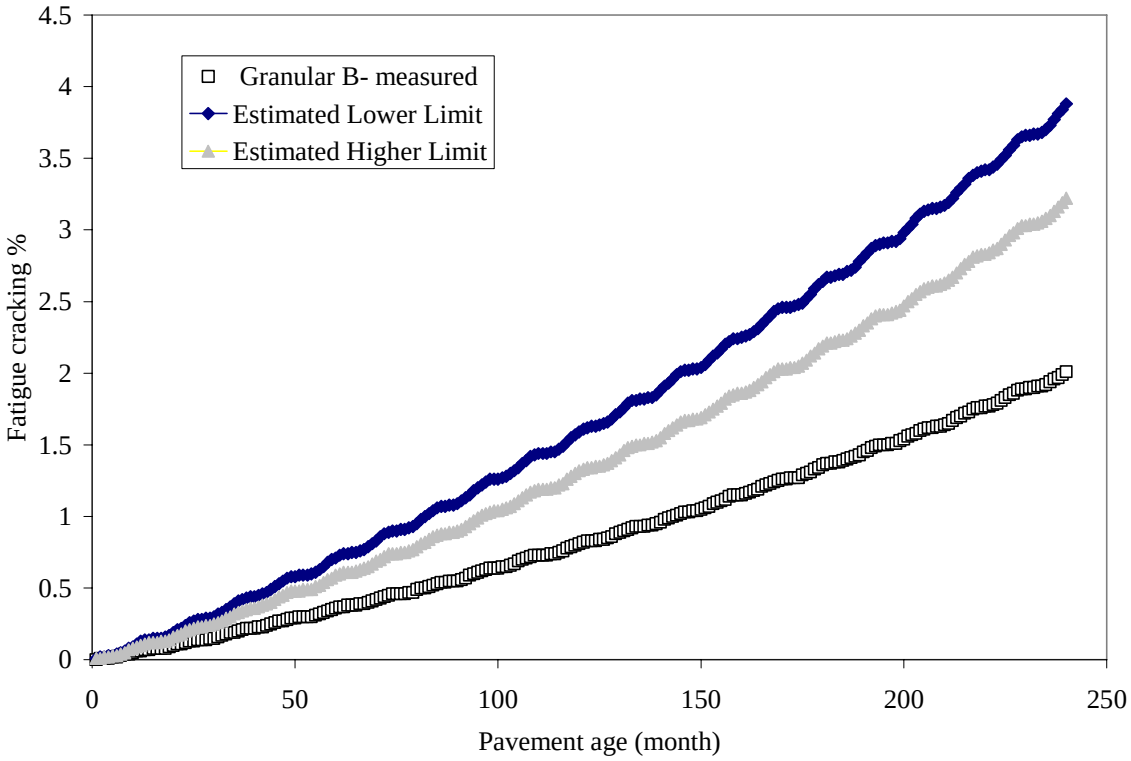

Figure 5.41 Fatigue Cracking for Granular B

CHAPTER 6

Conclusions and Recommendations

The proposed AASHTO Design Guide represents a radical change in the way pavements are analyzed and designed. The implementation of mechanistic principles in parts of the analytical model promotes design based on a relatively accurate assessment of the state of stresses and strains, compared with earlier versions of AASHTO guides. However, this first attempt at producing a mechanistic approach will require further improvements to produce reliable design solutions and to address user expectations related to a variety of issues encountered by road engineers.

(a) The structure module still relies on linear elastic analysis in contrast to typical field observations suggesting that the response is viscoelastic/plastic in nature. With the implementation of linear elasticity, it will not be possible to predict mechanistically components of the strain that translate into permanent deformations (rutting and cracking). The proposed model performs structural analysis to determine the elastic response and then proceeds to estimate the magnitude of various distress types, using empirical performance prediction models. Verification of the accuracy of the different modules and their calibration will take considerable time. However, the design of the software, which involves separate modules for the different functions, will make it easy to replace those proven inaccuracies with improved versions.

(b) Evaluation of the structural model was not possible in this study, because the calculated stresses and strains were not displayed in the current beta version of the proposed AASHTO 2002 model.

(c) Although the design software refers to a finite element model for capturing non-linear response of unbound pavement layers, the current version is blocked, because of some adjustment proposed by the reviewers of the beta version. Accordingly, Level 1 inputs were used for AC and only Level 3 inputs for unbound materials were used in this study. Results of model runs performed in this study to evaluate the sensitivity of the proposed Design Guide to variations in parameters with a known impact on performance, reflect the following.

- Model applications for predicting permanent deformation, as the performance criteria to be used in selecting a design proved to be effective for AC layers and showed sensitivity to the thickness of the AC layer and to the mix stiffness associated with the binder used in manufacturing the AC mix. They also responded clearly to changes in traffic volume and operating speed. Construction related parameters, such as the percent of air voids in the mix and effective binder contents are effective in input Level 3 rather than Level 1. The predictive equation used in Levels 2 and 3 included the percent of air voids and the mix effective binder contents parameters as direct inputs that contribute to the determination of the dynamic modulus. Accordingly, Level 1 applications should be complemented

by laboratory tests performed on samples prepared at the as built air voids content and effective binder content.

- Apparently, the model is less successful in addressing analysis requirements related to unbound materials. The model lacks sensitivity toward variations made in this study to parameters known to influence performance, such as the base course depth and the resilient modulus, where model predictions of permanent deformation showed little or no effect.

  The use of nonlinear analysis is recommended in mechanistic-based models to capture the real behaviour of unbound materials. The performance of the model is expected to improve when the nonlinear behaviour of unbound materials is included in the analysis and the model recalibrated to local conditions taking into consideration the contribution of field individual layers to the total permanent deformation.

  The NRC is performing R&D program involving modifications to the current AASHTO resilient modulus test protocol geared toward developing a process for modeling permanent deformation of unbound materials. Future research effort is expected to incorporate AC viscoelastic behaviour and permanent deformation in the structural model and reduce dependency on the empirical models included in the proposed Design Guide.

- Sensitivity to climatic conditions has been demonstrated in the higher rutting accumulated in warm regions compared with relatively cold regions.
- The model proved sensitive to variables with known influence on the resistance of AC mixes to fatigue cracking. This type of fatigue related damage is well defined in the literature and most models use an approach similar to that adopted in the proposed Guide.
  However, it is essential to calibrate carefully the transfer function by applying appropriate calibration parameters so the predicted distress can match field observations. Such a process will be needed in the calibration of the proposed Guide.

- Additional research is needed to address issues related to fatigue top-down cracking and for the development of mechanistic based models to replace the one currently incorporated in the Design Guide. Construction related variables should be studied to quantify their contribution to the deterioration of pavement structures. It is necessary to identify the effects of relevant construction practices, in particular compaction methods, as potential factors that influence the evolution of pavement cracking.
- Research is needed to address issues related to reflection cracking and to develop mechanistic-based models for use in the Design Guide. Such an approach will improve analysis and design of HMA overlays.
- Considering the fact that current testing facilities are not capable of satisfying requirements of the resilient modulus and dynamic modulus tests, users of the model will rely mainly on level 3 inputs for both the AC and unbound materials.

Because of the approximate nature of the mechanistic response used in Level 3, which predicts the modulus using physical properties, the results of the evaluation highlight the importance of using a well-executed material characterization process (Level 1) to the success of the proposed AASHTO Design Guide. The following conclusions are based on the results of the evaluation performed in this study.

- The model reflected sensitivity to variation in AC mix types with unique physical and mechanical properties. Performance predictions produced using the proposed AASHTO Design Guide while using laboratory-measured dynamic modulus values as input Level 1 are in agreement with performance patterns established by the current practice and those reported in the literature.
- However, AC dynamic modulus estimates made using the predictive equation incorporated in the Guide proved to be substantially different from the measured values. The average percent error calculated considering data produced by the predictive equation vs. measured dynamic modulus amounted to 77%. The error in estimating the modulus (input Level 3) led to underestimation of accumulated damage related to permanent deformation by 10% to 60% depending on the binder used in the mix, which consequently results in undersigning the road structure.
- Similarly, input Level 3 for unbound materials, mainly based on the correlation between physical properties (including the AASHTO classification) and the resilient modulus, produced unreliable values when compared with actual measurements made in the laboratory. Applications based on a modulus estimate obtained using the Guide proposed values to run the software resulted in substantially different performance predictions compared with those produced using measured modulus values. This study has shown a difference that ranges from -20% to +25% in the prediction of unbound layer rutting.

It is highly recommended to use a laboratory-measured dynamic modulus as the first choice. However, in the absence of adequate facilities and enough expertise for conducting the tests necessary to measure the required mechanical properties, reliance will be on performing design exercises using input Levels 2 and 3. To produce more reliable pavement design solutions using these two levels, this study proposes a scheme for building a database (Material Library) for potential Canadian users of the proposed Guide. The Library may be populated with generic dynamic modulus values of local AC mixes and resilient moduli of commonly used unbound materials. Implementation of such generic properties in running the proposed design software will result in lower design errors compared with those produced using moduli estimated from correlations established for the proposed Guide. These minor errors associated with the use of generic properties may be minimized by introducing additional results to the database from tests performed on possible local alternatives that reflect variations in the real practice.

(d) The accuracy of distress prediction models depends on effective calibration and validation using reliable sources of data. The review of the calibration studies associated with the models incorporated in the Guide has been impeded by the lack of required information in the LTPP as well as the CSHRP sections. It is imperative to plan and identify data needs to calibrate and validate mechanistic-based models and utilize advanced instrumentation to monitor the performance of individual pavement layers.

REFERENCES:

1. Statistic Canada Agency, "*Local Government Financial Management Statistics-Capital Expenditures*", Index 1733, 2003.
2. David Croney, Paul Croney. Design and Performance of Road Pavements, Mc-Graw Hill.
3. Belgian Road research Center, "Advanced Models for Analytical Design of European Pavement Structure"
4. Guide for Mechanistic-Empirical Design of New and Rehabilitated Pavement Structures – AASHTO 2002. American Association of State Highway and Transportation Officials, Washington, D.C.
5. The Asphalt Institute, "*Thickness Design, Asphalt Pavements for Highways and Streets*" Manual Series No 1, The Asphalt Institute, Lexington, KY,1991.
6. National Crushed Stone Association, "Flexible *Pavement Design Guide for Highways*", NCSA Publication, Washington D.C., 1972.
7. Department of Transportation U.S.,"*AASHO Interim Guide for the Design of Rigid and Flexible Pavements*" published by the American Association of State Highway officials, Washington D.C. 1961
8. Department of Transportation, U.S.,"*AASHTO Interim Guide for the Design of Pavement Structures*" published by the American Association of State Highway and Transportation officials, Washington D.C. 1972
9. Department of Transportation, U.S.,"*AASHTO Guide for the Design of Pavement Structures*" published by the American Association of State Highway and Transportation officials, Washington D.C. 1986
10. Department of Transportation, U.S., "AASHTO Guide for Design of Pavement Structures (1993)". American Association of State Highway and Transportation Officials, Washington, D.C. 1993
11. Transportation Association of Canada (TAC), Canadian Strategic Highway Research Program (C-SHRP), "Pavement Structural Design Practices Across Canada" , C-SHRP Technical Brief No. 23, Ottawa, Ontario, April2002.
12. Asphalt Institute, "SuperPave Mix Design Manual", SuperPave Series No. 2 (SP-2), 3rd Edition, 2001.
13. The Asphalt Institute, "Mix Design Methods for Asphalt Concrete and Other Hot-Mix Types", Manual series No. 2 (MS-2) 6th edition 1997.
14. Mase, George Thomas. "Continuum Mechanics for Engineers", CRC Press, 2nd edition
15. Charles W. Schwartz (2005). *Evaluation of the Witczak Dynamic Modulus Prediction Model*. TRB Annual meeting 2005.
16. Hopman, P.C, "VEROAD: A Viscoelastic Multilayer Program", 75th TRB meeting, Transportation Research Record 1539, Washington D.C. USA, 1996, pp. 72-80.
17. Sayegh, G. 1967. Viscoelastic Properties of Bituminous Mixtures. *Proceedings of the 2nd International conference on structural design of asphalt pavement*, pp. 743-755. Held at Rackham Lecture Hall, University of Michigan, Ann Arbor, USA

18. Hopman, P.C, "VEROAD: A viscoelastic multilayer program", 75th TRB meeting, Transportation Research Record 1539, Washington D.C. USA, 1996, pp.72-80.

19. Design Guide Documentation. Appendix HH Field Calibration of the Thermal Cracking Models.

20. A.P. S. Selvadurai. *Elastic Analysis of Soil Foundation Interaction*". Elsevier Scientific Publishing Company, New York, 1979- ISBN 0-444-41663-3 (vol.17).

21. Dragos Andrei, Mathew W. Witzack, Charles W.Schwartz, and Jacob Uzan. *Harmonized Resilient Modulus Test Method for Unbound Pavement Materials.* Transportation Research record: Journal of the Transportation Research Board, No. 1874, TRB, National Research Council, Washington, D.C., 2004, pp.29-37

22. Witzack, M. W., and J. Uzan. The universal Airport Design System, Report I of IV: Granular Material Characterization. Department of Civil Engineering, University of Maryland, College Park, 1988.

23. Yang H. H. *Pavement Analysis and Design.* Prentice Hall, Englewood Cliffs, New Jersey 1993.

24. American Association State Highway and Transportation Officials (AASHTO), "Resistance to Plastic Flow of Bituminous Mixtures Using Marshall Apparatus", AASHTO Designation: T245.

25. Ontario Ministry of Transportation (MTO), Ontario Provincial Standard Specification, OPSS 1149-1152, Ottawa, Ontario, July 1990

26. American Association State Highway and Transportation Officials (AASHTO), "Short and Long Term Aging of Hot Mix Asphalt", AASHTO Designation: PP2

27. American Society for Testing and Materials (ASTM), "Standard Test Method for Dynamic Modulus of Asphalt Mixtures", ASTM D3497-79 (1995)

28. American Association State Highway and Transportation Officials (AASHTO), "Standard Method of Test for Bulk specific gravity of Compacted Bituminous Mixtures Using Saturated Surface-Dry Specimens", AASHTO Designation: T166-94

29. American Association State Highway and Transportation Officials (AASHTO), "Standard Method of Test for Theoretical Maximum specific gravity and Density of Bituminous Paving Mixtures", AASHTO Designation: 269-97

30. American Society for Testing and Materials. "ASTM D 2493 Viscosity-Temperature Chart for Asphalts," *1998 Annual Book of ASTM Standards*, Vol. 0.403, pp. 230-234.

31. American Association State Highway and Transportation Officials (AASHTO), "Classification of Soils and Soil-Aggregate Mixtures for Highway Construction Purposes", AASHTO Designation: M 145

32. Design Guide Documentation. Appendix II Calibration of Fatigue cracking models for flexible pavements.
33. Interim Report: Chapters 1 and 2, NCHRP 1-42: Top-Down Fatigue Cracking of Hot –Mix Asphalt Layers. Advanced Asphalt Technologies, LLC. May 27,2004
34. Design Guide Documentation. Appendix HH Field Calibration of the Thermal Cracking Models.
35. Waldhoff, A.S., Buttlar, W.G., and J. Kim "Evaluation of Thermal Cracking at Mn/ROAD Using the Superpave IDT, *Proceeding of the Canadian Technical Asphalt Association*, 45th Annual Conference, Winnipeg, Manitoba, Polyscience Publications, Inc., Laval, Quebec, Canada, pp. 228-259, 2000.
36. Abd El Halim, A. O. 1986. Experimental and Field Investigation of the Influence of Relative Rigidity on the Problem of Reflection Cracking. For presentation and publication at the 1986 TRB Annual Conference, Washington, D.C. U.S.A.
37. Abd El Halim, A. O. (1985). "Influence of relative rigidity on the problem of reflection cracking." Transportation Research Record 1007, Transportation Research Board, Washington, D.C., 53- 58
38. Abd El Halim, A. O., Phang, W., and Hass, R.C. (1987). "Realizing structural design objectives through minimizing of construction induced cracking." Proc., 6th Int. Conference on Structural Design of Asphalt Pavements, Univ. of Michigan, Ann Arbor, Mich., Vol 1, 965-970.
39. Abd El Halim, A. O., Ralf Haas "Process and case illustration of construction Innovation" Journal of construction Engineering and management ASCE/July/August 2004
40. Abd El Halim, A. O., Ralf Haas "Process and case illustration of construction Innovation" Journal of construction Engineering and management ASCE/July/August 2004
41. Zubair Ahmed, Ivana Marukic, Sameh Zaghloul, Nick Vitillo, " Validation of Enhanced Integrated Climatic Model Predictions Using New Jersey Seasonal Monitoring Data" TRB 84th annual Meeting- January,2005.
42. Design Guide Documentation. Appendix GG- Calibration of Permanent Models for Flexible Pavements.
43. Walaa E.I. Khogali and ElHussein H. Mohamed. "*Novel Approach for Characterization of Unbound Materials"*. Transportation Research record: Journal of the Transportation Research Board, No. 1874, TRB, National Research Council, Washington, D.C., 2004, pp.38-46
44. Design Guide Documentation. Appendix II Calibration of Fatigue cracking models for flexible pavements.
45. Yang H. Huang (1993). Pavement Analysis and Design. Prentice-Hall, Inc, New Jersey
46. Asphalt Institute. 1991. Thickness Design – Asphalt Pavements for Highways and Streets. Manual Series No.1 (MS-1), Lexington, KY.

47. O.A. Fonseca and M.W. Witczak, “A Prediction Methodology for the Dynamic Modulus of In Place Aged Asphalt Mixture”, Journal of the Association of Asphalt Paving Technologist, vol. 65,1996, pp. 532-565.

48. “*Assessing Pavement Layer Condition Using Deflection Data*”, (NCHRP 10-48), Transportation Research Board, Lockbox 289, Washington, DC 20055.

APPENDIX A

Asphalt Concrete and Unbound Materials Inputs and Related Tests Specifications

Asphalt Mix					Structure Layer 1 – Asphalt Concrete
Property	**Data Input Level**			*cedure*	
	1	2	3		
Gradation		ret ¾"; $^3/_8$"; #4; pass #200	ret ¾"; $^3/_8$"; #4; pass #200	AASHTO T30	
Stiffness Master Curve	E*			AASHTO TP62	
Asphalt Binder					
Property	**Data Input Level**			*Procedure*	
	1	2	3		
Performance Binder	Test Result	Test Result		AASHTO T315	
Conventional Binder					
Viscosity	Test Result	Test Result		AASHTO T201, T202, T316	
Penetration	Test Result	Test Result		AASHTO T49	
Specific Gravity	Test Result	Test Result		ASTM D 70	
Softening Point	Test Result	Test Result		ASTM D 36	
Performance Grade			A & VTS	Select Grade	
Viscosity Grade			A & VTS	Select Grade	
Penetration Grade			A & VTS	Select Grade	
Property	**Data Input Level**			*Procedure*	
	1	2	3		
Poisson's Ratio	Calculated	Calculated	Calculated	M-E Design Guide	
Vbe	Calculated	Calculated	Calculated	AASHTO R 35	
Va	Test Result	Test Result	Test Result	AASHTO T269	
Unit Weight	Test Result	Test Result	Test Result	AASHTO T166	

Thermal Conductivity	Test Result			ASTM E 1952	
Heat Capacity	Test Result			ASTM D 2766	
Thermal Cracking					
Property	**Data Input Level**			*Procedure*	
Indirect Tension	@ 3 temps	@ 1 temp	Defaults	AASHTO T322	
Mix Coefficient of Thermal Contraction					
VMA	Test Result	Test Result	Test Result	AASHTO R35	
Aggregate CTC	Test Result	Test Result	Test Result	ASTM D4535	

Level 1					
Structure	**Drainage & Surface Property**	**Property**	**Test**	**Procedure**	**Typical Range of Values**
		Surface Shortwave Absorptivity	n/a	Weathered Asphalt Pavement New Asphalt Pavement	0.80 – 0.90 **0.90 – 0.98**
	Asphalt Concrete Layer	**Asphalt Mix**			
		Property	**Test**	**Procedure**	**Typical Range of Values**
		Master Stiffness Curve	Dynamic Modulus (E*)	AASHTO TP 62-03	Varies
		Asphalt Binder			
		Property	**Test**	**Procedure**	**Typical Range of Values**
		Performance Binder	G* & δ, after RTFO	AASHTO T 315	AASHTO M 320
		Conventional Binder	Viscosities	AASHTO T 201, T 202, T 316 or ASTM D4402	AASHTO M 226
			Penetration	AASHTO T 49	AASHTO M 20
			Specific Gravity	ASTM D70	Varies
			Softening Point	ASTM D36	Varies

		Asphalt General			
		Property	**Test**	**Procedure**	**Typical Range of Values**
		Poisson's Ratio	Calculation	M-E Software	0.15 - .50
		Vbe	Calculation	AASHTO R 35	Varies
		Va	Air Voids in Compacted HMA	AASHTO T 269	Varies
		Unit Weight (γ)	Gmb * 62.4	AASHTO T 166	Varies
		Thermal Conductivity	HMA Thermal Conductivity	ASTM E 1952	0.67 BTU/hr-ft-ºF
		Heat Capacity	HMA Heat Capacity	ASTM D2766	0.23 BTU/lb-ºF
	Thermal Cracking	**Property**	**Test**	**Procedure**	
		Indirect Tension Tests	Creep & Strength	AASHTO T 322 @ 3 temps	Varies
		Mix Coefficient of Thermal Contraction	VMA Aggregate CTC	AASHTO R 35 ASTM D 4535	Varies 21 to 37 /^{o}C
Level 2					
Structure	**Drainage & Surface Property**	**Property**	**Test**	**Procedure**	**Typical Range of Values**
		Surface Shortwave Absorptivity	n/a	Weathered Asphalt Pavement New Asphalt Pavement	0.80 – 0.90 **0.90 – 0.98**
	Layer	**Asphalt Mix**			
		Property	**Test**	**Procedure**	**Typical Range of Values**
		Aggregate Gradation	ret 3/4"; ret 3/8"; ret #4; pass #200	AASHTO T 30	Varies
		Asphalt Binder			
		Property	**Test**	**Procedure**	**Typical Range of Values**
		Performance Binder	G* & δ, after RTFO	AASHTO T 315	AASHTO M 320
		Conventional Binder	Viscosities	AASHTO T 201, T 202, T 316 or ASTM D4402	AASHTO M 226

			Penetration	AASHTO T 49	AASHTO M 20
			Specific Gravity	ASTM D70	Varies
			Softening Point	ASTM D36	Varies
		Asphalt General			
		Property	**Test**	**Procedure**	**Typical Range of Values**
		Poisson's Ratio	Calculation	M-E Software	0.15 - .50
		Vbe	Calculation	AASHTO R 35	Varies
		Va	Air Voids in Compacted HMA	AASHTO T 269	Varies
		Unit Weight (γ)	Gmb * 62.4	AASHTO T 166	Varies
		Thermal Conductivity	HMA Thermal Conductivity	ASTM E 1952	0.67 BTU/hr-ft-^{o}F
		Heat Capacity	HMA Heat Capacity	ASTM D2766	0.23 BTU/lb-^{o}F
	Thermal Cracking	**Property**	**Test**	**Procedure**	**Typical Range of Values**
		Indirect Tension Tests	Creep & Strength	AASHTO T 322 @ 1 temp	Varies
		Mix Coefficient of Thermal Contraction	VMA Aggregate CTC	AASHTO R 35 ASTM D 4535	Varies 21 to 37 /^{o}C
Level 3					
Structure	**Drainage & Surface Property**	**Property**	**Test**	**Procedure**	**Typical Range of Values**
		Surface Shortwave Absorptivity	n/a	Weathered Asphalt Pavement New Asphalt Pavement	0.80 – 0.90 **0.90 – 0.98**
	Layer	**Asphalt Mix**			
		Property	**Test**	**Procedure**	**Typical Range of Values**
		Aggregate Gradation	ret 3/4"; ret 3/8"; ret #4; pass #200 sieves	AASHTO T30	Varies
		Asphalt Binder			
		Property	**Test**	**Procedure**	**Typical Range of Values**

		Performance Grade	A & VTS	Select Grade	Table 2.2.10
		Viscosity Grade	A & VTS	Select Grade	Table 2.2.11
		Penetration Grade	A & VTS	Select Grade	Table 2.2.12
		Asphalt General			
		Property	**Test**	**Procedure**	**Typical Range of Values**
		Poisson's Ratio	Calculation	M-E Software	0.15 - .50
		Vbe	Calculation	AASHTO R 35	Varies
		Va	Air Voids in Compacted HMA	AASHTO T 269	Varies
		Unit Weight (γ)	Gmb * 62.4	AASHTO T 166	Varies
		Thermal Conductivity	HMA Thermal Conductivity	ASTM E 1952	0.67 BTU/hr-ft-^{o}F
		Heat Capacity	HMA Heat Capacity	ASTM D2766	0.23 BTU/lb-^{o}F
	Thermal Cracking	**Property**	**Test**	**Procedure**	**Typical Range of Values**
		Indirect Tension Tests	Creep & Strength	Default Table 2.2.20	Varies
		Mix Coefficient of Thermal Contraction	VMA Aggregate CTC	AASHTO R 35 ASTM D 4535	Varies 21 to 37 /^{o}C

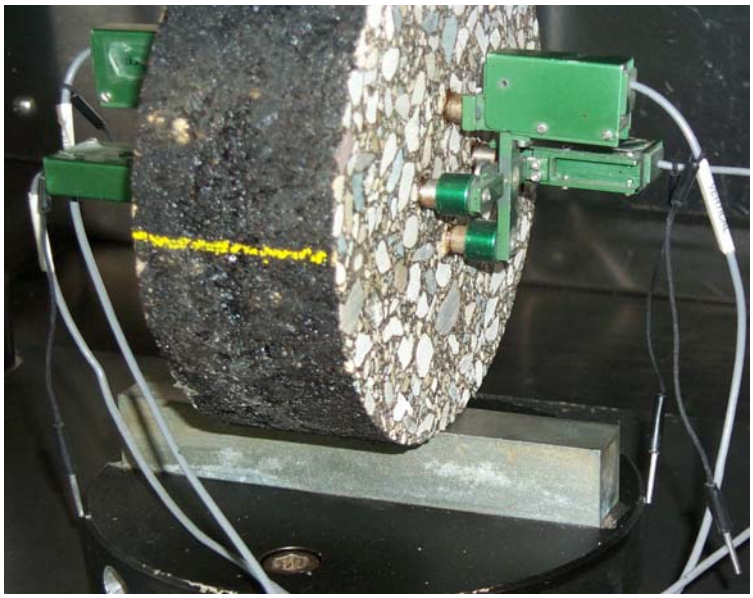

The Indirect Tensile Creep (ITC) test (AASHTO T 315-02, AASHTO T 322-03)

UNBOUND MATERIALS

	AASHTO T 307	NCRHP 1-28A
Loading Device	Electrohydraulic Electro pneumatic Top-Loading, closed loop	Electohydraulic Top-Loading, closed loop
Load Measurement	Electronic load cell located between the actuator and the chamber piston rod inside the triaxial cell	Electronic load cell located inside the triaxial cell
Load shape	Haversine-shaped load pulse	Haversine-shaped load pulse
Strain Measurement	Measured externally Two spring loaded Linear Variable Differential Transducers (LVDT's)	Measured internally Optical extensometer Non-contact sensors Clamps attached to the specimen
Cycle Time	Pneumatic Load Duration - 0.1 sec. Rest period – 0.9 to 3.0 sec	Base/subbbase materials Load Duration – 0.1 sec. Rest period – 0.9 sec.
	Hydraulic Load Duration - 0.1 sec. Rest period – 0.9 to 3.0 sec	Subgrade material Load Duration – 0.2 sec Rest period – 0.8 sec

Types of Materials	Type 1 Materials Untreated granular base/subbase All untreated subgrade soils < 70 % passing No. 10 sieve < 20 % passing No. 200 sieve	Type 1 Materials Unbound granular base/subbase Untreated subgrade Maximum particle size > 3/8”
	Type 2 Materials All materials not meeting Type 1 Thin wall tube samples	Type 2 Materials Unbound granular base/subbase Untreated subgrade Maximum particle size > 3/8” < 10 % passing No. 200 sieve
	N/A	Type 3 Materials Untreated subgrade Maximum particle size <3/8” > 10 % passing No. 200 sieve
	N/A	Type 4 Materials Undisturbed samples
Specimen Compaction	Vibratory Type 1 Soils Type 2 Soils Static Loading Type 2 Soils Kneading Uniform Density Gradient	Type 1 Materials Impact Vibratory Type 2 Materials Vibratory Type 3 Materials Impact Kneading Type 4 Materials (Undisturbed)

Soils and Unbound Material Inputs				
Strength Inputs				
Material Property	**Level**			*cedure*
	1*	2	3	
Resilient Modulus, M_r	X	X	X	AASHTO T307 or NCHRP 1-28A
CBR*		X		AASHTO T193
R-value**		X		AASHTO T190
Layer Coefficient, a_i**		X		AASHTO Guide for the Design of Pavement Structures

PI and Gradation		X		AASHTO T27 and AASHTO T90
Dynamic Cone Penetrometer		X		ASTM D 6951
Soil Classification			X	AASHTO M 145 Or ASTM D2487

* Level 1 Resilient Modulus Testing is only applicable for new asphalt pavement design.
** Only one of the five properties (CBR, Layer Coefficient, etc) is needed for Level 2.

Level 2 Correlation Equations:

Strength/Index Property	Model	Comments
CBR	$M_r = 2555(CBR)^{0.64}$	CBR = California Bearing Ratio, percent
R-value	$M_r = 1155 + 555R$	R = R-value
AASHTO layer coefficient	$M_r = 30000\left(\frac{a_i}{0.14}\right)$	a_i = AASHTO layer coefficient
PI and gradation*	$CBR = \frac{75}{1+0.728(wPI)}$	wPI = P200*PI P200= percent passing No. 200 sieve size PI = plasticity index, percent
DCP*	$CBR = \frac{292}{DCP^{1.12}}$	CBR = California Bearing Ratio, percent DCP =DCP index, mm/blow

Material Group Category	Type Design	Input Level	Description*
Bedrock	New	1-2	• None of these levels are considered applicable for bedrock cc
		3	• User selects typical design values: Solid, Massive Bedrock Typical ranges: 750-2000 ksi Default Value: 1000 ksi Highly Fractured, Weathered Typical ranges: 250-1000 ksi Default Value: 500 ksi
	Rehab	1-2	• None of these levels are considered applicable for bedrock cc
		3	• User selects typical design values: Solid, Massive Bedrock Typical ranges: 750-2000 ksi Default Value: 1000 ksi Highly Fractured, Weathered Typical ranges: 250-1000 ksi Default Value: 500 ksi

Soils and Unbound Material Inputs

Environmental Adjustment Inputs

Material Property	Level		
	1	2	3
Plasticity Index	AASHTO T90	N/A	N/A
Gradation	AASHTO T27	N/A	N/A
Specific Gravity	AASHTO T99 AASHTO T180	Calculated from PI and Gradation	N/A
Maximum Dry Unit Weight	AASHTO T99 AASHTO T180	Calculated from PI and Gradation	Assumed Value
Optimum Moisture Content	AASHTO T99 AASHTO T180	Calculated from PI and Gradation	***N/A***
Saturated Hydraulic Conductivity	AASHT0 T215	Calculated from PI and Gradation	N/A
Degree of Saturation	N/A	Calculated from w_{opt}, $_{dmax}$, G_s	N/A

Appendix B

Typical Analysis Run Using Proposed AASHTO 2002 Design Guide

Project: level1.dgp

General Information

Description:

Design Life	20 years
Base/Subgrade construction:	September, 2004
Pavement construction:	September, 2004
Traffic open:	October, 2004
Type of design	Flexible

Analysis Parameters

Analysis type	Probabilistic

Performance Criteria

	Limit	Reliability
Initial IRI (in/mi)	63	
Terminal IRI (in/mi)	172	90
AC Surface Down Cracking (Long. Cracking) (ft/500):	1000	90
AC Bottom Up Cracking (Alligator Cracking) (%):	25	90
AC Thermal Fracture (Transverse Cracking) (ft/mi):	1000	90
Permanent Deformation (AC Only) (in):	0.25	90
Permanent Deformation (Total Pavement) (in):	0.75	90

Location:		
Project ID:		
Section ID:		
	Principal Arterials - Others	
Date:	13/02/2004	
Station/milepost format:	Miles: 0.000	
Station/milepost begin:		0
Station/milepost end:		10
Traffic direction:	East bound	

Default Input Level

Default input level	Level 3, Default and historical agency values.

Traffic

Initial two-way aadtt:	1000
Number of lanes in design direction:	2
Percent of trucks in design direction (%):	50
Percent of trucks in design lane (%):	95
Operational speed (mph):	25

Monthly Adjustment Factors (Level 3, Default MAF)

Month	Vehicle Class									
	Class 4	Class 5	Class 6	Class 7	Class 8	Class 9	Class 10	Class 11	Class 12	Class 13
January	1.00	1.00	1.00	1.00	1.00	1.00	1.00	1.00	1.00	1.00
February	1.00	1.00	1.00	1.00	1.00	1.00	1.00	1.00	1.00	1.00
March	1.00	1.00	1.00	1.00	1.00	1.00	1.00	1.00	1.00	1.00
April	1.00	1.00	1.00	1.00	1.00	1.00	1.00	1.00	1.00	1.00

May	1.00	1.00	1.00	1.00	1.00	1.00	1.00	1.00	1.00	1.00
June	1.00	1.00	1.00	1.00	1.00	1.00	1.00	1.00	1.00	1.00
July	1.00	1.00	1.00	1.00	1.00	1.00	1.00	1.00	1.00	1.00
August	1.00	1.00	1.00	1.00	1.00	1.00	1.00	1.00	1.00	1.00
September	1.00	1.00	1.00	1.00	1.00	1.00	1.00	1.00	1.00	1.00
October	1.00	1.00	1.00	1.00	1.00	1.00	1.00	1.00	1.00	1.00
November	1.00	1.00	1.00	1.00	1.00	1.00	1.00	1.00	1.00	1.00
December	1.00	1.00	1.00	1.00	1.00	1.00	1.00	1.00	1.00	1.00

Vehicle Class Distribution

(Level 3, Default Distribution)

AADTT distribution by vehicle class

Class 4	1.3%
Class 5	8.5%
Class 6	2.8%
Class 7	0.3%
Class 8	7.6%
Class 9	74.0%
Class 10	1.2%
Class 11	3.4%
Class 12	0.6%
Class 13	0.3%

Hourly truck traffic distribution

by period beginning:

Midnight	2.3%	Noon	5.9%
1:00 am	2.3%	1:00 pm	5.9%
2:00 am	2.3%	2:00 pm	5.9%
3:00 am	2.3%	3:00 pm	5.9%
4:00 am	2.3%	4:00 pm	4.6%
5:00 am	2.3%	5:00 pm	4.6%
6:00 am	5.0%	6:00 pm	4.6%
7:00 am	5.0%	7:00 pm	4.6%
8:00 am	5.0%	8:00 pm	3.1%
9:00 am	5.0%	9:00 pm	3.1%
10:00 am	5.9%	10:00 pm	3.1%
11:00 am	5.9%	11:00 pm	3.1%

Traffic Growth Factor

Vehicle Class	Growth Rate	Growth Function
Class 4	3.0%	Compound
Class 5	3.0%	Compound
Class 6	3.0%	Compound
Class 7	3.0%	Compound
Class 8	3.0%	Compound
Class 9	3.0%	Compound
Class 10	3.0%	Compound
Class 11	3.0%	Compound
Class 12	3.0%	Compound
Class 13	3.0%	Compound

Traffic -- Axle Load Distribution Factors

Level 3: Default

Traffic -- General Traffic Inputs

Mean wheel location (inches from the lane marking):	18
Traffic wander standard deviation (in):	10
Design lane width (ft):	12

Number of Axles per Truck

Vehicle Class	Single Axle	Tandem Axle	Tridem Axle	Quad Axle
Class 4	1.62	0.39	0.00	0.00
Class 5	2.00	0.00	0.00	0.00
Class 6	1.02	0.99	0.00	0.00
Class 7	1.00	0.26	0.83	0.00
Class 8	2.38	0.67	0.00	0.00
Class 9	1.13	1.93	0.00	0.00
Class 10	1.19	1.09	0.89	0.00
Class 11	4.29	0.26	0.06	0.00
Class 12	3.52	1.14	0.06	0.00
Class 13	2.15	2.13	0.35	0.00

Axle Configuration

Average axle width (edge-to-edge) outside dimensions, ft):	8.5
Dual tire spacing (in):	12

Axle Configuration

Single Tire (psi):	120
Dual Tire (psi):	120

Average Axle Spacing

Tandem axle(psi):	51.6
Tridem axle(psi):	49.2
Quad axle(psi):	49.2

Climate

icm file:	C:\DG2002\Projects\dallas.icm
Latitude (degrees.minutes)	32.54
Longitude (degrees.minutes)	-97.02
Elevation (ft)	559
Depth of water table (ft)	30

Structure--Design Features

Structure--Layers

Layer 1 -- Asphalt concrete

Material type: Asphalt concrete
Layer thickness (in): 10

General Properties

General
Reference temperature (F°): 70

Volumetric Properties as Built
Effective binder content (%): 10.5
Air voids (%): 5.9
Total unit weight (pcf): 151

Poisson's ratio: 0.35 (user entered)

Thermal Properties
Thermal conductivity asphalt (BTU/hr-ft-F°): 0.67
Heat capacity asphalt (BTU/lb-F°): 0.23

Asphalt Mix

Number of temperatures: 5
Number of frequencies: 6

Temperature	Mixture E* (psi)					
°F	0.1	0.5	1	5	10	25
15.8	2E+06	2E+06	2E+06	2E+06	3E+06	3E+06
40	752930	1E+06	1E+06	2E+06	2E+06	2E+06
70	164415	259400	319020	512560	645725	846635
100	44810	63095	76300	120730	149020	202140
130	30525	37830	42245	56325	68710	87100

Asphalt Binder

Option: Superpave binder test data

Temperature	Angular frequency = 10 rad/sec	
°F	G*, psi	Delta (°)
59	2605000	49.75
77	572800	55.84
95	120800	62.58
113	23440	69.3
140	3267	77.96

Layer 2 -- A-3

Unbound Material: A-3

Thickness(in): 18

Strength Properties

Input Level: Level 3
Analysis Type: ICM inputs (ICM Calculated Modulus)
Poisson's ratio: 0.35
Coefficient of lateral pressure,Ko: 0.5
Modulus (input) (psi): 29000

ICM Inputs

Gradation and Plasticity Index

Plasticity Index, PI: 0
Passing #200 sieve (%): 10
Passing #4 sieve (%): 80
D60 (mm): 0.2

Calculated/Derived Parameters

Maximum dry unit weight (pcf): 126 (derived)
Specific gravity of solids, Gs: 2.65 (derived)
Saturated hydraulic conductivity (ft/hr): 0.0223 (derived)
Optimum gravimetric water content (%): 9.2 (derived)
Calculated degree of saturation (%): 78 (calculated)

Soil water characteristic curve parameters: Default values

Parameters	Value
a	2.89
b	7.5
c	0.488
Hr.	7.65

Layer 3 -- A-7-6

Unbound Material: A-7-6
Thickness(in): Semi-infinite

Strength Properties

Input Level: Level 3
Analysis Type: ICM inputs (ICM Calculated Modulus)
Poisson's ratio: 0.35
Coefficient of lateral pressure,Ko: 0.5
Modulus (input) (psi): 8000

ICM Inputs

Gradation and Plasticity Index

Plasticity Index, PI: 40
Passing #200 sieve (%): 90
Passing #4 sieve (%): 99
D60 (mm): 0.01

Calculated/Derived Parameters

Maximum dry unit weight (pcf):	82.2 (derived)
Specific gravity of solids, Gs:	2.77 (derived)
Saturated hydraulic conductivity (ft/hr):	3.25e-005 (derived)
Optimum gravimetric water content (%):	28.8 (derived)
Calculated degree of saturation (%):	89.4 (calculated)
Soil water characteristic curve parameters:	Default values

Parameters	Value
a	750
b	0.911
c	0.772
Hr.	47500

Distress Model Calibration Settings - Flexible

AC Fatigue — Level 3 (Nationally calibrated values)

k1	0.0043
k2	3.9492
k3	1.281

AC Rutting — Level 3 (Nationally calibrated values)

k1	-3.449
k2	1.5606
k3	0.4791
Standard Deviation Total Rutting (RUT):	0.1587*POWER(RUT,0.4579)+0.001

Thermal Fracture — Level 3 (Nationally calibrated values)

k1	5
Std. Dev. (THERMAL):	0.2474 * THERMAL + 10.619

CSM Fatigue — Level 3 (Nationally calibrated values)

k1	1
k2	1

Subgrade Rutting — Level 3 (Nationally calibrated values)

Granular:

k1	1.673

Fine-grain:

k1	1.35

AC Cracking

AC Top Down Cracking

C1 (top)	7

C2 (top)	3.5
C3 (top)	0
C4 (top)	1000
Standard Deviation (TOP)	200 + 2300/(1+exp(1.072-2.1654*log(TOP+0.0001)))

AC Bottom Up Cracking

C1 (bottom)	1
C2 (bottom)	1
C3 (bottom)	0
C4 (bottom)	6000
Standard Deviation (TOP)	32.7 + 995.1 /(1+exp(2-2*log(BOTTOM+0.0001)))

CSM Cracking

C1 (CSM)	1
C2 (CSM)	1
C3 (CSM)	0
C4 (CSM)	1000
Standard Deviation (CSM)	CTB*1

IRI

IRI Flexible Pavements with GB

C1 (GB)	0.0463
C2 (GB)	0.0012
C3 (GB)	0.1834
C4 (GB)	0.0038
C5 (GB)	0.0074
C6 (GB)	0.0012
Std. Dev (GB)	0.387

IRI Flexible Pavements with ATB

C1 (ATB)	0.01
C2 (ATB)	0.0005
C3 (ATB)	0.0024
C4 (ATB)	18.36
C5 (ATB)	0.9694
Std. Dev (ATB)	0.292

IRI Flexible Pavements with CSM

C1 (CSM)	0.0073
C2 (CSM)	0.0765
C3 (CSM)	0.0001
C4 (CSM)	0.0084
C5 (CSM)	0.0002
Std. Dev (CSM)	0.229

Project: level1.dgp
Reliability Summary

Performance Criteria	Distress Target	Reliablity Target	Distress Predicted	Reliability Predicted	Acceptable
Terminal IRI (in/mi)	172	90	148.7	82.52	Fail
AC Surface Down Cracking (Long. Cracking) (ft/500):	1000	90	2.3	98.02	Pass
AC Bottom Up Cracking (Alligator Cracking) (%):	25	90	0.4	99.999	Pass
AC Thermal Fracture (Transverse Cracking) (ft/mi):	1000	90	1	99.999	Pass
Permanent Deformation (AC Only) (in):	0.25	90	0.52	1.05	Fail
Permanent Deformation (Total Pavement) (in):	0.75	90	0.79	39.65	Fail

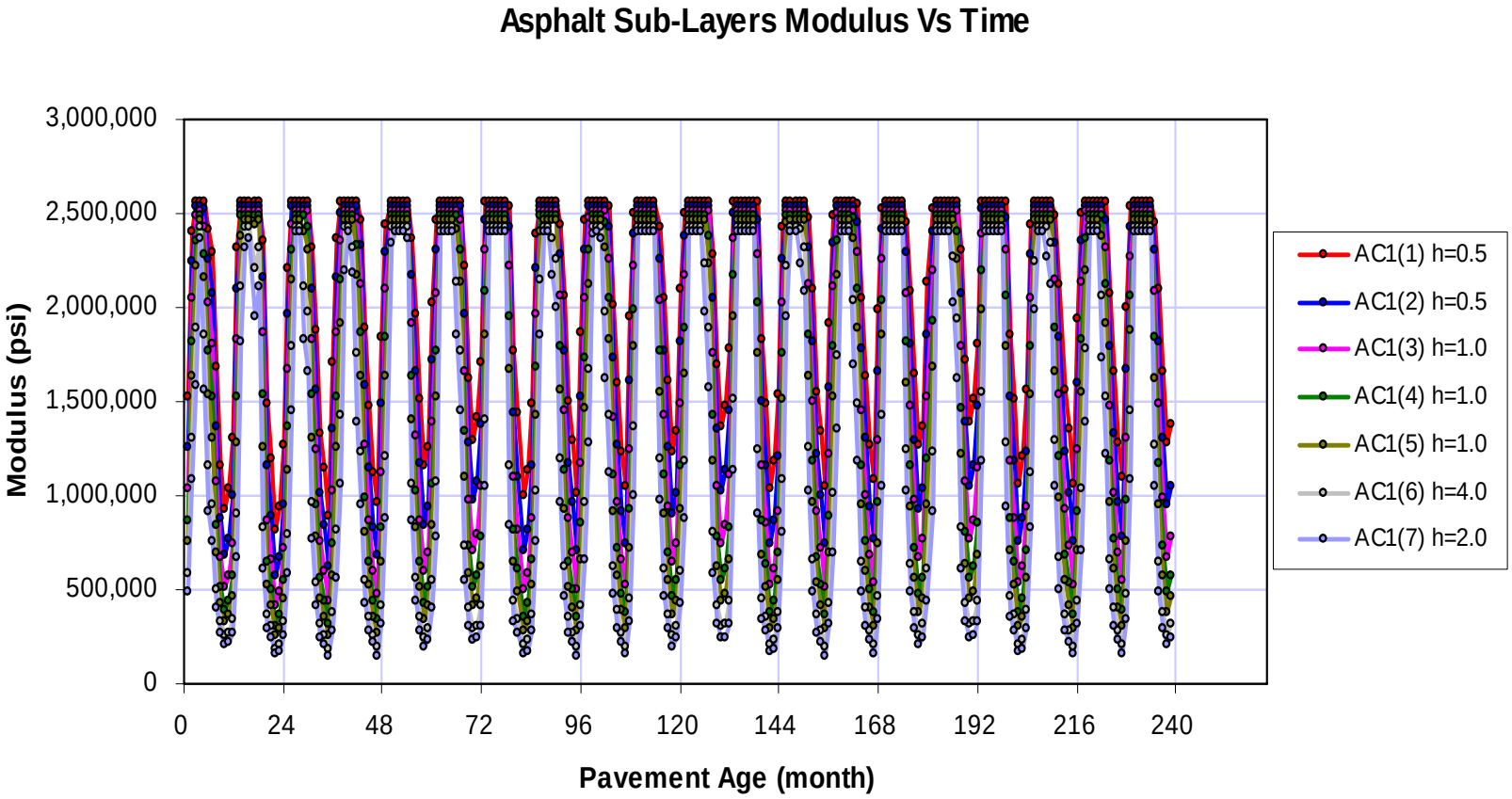
Asphalt Sub-Layers Modulus Vs Time
Modulus (psi)
3,000,000
2,500,000
2,000,000
1,500,000
1,000,000
500,000
0
0
24
48
72
96
120
144
168
192
216
240
Pavement Age (month)
AC1(1) h=0.5
AC1(2) h=0.5
AC1(3) h=1.0
AC1(4) h=1.0
AC1(5) h=1.0
AC1(6) h=4.0
AC1(7) h=2.0

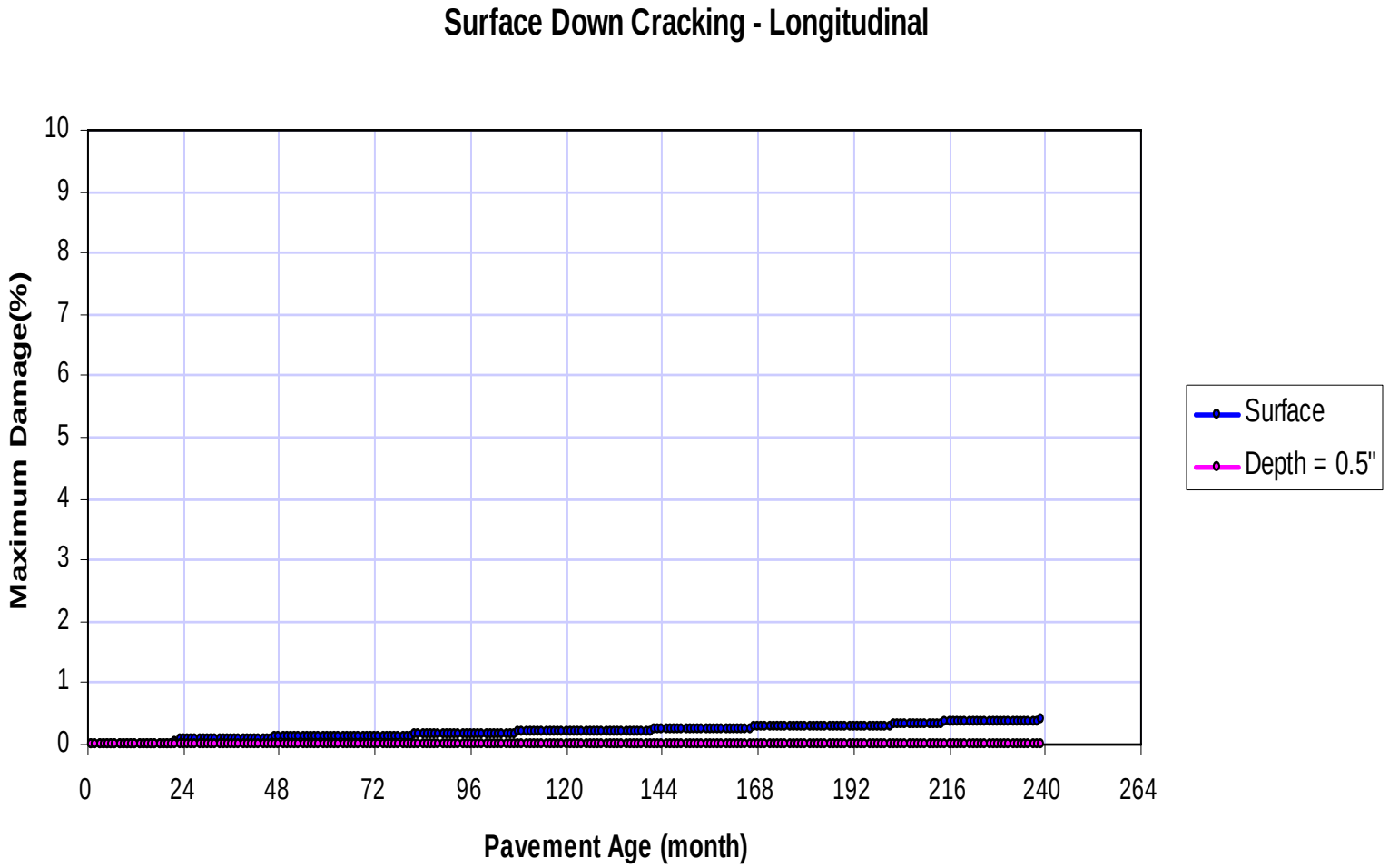
Surface Down Cracking - Longitudinal
Maximum Damage(%)
10
9
8
7
6
5
4
3
2
1
0
0
24
48
72
96
120
144
168
192
216
240
264
Pavement Age (month)
Surface
Depth = 0.5"

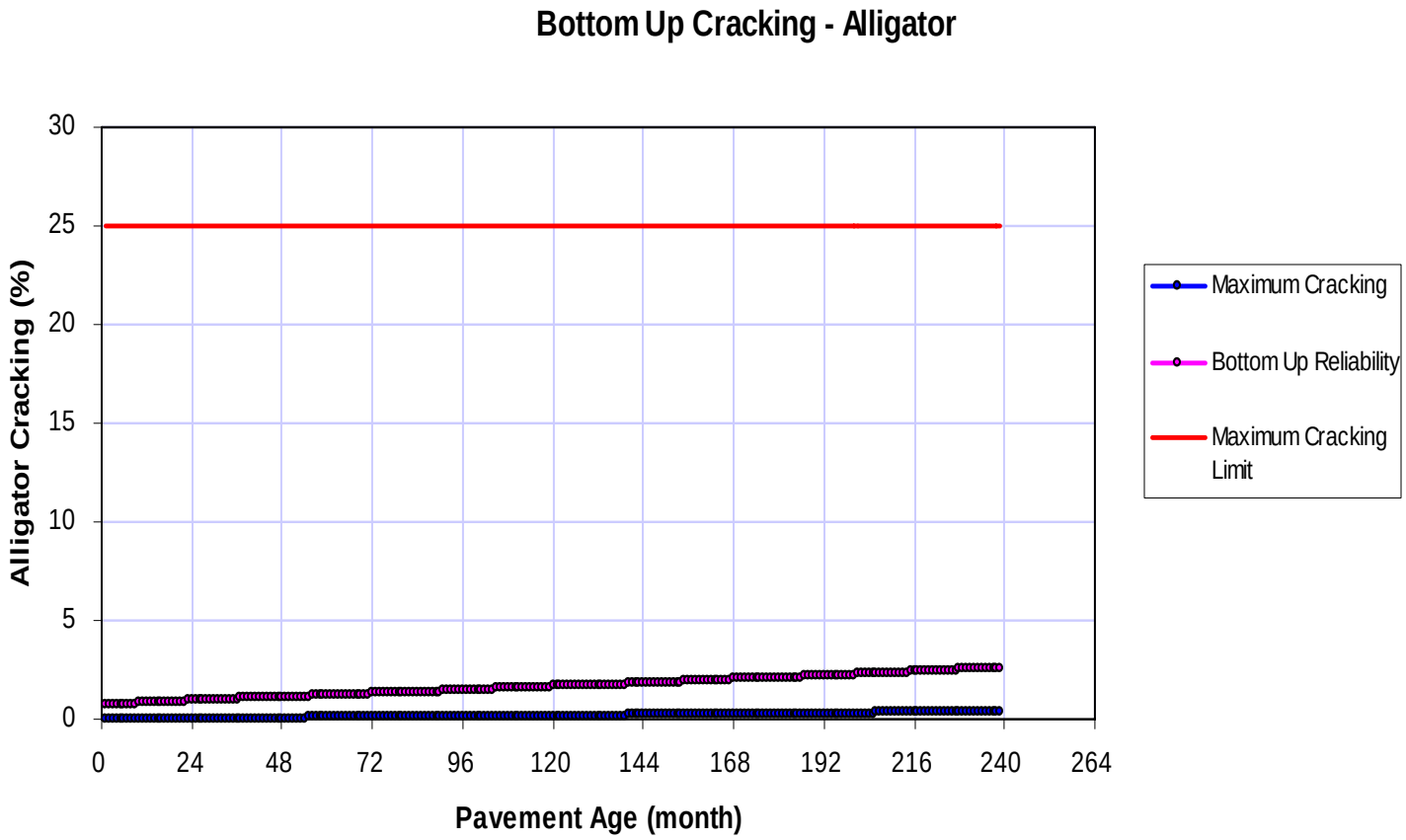
Bottom Up Cracking - Alligator
Alligator Cracking (%)
30
25
20
15
10
5
0
0
24
48
72
96
120
144
168
192
216
240
264
Pavement Age (month)
Maximum Cracking
Bottom Up Reliability
Maximum Cracking Limit

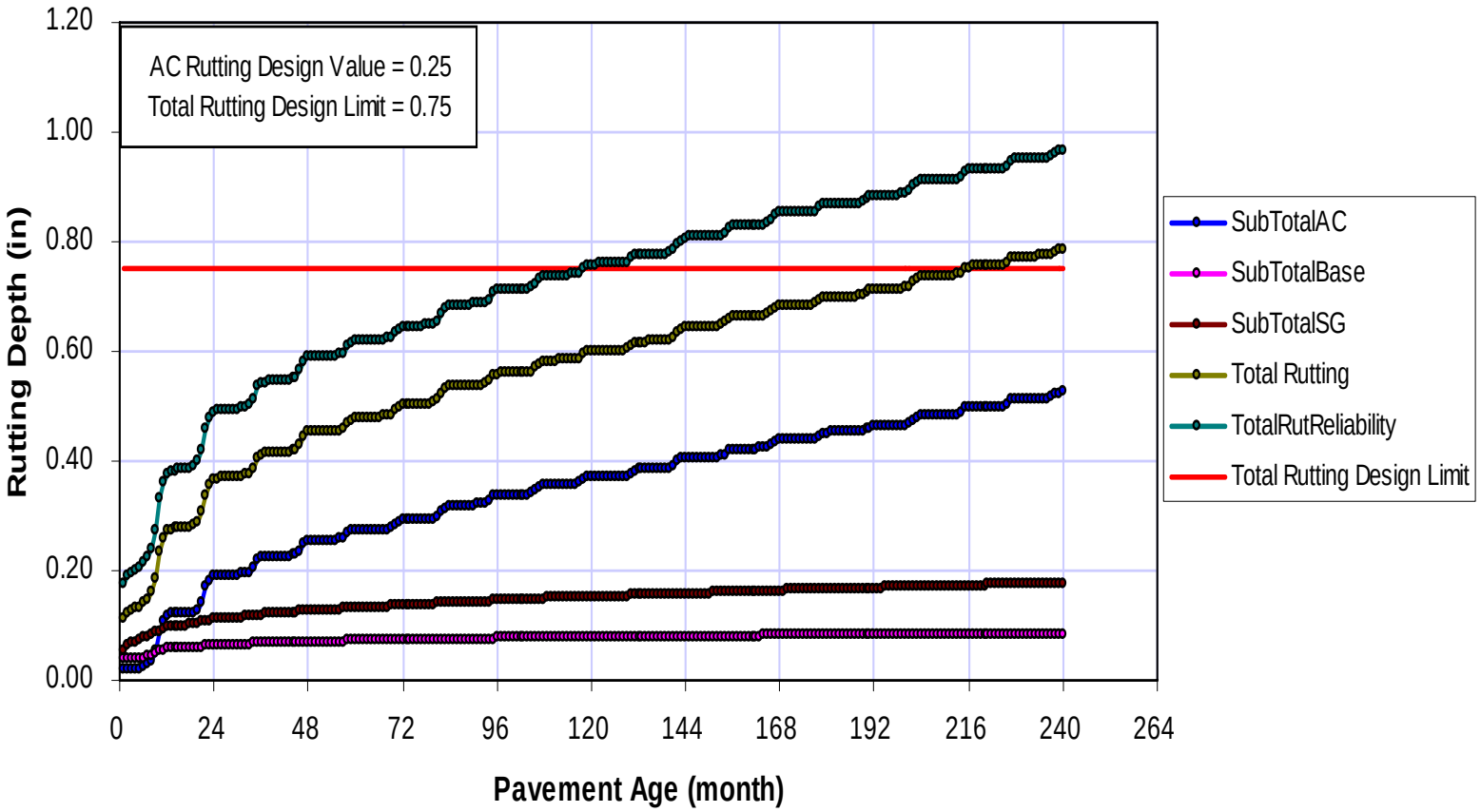
Permanant Deformation: Rutting
AC Rutting Design Value = 0.25
Total Rutting Design Limit = 0.75
Rutting Depth (in)
1.20
1.00
0.80
0.60
0.40
0.20
0.00
0
24
48
72
96
120
144
168
192
216
240
264
Pavement Age (month)
SubTotalAC
SubTotalBase
SubTotalSG
Total Rutting
TotalRutReliability
Total Rutting Design Limit

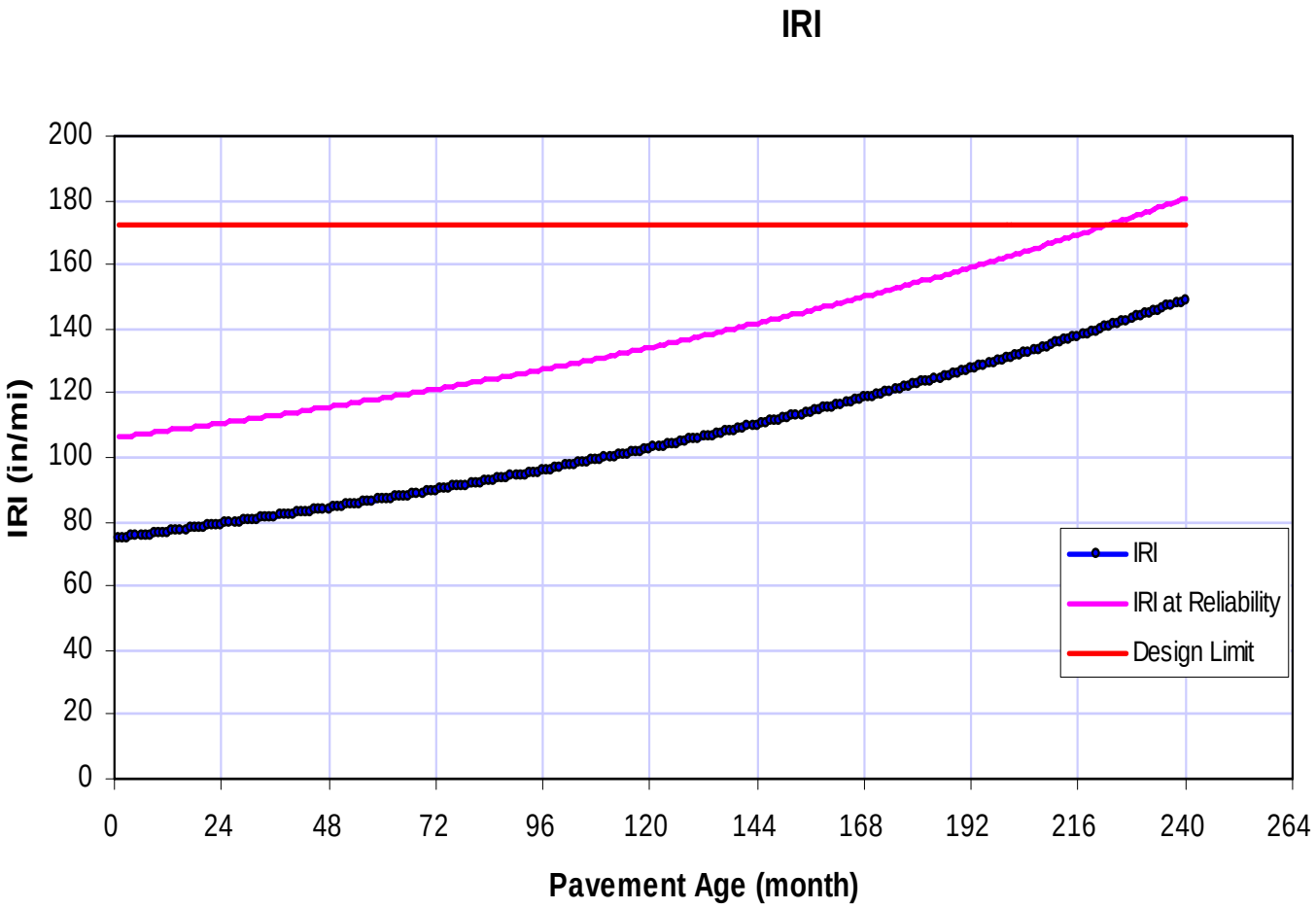
IRI
200
180
160
140
120
100
80
60
40
20
0
IRI (in/mi)
0
24
48
72
96
120
144
168
192
216
240
264
Pavement Age (month)
IRI
IRI at Reliability
Design Limit